

EFFECT OF SLIDING SPEED AND RISE IN TEMPERATURE AT THE CONTACT INTERFACE ON COEFFICIENT OF FRICTION DURING FULL SLIDING OF SS304

Thesis

Submitted in partial fulfillment of the requirements for degree of

DOCTOR OF PHILOSOPHY

by

PALANI KUMAR. P



DEPARTMENT OF WATER RESOURCES & OCEAN ENGINEERING,

NATIONAL INSTITUTE OF TECHNOLOGY KARNATAKA,

SURATHKAL, MANGALORE - 575 025

APRIL – 2022

**Effect of sliding speed and rise in temperature
at the contact interface on coefficient of
friction during full sliding of SS304**

Thesis

Submitted in partial fulfillment of the requirements for degree of
DOCTOR OF PHILOSOPHY

by

PALANI KUMAR. P



**DEPARTMENT OF WATER RESOURCES & OCEAN ENGINEERING
NATIONAL INSTITUTE OF TECHNOLOGY KARNATAKA,
SURATHKAL, MANGALORE - 575 025**

April – 2022

**EFFECT OF SLIDING SPEED AND RISE IN
TEMPERATURE AT THE CONTACT INTERFACE
ON COEFFICIENT OF FRICTION DURING FULL
SLIDING OF SS304**

Submitted in partial fulfillment of the requirements for degree of
DOCTOR OF PHILOSOPHY

by
PALANI KUMAR. P
155101AM15F05

Under the guidance of

Dr. Subrahmanya Kundapura

Assistant Professor

Department of Water Resources and Ocean Engineering

Dr. N. Gnanasekaran

Assistant Professor

Department of Mechanical Engineering



**DEPARTMENT OF WATER RESOURCES & OCEAN ENGINEERING
NATIONAL INSTITUTE OF TECHNOLOGY KARNATAKA,
SURATHKAL, MANGALORE - 575 025**

April – 2022

DECLARATION

I hereby *declare* that the Research Thesis entitle **EFFECT OF SLIDING SPEED AND RISE IN TEMPERATURE AT THE CONTACT INTERFACE ON COEFFICIENT OF FRICTION DURING FULL SLIDING OF SS304**

Which is being submitted to the **National Institute of Technology Karnataka, Surathkal**, in partial fulfillment of the requirements for the award of the Degree of **Doctor of Philosophy** in the Department of **Water Resources and Ocean Engineering**, is a *bonafide report of the research work carried out by me*. The material contained in this Research Thesis has not been submitted to any University or Institution for the award of any degree.

P.K.S.
25/04/22

155101 AM15F05, PALANI KUMAR. P



Department of Water Resources and Ocean Engineering

Place: NITK-Surathkal

Date: 25-04-2022

CERTIFICATE

This is to *certify* that the Research Thesis entitled **EFFECT OF SLIDING SPEED AND RISE IN TEMPERATURE AT THE CONTACT INTERFACE ON COEFFICIENT OF FRICTION DURING FULL SLIDING OF SS304** submitted by **PALANI KUMAR. P (Register Number;155101 AM15F05)**, as the record of the research work carried out by him, is *accepted as the Research Thesis submission* in partial fulfilment of the requirements for the award of degree of Doctor of Philosophy.


28/04/2022
Research Guides 
28/04/2022
(Dr. Subrahmanya Kundapura and Dr. N. Gnanasekaran)




Chairman – DRPC
(Prof. Dodamani B M)

Chairman (DRPC)
Dept. of Water Resources & Ocean Engineering

ABSTRACT

Most of the marine, aerospace, mechanical, civil components undergo cyclic loading. When two metal bodies slide or move relative to one another, there will be a mechanical energy loss as a result of friction. In the majority of dry sliding scenarios, it is appropriate to assume that all frictional energy is transferred as heat to the contacting bodies. Frictional heating is what causes the temperature of the sliding bodies to rise, particularly at the contact interface. The temperature on the contact interface may be high enough to have a substantial influence on the outcomes of the sliding mechanism. The following are some of the potential effects of high sliding surface temperatures: surface melting, oxidation, oxidation wear, deterioration of solid, thermo elastic instabilities, and thermo cracking of the sliding components. When two metals are in contact and subjected to friction, heat is generated at the contact interface which plays a vital role in the field of tribology. Pin-on-disk apparatus is used to examine materials sliding. The current research work focuses on the effect of sliding speeds, normal loads, and temperature rise at the contact interface of SS304 alloys subjected to full sliding experiments. Dry sliding experiments were conducted on Rotary Type Pin-on-Disk Tribometer and Finite Element Modelling was carried out using ANSYS Software. Cylindrical pins of radius 3 mm, height 30 mm, and circular disk of diameter 165 mm having flat surface were fabricated to simulate Hertzian contact configuration. Experiments were conducted at three different sliding speeds of 1 m/s, 2 m/s, and 3 m/s under normal load of 1 kg, 1.5 kg and 2 kg and two different wear tracks of diameter (60 mm and 120 mm) respectively. Dry sliding experiments were conducted up to time of 200 s. The rise in temperature were measured using K-type thermocouples and they were located to the pins at 4 mm and 7 mm distance from the contact interface. The temperature and heat flux at the contact surface was predicted using inverse heat transfer method obtained during Pin on Disk experiment. Evolution of pin temperature at the contact interface obtained from Finite Element Analysis results is in good agreement with the experimental result.

Keywords: SS304 alloys, sliding speed, heat flux, temperature, Finite Element Analysis.

TABLE OF CONTENTS

ABSTRACT	i
TABLE OF CONTENTS	ii
LIST OF FIGURES	iv
LIST OF TABLES	x
1. INTRODUCTION	1
1.1 General	1
1.2 Background and Motivation	3
1.3 Structure of the thesis	6
2. LITERATURE SURVEY	7
2.1 Literature review	7
2.1.1 Effect of normal load and sliding speed	8
2.1.2 Effect of contact temperature	12
2.1.3 Inverse heat transfer	15
2.1.4 Finite Element Method (FEM) models	17
2.2 Problem Formulation	22
2.3 Aim and objectives	23
3. DETAILS OF ROTARY-TYPE DRY SLIDING EXPERIMENTS	25
3.1 Material	25
3.1.1 Measuring Surface Roughness (Ra)	27
3.2 Experimental Setup	29
3.3 Identification of Optimum location for pasting thermocouples through Finite Element Analysis	33

3.3.1	Finite element model	33
3.3.2	Boundary condition and application of pressure	33
4.	ONE DIMENSIONAL INVERSE HEAT TRANSFER MODEL AND FINITE ELEMENT MODELING	37
4.1	Mathematical modelling to estimate surface temperature	37
4.2	Finite Element Modeling	39
4.2.1	Pin and Disk Geometric Parameters and Material Properties	39
4.2.2	Meshing Parameter, Boundary Conditions and Loading	41
5.	RESULTS AND DISSCUSSION	45
5.1	Friction behavior	45
5.2	Wear behavior	50
5.3	Analysis of worn-out disks track surface	55
5.4	Variation of coefficient of friction over sliding distance	58
5.5	Variation of temperature over sliding distance	59
5.6	Variation of temperature over sliding speeds and normal loads	60
5.7	Finite Element Analysis results	67
5.8	Validation of finite element models against experiment results	77
6.	CONCLUSIONS	89
6.1	Limitations of the study	90
6.2	Scope for future work	91
	SELECTED REFERENCES	92
	PUBLICATIONS BASED ON PRESENT RESEARCH WORK	100
	CURRICULUM VITAE	103

LIST OF FIGURES

Figure 1.1	Schematic diagram of (a) Rotary type sliding wear test and (b) Reciprocating type sliding wear test	3
Figure 2.1	Effect of normal load on (a) wear and (b) friction Sharma (2001)	9
Figure 2.2	Effect of sliding velocity on (a) wear and (b) friction Sharma (2001)	10
Figure 2.3	Coefficient of friction at different applied normal loads (Sachin M. et al., 2014)	11
Figure 2.4	Coefficient of friction vs sliding velocity (Mohammad, 2013)	11
Figure 2.5	Various phenomena occurring during sliding process for a ball-on-flat sliding contact (Gwidon W. Stachowiak, 2005)	12
Figure 2.6	Predicted maximum contact temperature during sliding velocity	12
Figure 2.7	Change of contact temperature increment with time for sliding velocity 0.5 m/s	14
Figure 2.8	The contact temperature was measured by thermocouple	14
Figure 2.9	Finite element mesh details of fretting wear test (Cruzado <i>et al.</i> , 2013)	18
Figure 2.10	Abaqus model of the fretting test (C. Gandiolle and S. Fouvry, 2015)	18
Figure 2.11	Comparison of experimental Observation and FEA- computed temperatures of Pin at (a) 4 mm and (b) 6 mm distance from the sliding surface	19
Figure 2.12	(a) total heat flux and (b) temperature variation due to friction shows the FEM analysis of pin model (C.R. Raghavendra et.al. (2018))	21
Figure 3.1	Schematic diagram of Stainless-Steel rod used for (a) Circular Disk and (b) Cylindrical Pin preparation	27
Figure 3.2	Schematic representation of surface roughness (Ra) measured at different location on pin and disk specimens	28
Figure 3.3	Schematic representation of pin-on-disk tribometer equipment	29
Figure 3.4	Top view of pin-on-disk tribometer equipment	30

Figure 3.5	Schematic representation of Pin and disk specimen dimensions	31
Figure 3.6	Pin-on-disk tribometer used for friction test	32
Figure 3.7	Schematic representation of a weary disk and pin used to measure total wear volume	33
Figure 3.8	von Mises stress distribution over solid cylinder-flat for the pin with hole (2 mm, 3 mm, 4 mm, 5 mm and 6 mm) and with-out hole	34
Figure 3.9	von Mises stress distribution over solid cylinder-flat for the pin with hole (7 mm, 8 mm, 9 mm, and 10 mm)	34
Figure 3.10	Schematic representation of temperature measurement points with K- Type thermocouples in pin specimen	35
Figure 3.11	Temperatures measured at 4 mm and 7 mm locations using thermocouples from contact interface during dry sliding experiments on SS304 alloy	36
Figure 4.1	Flowchart of the heat flux estimation process (Chen, et al 2014, Sun Z et al 2011)	39
Figure 4.2	Geometry of pin-on-disk finite element model (60 mm Track)	40
Figure 4.3	Geometry of pin-on-disk finite element model (120 mm Track)	41
Figure 4.4	Element (SOLID90) considered for finite element analysis(ANSYS Workbench Manual)	42
Figure 4.5	Solid element mesh of the Pin-on-disk model (60 mm Track)	43
Figure 4.6	Solid element mesh of the Pin-on-disk model (120 mm Track)	43
Figure 4.7	Schematic representation of Boundary Conditions considered for Pin-on-disk model	44
Figure 5.1	Variation of coefficient of friction with respect to time at different sliding speeds and normal loads for 60 mm track diameter	46
Figure 5.2	Variation of coefficient of friction with respect to time at different sliding speeds and normal loads for 120 mm track diameter	47
Figure 5.3	Worn surfaces of wear track 60 mm diameter for three different	49

	normal loads and sliding speeds	
Figure 5.4	Worn surfaces of wear track 120 mm diameter for three different normal loads and sliding speeds	50
Figure 5.5	Variation of wear volume with varying time at different sliding speeds and normal loads for track diameter of 60 mm	51
Figure 5.6	Variation of wear volume with varying time at different sliding speeds and normal loads for track diameter of 120 mm	52
Figure 5.7	Optical microscopy image for damage disks at 60 mm track surface	56
Figure 5.8	Optical microscopy image for damage disks at 120 mm track surface	57
Figure 5.9	Coefficient of friction vs. sliding distance	58
Figure 5.10	Temperature vs. sliding distance	60
Figure 5.11	Estimated heat flux at contact interface of SS304 alloy	61
Figure 5.12	Estimated surface temperature at contact interface of SS304 alloy	61
Figure 5.13	Variation of heat flux with respect to time (60 mm track diameter) for three different sliding speeds 1 m/s, 2 m/s, and 3 m/s under normal load of (a) 1 kg (b) 1.5 kg and (c) 2 kg	63
Figure 5.14	Variation of heat flux with respect to time (120 mm track diameter) for three different sliding speeds 1 m/s, 2 m/s, and 3 m/s under normal load of (a) 1 kg (b) 1.5 kg and (c) 2 kg	64
Figure 5.15	Temperature distribution between pin and disk over 200 s of sliding for a 60 mm diameter track using a Finite Element model (1 kg, 1 m/s)	67
Figure 5.16	Temperature distribution between pin and disk over 200 s of sliding for a 60 mm diameter track using a Finite Element model (1 kg, 2 m/s).	68
Figure 5.17	Temperature distribution between pin and disk over 200 s of sliding for a 60 mm diameter track using a Finite Element model (1 kg, 3 m/s).	68
Figure 5.18	Temperature distribution between pin and disk over 200 s of	69

	sliding for a 60 mm diameter track using a Finite Element model (1.5 kg, 1 m/s).	
Figure 5.19	Temperature distribution between pin and disk over 200 s of sliding for a 60 mm diameter track using a Finite Element model (1.5 kg, 2 m/s).	69
Figure 5.20	Temperature distribution between pin and disk over 200 s of sliding for a 60 mm diameter track using a Finite Element model (1.5 kg, 3 m/s).	70
Figure 5.21	Temperature distribution between pin and disk over 200 s of sliding for a 60 mm diameter track using a Finite Element model (2 kg, 1 m/s).	70
Figure 5.22	Temperature distribution between pin and disk over 200 s of sliding for a 60 mm diameter track using a Finite Element model (2 kg, 2 m/s).	71
Figure 5.23	Temperature distribution between pin and disk over 200 s of sliding for a 60 mm diameter track using a Finite Element model (2 kg, 3 m/s).	71
Figure 5.24	Temperature distribution between pin and disk over 200 s of sliding for a 120 mm diameter track using a Finite Element model (1 kg, 1 m/s).	72
Figure 5.25	Temperature distribution between pin and disk over 200 s of sliding for a 120 mm diameter track using a Finite Element model (1 kg, 2 m/s).	72
Figure 5.26	Temperature distribution between pin and disk over 200 s of sliding for a 120 mm diameter track using a Finite Element model (1 kg, 3 m/s).	73
Figure 5.27	Temperature distribution between pin and disk over 200 s of sliding for a 120 mm diameter track using a Finite Element model (1.5 kg, 1 m/s).	73
Figure 5.28	Temperature distribution between pin and disk over 200 s of sliding for a 120 mm diameter track using a Finite Element	74

	model (1.5 kg, 2 m/s).	
Figure 5.29	Temperature distribution between pin and disk over 200 s of sliding for a 120 mm diameter track using a Finite Element model (1.5 kg, 3 m/s).	74
Figure 5.30	Temperature distribution between pin and disk over 200 s of sliding for a 120 mm diameter track using a Finite Element model (2 kg, 1 m/s).	75
Figure 5.31	Temperature distribution between pin and disk over 200 s of sliding for a 120 mm diameter track using a Finite Element model (2 kg, 2 m/s).	75
Figure 5.32	Temperature distribution between pin and disk over 200 s of sliding for a 120 mm diameter track using a Finite Element model (2 kg, 3 m/s).	76
Figure 5.33	Temperature comparison between experimental and FE-simulated data (1 kg, 1 m/s) (a) evolution of the pin temperature at contact interface (b) Pin temperature evolution at 4 mm location (c) pin temperature evolution at 7 mm location for track diameter 60 mm.	78
Figure 5.34	Temperature comparison between experimental and FE-simulated data (1.5 kg, 1 m/s) (a) evolution of the pin temperature at contact interface (b) Pin temperature evolution at 4 mm location (c) pin temperature evolution at 7 mm location for track diameter 60 mm.	79
Figure 5.35	Temperature comparison between experimental and FE-simulated data (2 kg, 1 m/s) (a) evolution of the pin temperature at contact interface (b) Pin temperature evolution at 4 mm location (c) pin temperature evolution at 7 mm location for track diameter 60 mm.	80
Figure 5.36	Temperature comparison between experimental and FE-simulated data (1 kg, 1 m/s) (a) evolution of the pin temperature at contact interface (b) Pin temperature evolution at 4 mm	81

location (c) pin temperature evolution at 7 mm location for track diameter 120 mm.

Figure 5.37 Temperature comparison between experimental and FE- 82
simulated data (1.5 kg, 1 m/s) (a) evolution of the pin
temperature at contact interface (b) Pin temperature evolution at
4 mm location (c) pin temperature evolution at 7 mm location for
track diameter 120 mm.

Figure 5.38 Temperature comparison between experimental and FE- 83
simulated data (2 kg, 1 m/s) (a) evolution of the pin temperature
at contact interface (b) Pin temperature evolution at 4 mm
location (c) pin temperature evolution at 7 mm location for track
diameter 120 mm.

LIST OF TABLES

Table 3.1	Chemical Composition of Stainless Steel (SS304 grade)	25
Table 3.2	Properties of Stainless Steel (SS304 grade)	26
Table 3.3	Surface Roughness values of Stainless Steel (SS304 grade)	28
Table 3.4	Experimental parameters used for dry sliding pin on disk experiments	30
Table 4.1	Geometric parameters and engineering properties of cylindrical pin and Circular disk	40
Table 4.2	Mesh Details of pin-on-disk finite element models	43
Table 4.3	Values of Convection Coefficient applied to various surfaces of pin on disk model and Ambient Temperature used in the study (Sagar, 2016)).	44
Table 5.1	Coefficient of friction stabilization value at different sliding speeds with different Normal loads	45
Table 5.2	Comparison of wear volume stabilization value at different Normal loads and different sliding speeds with 60 mm and 120 mm track diameter	53
Table 5.3	Temperature values obtained by conducting experiment for track diameter 60 mm	66
Table 5.4	Temperature values obtained by conducting experiment for track diameter 120 mm	66
Table 5.5	Temperature values obtained by finite element analysis for track diameter 60 mm at pin surfaces	76
Table 5.6	Temperature values obtained by finite element analysis for track diameter 120 mm at pin surfaces	77
Table 5.7	Comparison of maximum surface temperature between experiments and FEA for Track Diameter 60 mm	84
Table 5.8	Comparison of maximum surface temperature between experiments and FEA for a Track Diameter 60 mm at 4mm location	84
Table 5.9	Comparison of maximum surface temperature between	85

experiments and FEA for a Track Diameter 60 mm at 7 mm location

Table 5.10	Comparison of surface temperature from experimental to FEA values for Track Diameter 120 mm	85
Table 5.11	Comparison cylindrical pin temperature 4 mm location from experimental to FEA values for Track Diameter 120 mm	86
Table 5.12	Comparison of cylindrical pin temperature 7 mm location from experimental to FEA values for Track Diameter 120 mm	86

CHAPTER 1

INTRODUCTION

1.1 General

Stainless steels represent quite an interesting material family, both from a scientific and commercial point of view, owing to their excellent qualities in terms of strength and ductility, combined with corrosion resistance. The austenitic structure provides stainless steels (SS304) with good ductility and formability. The common 18% chromium, 8% nickel Type 304 in particular shows good stretch-forming characteristics. Stainless steel alloys (SS304) are preferred for high-temperature applications and where fire resistance is needed. (Andrea Di Schino., 2020).

Most of the marine, aerospace, mechanical, civil components undergo cyclic loading. When two metal bodies slide or move relative to one another, there will be a mechanical energy loss as a result of friction. In the majority of dry sliding scenarios, it is appropriate to assume that all frictional energy is transferred as heat to the contacting bodies. Frictional heating is what causes the temperature of the sliding bodies to rise, particularly at the contact interface. The temperature on the contact interface may be high enough to have a substantial influence on the outcomes of the sliding mechanism. The following are some of the potential effects of high sliding surface temperatures: surface melting, oxidation, oxidation wear, deterioration of solid, thermo elastic instabilities, and thermo cracking of the sliding components. It's crucial to determine surface temperatures in sliding contacts because frictional heating can impact the operation of sliding components such as bearings, seals, brakes, and clutches (Francis Kennedy, Jr.1981).

Brake components can be tested for friction and wear using dynamometer measurements (dyno tests) or pin-on-disk tests. Since actual pads and Disks are used in dyno simulations, they better simulate actual braking conditions. Pin on Disk experiments, on the other hand, have many benefits, including shorter processing

periods, lower costs, the ability to help determine the dependency of friction and wear on operational circumstances, and the ability to relate the active damage mechanisms to the operating parameters. An appropriate model for measuring and monitoring the contact temperatures produced during sliding is required to effectively design a pin-on-Disk test and to interpret the results. Plain Pin-on-Disk experiments are very useful for obtaining detailed insights on wear processes and their effect in tribological behaviour (Saikko et al., (2017), Straffelini (2015), Kennedy (1984), Laraqui et al., (2009)).

Components of mechanical devices are either in rolling contact or in sliding contact. Contact surfaces are subjected to friction and wear in both rolling contacts and in sliding contacts. Wear leads to dimensional changes and eventual breakdown of the Mechanical components and consequently the entire machine. The material loss at the contact interface due to wear necessitates replacement of machine components. It is therefore necessary and essential to reduce wear. Wear rate should be reduced to improve performance of machine components. Coefficient of friction(μ) and wear rate are two parameters, which can be measured by conducting wear tests [Maged Elhefnawy et.al, (2020), Satyananda Kar et.al, (2020)]. Deterioration of material can be understood by observing coefficient of friction (μ) and wear rate at the contact interface. Wear rate was determined by conducting Pin-on-Disk experiments. In Pin-on-Disk experiments, materials slides against each other with various parameters such as contact geometry, normal load, and sliding velocity. Material wear process should be investigated to understand wear at the contact interface and to improve performance and life of machine [Meng, H. C et.al, (2001), Rudas, J. S et.al, (2013)]. Coefficient of friction (μ) and wear rate is a function of conditions, applied normal load, contact geometry, relative surface motion, sliding speed, surface roughness of the contact interface, stick/slip, temperature, relative humidity, etc [S. Guicciardi et.al, (2002), S.A. Alidokht et.al, (2013), H. Murthy et.al, (2016), Handbook, (2014)]. Many researchers [T. Ram Prabhu M et.al,(2019), Shiv Kumara et.al,(2011), T. Xinmin Lin et.al,(2015)] studied the frictional behaviour of two metals either in rolling contact or in sliding contact by conducting full sliding experiments. Extensive

procedural details were explained to measure the COF. Schematic diagrams of rotary type and reciprocating type sliding are shown in Figure. 1.1. Pin-on-disk tests [Dong H et.al,(1999)] were conducted between Ti6Al4V alloy and aluminium alloy. Increase of normal load and sliding speed resulted in increase of the wear rate. Reciprocating sliding experiments were conducting between Ti6Al4V alloy and aluminium alloy. Aluminium alloy showed higher hardness than the titanium alloy, and shows better resistance to abrasion [Wen-Lih Chen et.al,(2011)]

Coefficient of friction is defined as the ratio of forces acting parallel and perpendicular to the interacting surfaces when the surfaces are in relative motion (Peter J. Blau, 2008). Coefficient of friction is, a dimension less quantity, intrinsic property of two contacting surfaces which depends on number of parameters and the measurement of coefficient of friction is quite difficult in laboratory. The coefficient of friction is dependent on space and time, which requires a careful, extensive, and through study before designing the engineering components. Coefficient of friction of contacting materials is dependent on parameters such as normal pressure at contact surface, frequency of loading, duration of loading, mode of sliding, environment at contact interface, etc.

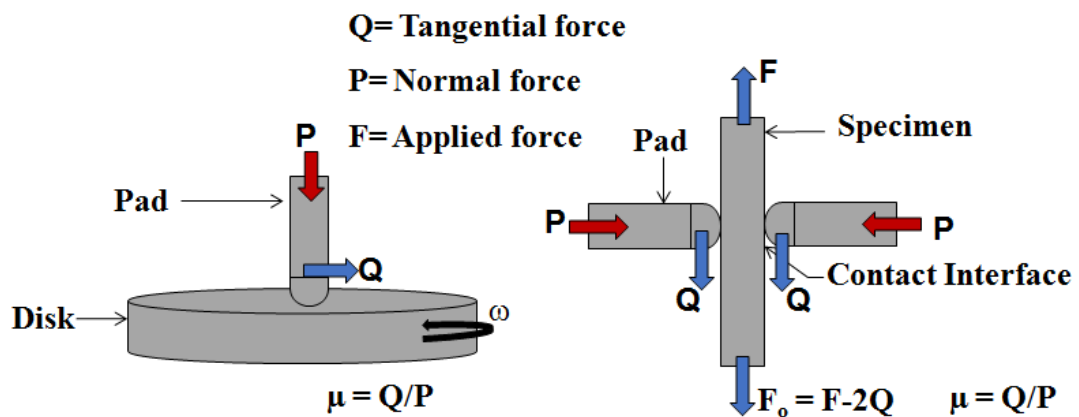


Figure. 1.1: Schematic diagram of (a) Rotary type sliding wear test and (b) Reciprocating type sliding wear test

1.2 Background and Motivation

Friction is associated with the conversion of energy. In practical cases up to 95% of friction generated is converted in the form of heat (Majcherczak D et al., 2007). The

heat generated by friction and its corresponding temperature field is affected by the change in motion, normal load applied at the contact interface and relative velocity of sliding components. The heats generated by friction and temperature field have more influence on the wear behaviour. Hence the life of material is affected. Attention is paid to the heat generation due to sliding, which plays a key role on the wear of material at the contact interface. When two materials slide against each other, temperature rise is caused at the contact surface between pin held in position by the pin holder and rotating disk. The frictional force between pin and disk is transformed into heat energy due to rotation of the disk. The frictional heat is measured by using thermocouples during the full sliding experiments conducted in dry sliding condition.

Many researchers (Bortoleto et al., 2013, Uthayakumar M. et.al.2013, Arul raj K et.al.,2019, Larson M. G et.al.,2017) have conducted full sliding friction experiments using rotary type Tribometer (Giovanni Straffelini., 2001) and to and fro reciprocating sliding experiments (Mohammad Asaduzzaman Chowdhury et al, 2000, Murthy et al., 2017). They explained detailed procedure to measure the coefficient of friction from their experiments and they also explained the effect of sliding speed (Peter J. Blau et al, 2000), normal load (Hosung Kong et al,1995), humidity (Laurence W. McKeen, 2010) and ambient temperature (Y.J.Heay et al, 1995) on coefficient of friction. From friction experiments, the researchers (Y.J.Heay et al, 1995; S.M.R. Mousavi Abarghouie et al, 2010; Dobromirski J M, 1992) have observed that 54 parameters are influencing coefficient of friction. To measure the friction coefficient, suitable fixtures are needed to run well-controlled reciprocating tests (Vadivuchezhian et al, 2011), if two components are under full sliding with respect to each other. For full sliding experiments, it is direct way to measure the coefficient of friction which is defined as the ratio between the tangential load and the normal load acting at the contact interface of the full sliding components. Some researchers (Ian Baker et al, 2015; K.Imado et al, 2003; B. R. Srinivasa Murthy et al, 1993) have studied the effect of rise in temperature at the contact interface on coefficient of friction obtained from full sliding experiments. They used only flat on flat contact in their study. But flat on

flat contact is not suitable for sliding since it removes the material as wear debris due to the presence of sharp corners (B. R. Srinivasa Murthy et al, 1993).

The prediction of the service life of a component with the highest accuracy possible is increasingly one of the key aspects in today's design philosophy of mechanical parts. The understanding of the different failure mechanisms is very important in determining the safety and reliability of a product. Furthermore, the financial cost associated with maintenance and durability of the parts of a product during the course of its life is ever more important in the design of new mechanical components. Maintenance and replacement costs of parts represent a significant contribution to the total operational cost throughout different areas of mechanical engineering, if taken into account over the total service life of components [Seemann, 2010]. The question of reliability and safety of a product requires a good understanding of its material properties and its behavior under specific loading conditions. Any lack of knowledge on how and when a part will fail is normally compensated by overestimating the loads and/or part dimensions in the design. Needless to say, an overestimation of the dimensions of a mechanical component will incur greater cost, weight and, in the case of engines, higher fuel consumption. All of these factors also lead to higher environmental impact. In a time where efficiency is one of the main design considerations in most transport industries, a lower fuel consumption is often prioritised over power or speed. This search for greater efficiency is one of the main driving factors behind the push towards a better understanding of the service life of components, but also towards the development of new materials. The motivation is from the fact that many machine components fail due to wear and estimation of wear during operation of the machine would lead to developing appropriate wear mitigation approaches. However, measurement of in-situ wear in machine components is very difficult, if not impossible. Finite element method (FEM) based numerical modeling of machine operation with appropriate models would enable estimation of contact temperature a-priori. However, accuracy of calculated temperature values strongly depends on the heat flux values. Hence, accurate modeling of inverse heat transfer technique is essential to estimate contact temperature accurately. Hence, this work

was taken up to establish the FEM modeling methodology to evaluate the evolution of surface temperature at the contact interface accurately in the ball-on-disc contact configuration in the form of pin-on-disc tribology test. This FEM model would lead towards establishing a fully functional FEM model extendable to real world components having contact pairs to estimate surface temperature at the contact interface a-priori. The accuracy of the pin on disc models is validated by comparing the results of the finite element analysis and experimental results.

1.3 Structure of the thesis

Chapter 1 provides an introduction to the stainless-steel alloys, components of mechanical devices, types of contacts, coefficient of friction, friction and motivation.

Chapter 2 contains literature review of the effect of normal load and sliding speed, contact temperature, inverse heat transfer, Finite Element Method (FEM) models, problem formulation and objectives of present research work.

Chapter 3 gives detail procedure of material selection, fabrication of cylindrical pin and circular disk specimens, measuring Surface Roughness, experimental setup and identification of optimum location for pasting thermocouples through finite element analysis.

Chapter 4 gives detail procedure of mathematical modelling to estimate surface temperature, Finite Element Modeling, Pin and Disk Geometric Parameters, Material Properties, Meshing Parameter, Boundary Conditions, and Loading.

Chapter 5 discusses about the results obtained by conducting rotary type dry sliding experiments conducted on cylindrical pin and circular disk model with two different track diameters, transient thermal analysis and their validation.

Chapter 6 is devoted to conclusions arising from this research study, limitations of present study and scope of future work, followed by references.

CHAPTER 2

LITERATURE SURVEY

2.1 Literature review

Numbers of researchers have reported about the tribological parameters of different alloys. Under this circumstance, it is necessary to evaluate tribological properties such as friction and wear characteristics under varying sliding speeds, sliding distance, surface roughness, time and temperature of different alloy and its composite. A survey of existing literature on rotary type sliding experiments and properties of contact interface along with various experimental setups developed to study these properties is presented in this section. Emphasis is laid on friction coefficient, its estimation, its variation and its effect on contact traction and subsequent failure of the components.

There are various factors which influence contact tractions and hence contribute to the failure of the components. Some of these factors are: shape of the two contacting surfaces, material properties, friction coefficient and environmental conditions (Peter J. Blau, 2001). Each of these factors need to be studied in detail in order to understand the fretting fatigue phenomenon. Johnson (1985) and Hills and Nowell (1994) have discussed the phenomenon of fretting from the contact mechanics point of view. Johnson (1985) explained the effect of different loadings like concentrated normal force, concentrated tangential force, distributed normal traction and distributed tangential traction on half space. While factors like shape of the contacting surfaces (Murthy et al., 2000) and material properties (Murthy et al., 2003) have been studied in detail for partial slip contacts, the effect of friction coefficient needs to be studied in detail. The studies related to friction coefficient under full sliding conditions were used to obtain contact tractions for partial slip fretting conditions. But in full sliding experiments, the transition of a full slip to partial slip is a critical phenomenon to be identified which promotes the fretting under mixed stick-slip condition (M. Helmi Attia and R. B. Waterhouse, 1992). The rise in contact temperature varies over a period of time due to continuous sliding of two metallic contacts. The rise in contact temperature depends on normal load, sliding velocity, mode of slip, type of material,

etc. (Raj K. Pandey and Mihir K. Ghosh, 1998; M.L. Rahaman and Liangchi Zhang, 2014; K.A. Laux et al., 2016). The present study focuses on understanding the effect of rise in contact temperature on the coefficient of friction under full sliding condition.

A brief review of available literature on related to specific topic of thesis is presented under the following headings: Effect of normal load and sliding speed; Effect of contact temperature; Inverse heat transfer; Finite Element Method (FEM) models.

2.1.1 Effect of normal load and sliding speed

Many researchers (Douglas Godfrey (1995), Kwok and Lim (1999), Sharma (2001)) tried to understand the phenomenon of friction and wear by conducting experiments using pin-on-disk tribometer and by observing the variation of friction with respect to change in various parameters such as normal load, geometry, relative surface motion, sliding velocity, temperature, etc. The normal load and sliding velocity are the deciding parameters which play an important role among these parameters. Generally, the fluctuation of friction is more on pin on disk setup which depends on sliding speeds and this fluctuation is due to non-uniformity of wear track (Douglas Godfrey, 1995). Adel Mahamood Hassan (2009) found the wear loss of Al–Mg–Cu alloys was reduced by increasing Cu content by weight up to 5%. He observed that SiC containing aluminum alloys resulted in higher coefficient of friction than aluminum-based alloys under similar test condition due to formation of tribofilm at the contact interface.

Wear and friction characteristics of Al6061 composites reinforced with garnet particulate were investigated by Sharma (2001) using a pin on disk tribometer. Tests were conducted by varying normal loads (10 N – 50 N) and sliding speeds (1.25 m/s – 3.05 m/s). When the wear rates are high, contact temperature increases and material attains plastic state. At high temperature an oxide layer, forms on contact surface, which prevents the conduction of temperature at the contact and deforms as debris due to accumulation of temperature at the contact. There was not much variation in wear rate up to 30 N normal load and then the wear rate increased with increase in the

normal load (Figure. 2.1). The wear rate also increased with increase in the sliding speed (Figure. 2.2). The friction coefficient increased with increasing normal load. But initially the friction coefficient decreased with increase in the sliding velocity and then increased. Basavarajappa S. et al. (2006) investigated Al 2219/SiCp-Gr Hybrid Metal Matrix Composites. They observed that the wear volume of Al 2219 increased after 20 N normal load with increasing normal load and wear rate increased with increase in sliding speed. Drastic increase in wear rate was observed after the sliding speed crossed 4.5 m/s.

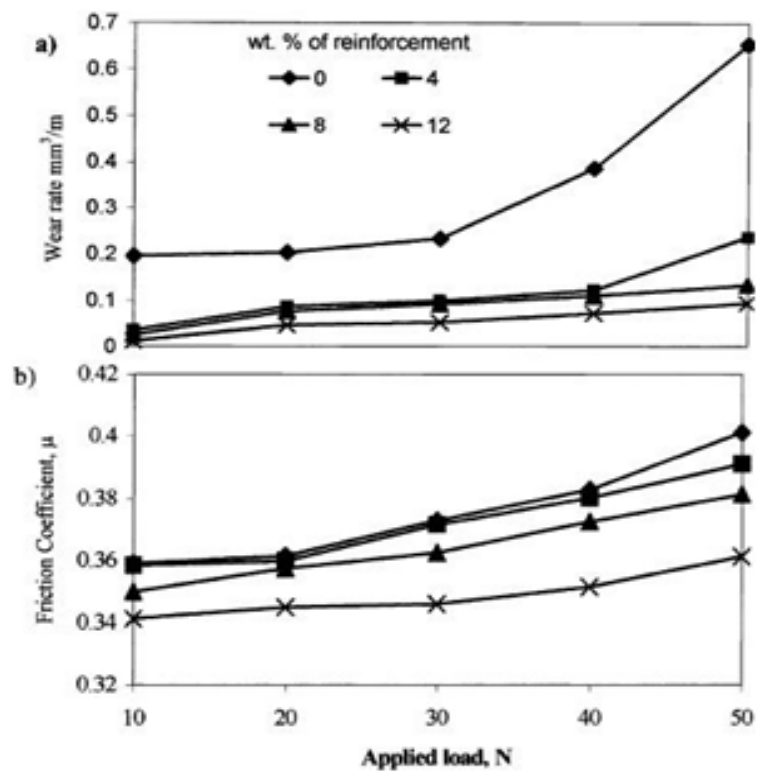


Figure 2.1: Effect of normal load on (a) wear and (b) friction Sharma (2001)

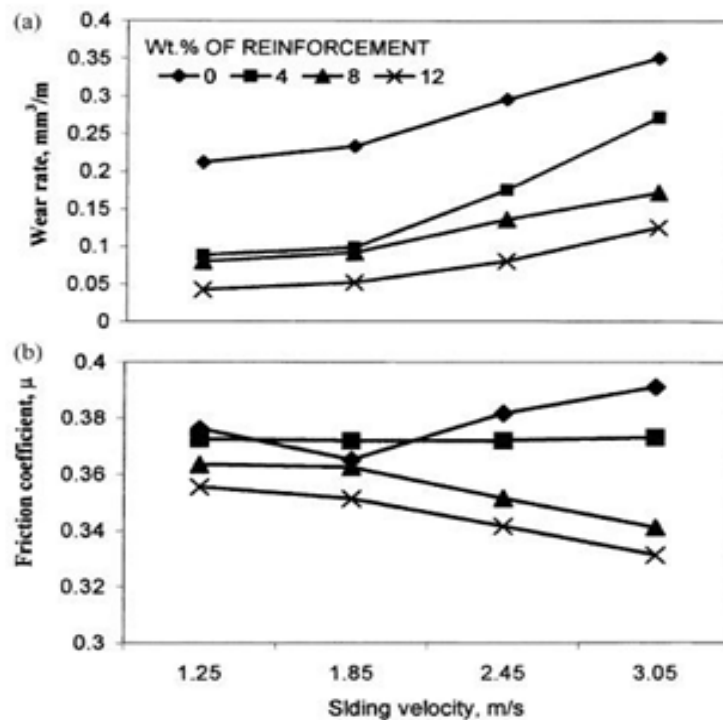


Figure 2.2: Effect of sliding velocity on (a) wear and (b) friction Sharma (2001)

Al /SiCP composite was used by Kwok and Lim (1999) to study the tribological behavior on high speed pin-on-disk tribometer and the coefficient of friction was studied at three different sliding velocities of 1 m/s, 12 m/s, 29 m/s when the normal load ranges from 30 N to 100 N. Generally, friction increases with sliding distance and stabilizes after threshold value of sliding distance. When the sliding speeds are high the coefficient of friction increases till some sliding distance and decreases due to melting of material and debris formation at higher sliding speeds. Generally, the wear rate increases with increase in applied normal load at contact when other parameters are not varying. But wear volume change is a complex phenomenon which changes with varying sliding speeds, sliding distance and material properties. The wear volume was low for low normal loads (regime I) but when the normal load and sliding speeds increase simultaneously material failed catastrophically due to adhesion effect (regime II). At higher sliding speeds melting of material surface and debris formation occur which changes the wear and friction characteristics (regime III). The wear and friction change at contact is due to rise in temperature while sliding which changes the physical and chemical properties of materials (Sharma, 2001).

Sachin M. et al. (2014) investigated on effect of cotton seed oil and SAE 40 oil on wear and friction characteristics of M2 steel. Experiments were conducted with normal loads (10N, 20N, 30 N) and sliding speeds (300 rpm, 600 rpm, 900 rpm). Coefficient of friction was decreased with increases in normal load for both dry and wet surface conditions (Figure 2.3). At lower normal load, the SAE 40 oil resulted less coefficient of friction, but as the increment in normal load cotton seed oil surfaces gave lower coefficient of friction. This research work explains the effect of normal load on friction coefficient values for SS304L and SS316 alloys under dry sliding condition at constant sliding speed. Mohammad Asaduzzaman Chowdhury (2013) observed the increase in coefficient of friction as the sliding velocity increased when SS 202 was sliding against SS 304 (Figure 2.4).

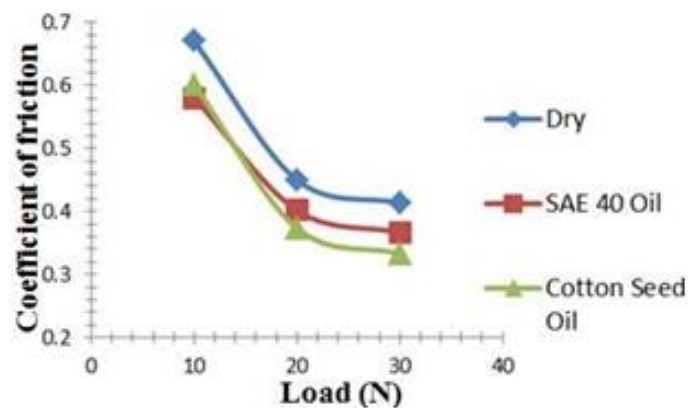


Figure 2.3: Coefficient of friction at different applied normal loads (Sachin M. et al., 2014)

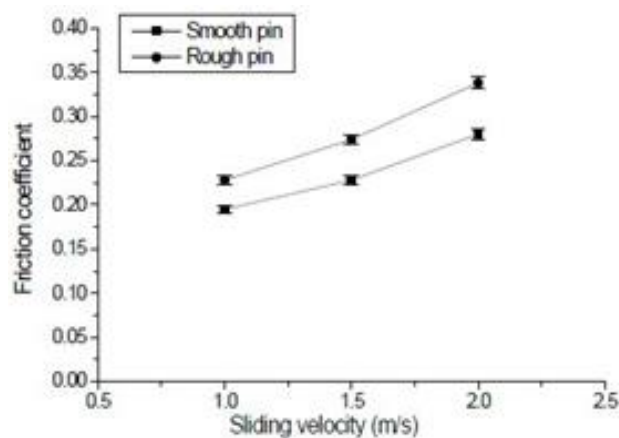


Figure 2.4: Coefficient of friction vs sliding velocity (Mohammad, 2013)

2.1.2 Effect of contact temperature

The part of dissipated energy during full sliding generates heat at contact surface. The generated heat flows through the specimen and pads by conduction (Figure 2.5). Researchers (Raj K. Pandey and Mihir K. Ghosh, 1998; M.L. Rahaman and Liangchi Zhang, 2014; K.A. Laux et al., 2016) studied the effect of normal load, sliding speed on contact temperatures for metals and polymers. M.L. Rahaman and Liangchi Zhang (2014) estimated the interface temperature during sliding of bulk metallic glass (BMG) pin on steel disk using pin-on-disk tribometer. The contact temperatures were estimated using BMG surface parameters. The contact temperature rise was more sensitive to sliding speed than applied normal load (Figure 2.6).

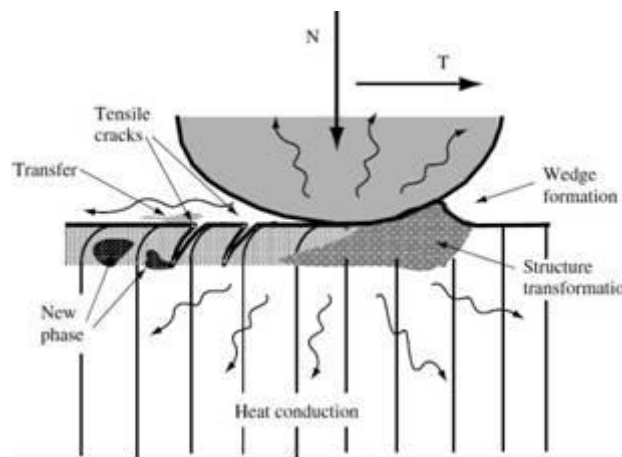


Figure 2.5: Various phenomena occurring during sliding process for a ball-on-flat sliding contact (Gwidon W. Stachowiak, 2005)

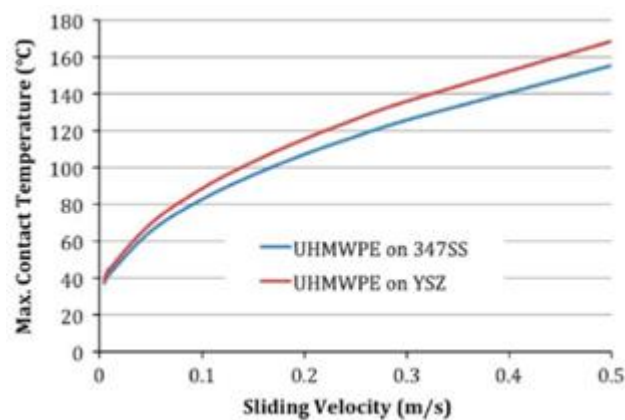


Figure 2.6: Predicted maximum contact temperature during sliding velocity

Kennedy et.al, conducted experiments to study effect of contact temperature on wear during pin on disk tribotesting. They used Ultra High Molecular Weight Poly-Ethylene (UHMWPE) pin of diameter 5 mm and 1.5 mm length was used. The disks of diameter 100 mm and thickness 10 mm was made of 347grade stainless steel and yttria-stabilized zirconia (YSZ). Contact temperature was observed up to sliding velocity of 0.5 m/s. The contact temperature increased up to 165 °C. Contact pressure of 10 MPa was applied while conducting the experiments. Analysis of contact temperature during the experiment using iron-based metallic pin and disc showed that the contact temperature increased at higher sliding velocity.

K. Imado et.al, conducted experiments to study contact temperature due to frictional heating of Ultra High Molecular Weight Poly-Ethylene (UHMWPE) bearing of diameter 51 mm and thickness of 6 mm. Cylinder on flat contact (hertzian contact model) consisted of flat sapphire glass of diameter 26 mm and thickness of 3 mm in contact with the UHMWPE bearing. Different contact pressures (8.3 MPa, 10.6 MPa and 12.7 MPa) and sliding speeds (40 mm/s and 50 mm/s) were used to study contact temperature due to frictional heating (Figure 2.7). Contact temperature increased by 12 °C in 30 minutes. The experiment was conducted using two different testing methods; oscillation type and reciprocating type to measure the contact temperature. Thermocouple of 0.3 mm diameter was used to measure contact temperature by placing the thermocouple at 0.5 mm from contact interface (Figure 2.8). At 12.7 MPa contact pressure and sliding speed of 50 mm/s the contact temperature increased by 8 °C to 10 °C. At 10.6 MPa contact pressure and sliding speed of 50 mm/s the contact temperature increased by 4 °C to 6 °C. At 8.3 MPa contact pressure and sliding speed of 50 mm/s the contact temperature increased by 3 °C to 4 °C. The contact temperature showed similar trend at sliding speed of 40 mm/s.

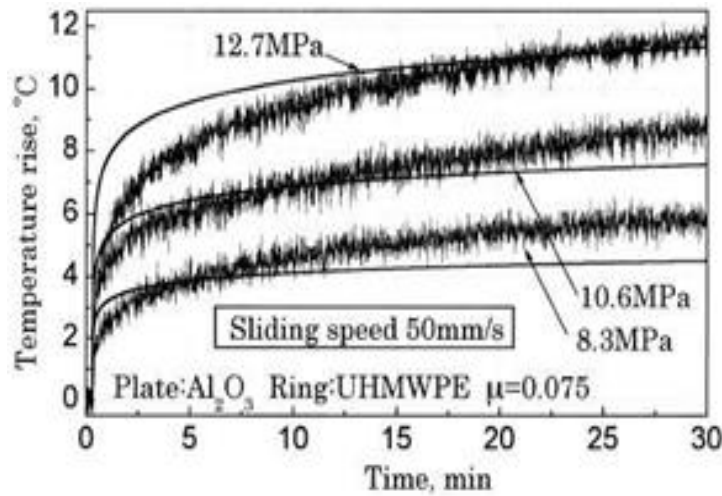


Figure 2.7: Change of contact temperature increment with time for sliding velocity 0.5 m/s

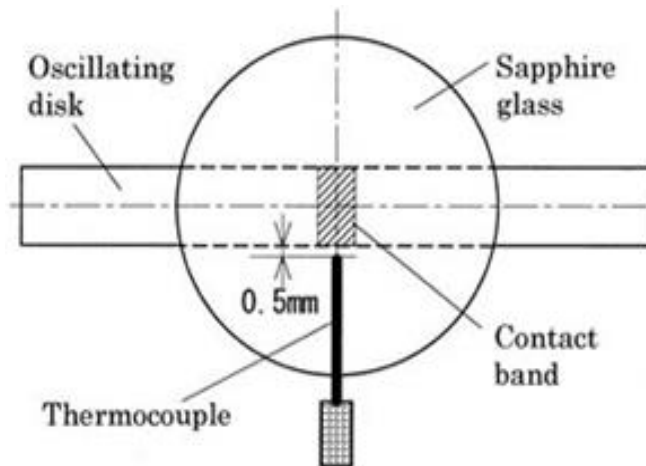


Figure 2.8: The contact temperature was measured by thermocouple

M.Uthayakumar et.al., (2012) have conducted the wear test using pin on disk tribometer. In this experiment they used aluminum cylindrical cast hybrid composite pin sliding against EN30 steel disk. They measured the rising temperature at contact surface using K-type thermocouple. Thermocouple was inserted in the pin at axial distance of 2 mm from the contact. The normal load and sliding speed were increased and the increase in pin temperature was measured.

K. Arul Raj et.al., (2018) have conducted experiment by using pin on disk tribometer to study the tribological and vibrational characteristics of AISI 316L tested at elevated temperature. The dimension of pin considered for the study was 4 mm diameter and

180 mm was diameter of disk were subjected to varying sliding velocities (0.5 m/s, 0.75 m/s and 1.5 m/s) with varying vacuum chamber temperature from 200 °C to 600 °C. The results revealed that at high temperature vibrations and speed is reduced. This can be due to reduction in stiffness of the material at varying vacuum chamber temperatures. During experiment increased vibration can lead to increase in wear rate.

2.1.3 Inverse heat transfer

Inverse heat transfer models are being used to estimate the temperature at locations where there are practical difficulties to measure temperature. Industrial processes like metal casting and welding in automobile industries and aerospace industries (Antonino Repaci, 1991) use inverse heat transfer models to estimate the source temperature. During casting of metal bodies, heat transfer coefficient between molten metal to body of metal cast is important to understand the metal solidification process, this can be estimated using inverse heat transfer methods. Friction stir welding, sliding of brake pad-disc contact of automobile produces heat at the contact interfaces. Direct measurement of contact temperatures is not feasible experimentally. Estimating these temperatures is important for engineering design of components. Beck et al., (1985) had done extensive studies on inverse heat conduction problems. They had derived different approaches to estimate the unknown heat source temperatures from the measured temperature data at selected points away from the heat source. Aweda and Adeyemi (2009) calculated heat transfer coefficients between steel mould and cast aluminium metal during squeeze casting of aluminium metal. They observed increase in heat transfer coefficient with increase in squeezing pressure and decrease in heat transfer coefficient with fall in solidification temperatures. The heat transfer coefficients were estimated using the Beck's non-linear solution as mentioned in Krishnan and Sharma (1996). Ana Paula Fernandes et al., (2015) developed analytical model, based on Green's function, to solve the inverse heat conduction problems. The model was used to estimate the interface temperature of tool-work-piece during machining process. The quality of resistance spot weld depends on dimension of nugget, which depends on the temperature at weld spot. Chunfeng Zhao et al., (2016) developed inverse heat conduction model based on

conjugate gradient method to estimate the temperatures at weld spot to estimate nugget dimension. Zhang et al., (2017) worked on estimation of interfacial heat transfer coefficient at metal-sand mould interface during low pressure casting using nonlinear inverse methods. In their investigation, they found the accuracy of results can be improved by considering temperature dependent thermo-physical properties of materials rather than considering the constant thermo-physical properties of materials. Shoubin Wang et al., (2018) solved two dimensional unsteady inverse heat conduction problem using boundary element method. The model proposed by the authors showed accurate results even though the measuring points are far away from the heat source. Raghavendra C. R. et al., (2019) worked on estimation of temperature rise due to dry sliding friction of aluminium metal against EN-32 steel. The temperatures were estimated using finite element method and validated using ANSYS simulation. Zhizhong Sun et al., (2011), Liping Chen et al., (2014) and Zhang A. et al., (2017) used finite difference method to develop inverse heat transfer algorithms. Borut Cerne et al., (2019) used semi-analytical methods to estimate flash temperatures and bulk temperatures at contact of gear teeth. Toshio Yoshimura & Kazushige Ikuta (1985); Srinivasa Raju et al., (2016); Christian Zeller et al., (2018) used Finite Element Method for transient thermal analysis. Researchers (Gupta et al., (2017); Vishweshwara et al., (2019) and Vishweshwara et al., (2020)) also used artificial intelligence to estimate heat flow in materials for inverse heat transfer problems. In the present study, efforts have been made to estimate the frictional heat at contact interface when two materials slide against each other; at such locations direct measurement of frictional heat is not practical. So, the temperature away from the contact interface due to frictional heat was measured to estimate the contact temperature. Inverse heat conduction model, using Finite Element Method and Beck's theorem, was developed and explained in this study.

Most of the researchers (Wang et al., 2010; Viktoria Westlund et al., 2018) have studied the wear and friction characteristics of aluminium alloys by considering steel material as counter face, having flat on flat contact configuration, during experiments. Few researchers (Dewan and Mohammad 2012; Shuaihang Pan et al., 2018) focused

on friction behaviour of aluminium to aluminium metal alloy during full sliding. In the present study, dry sliding experiments were conducted by considering the contact pair of aluminium to aluminium having cylinder on flat contact configuration. The influence of temperature, normal load and sliding speed on coefficient of friction was investigated by conducting experiments under full sliding condition and the results were discussed. This report is organized as follows: specimen preparation; procedure of dry sliding experiments at different temperatures; estimation of frictional heat at different loading conditions; observation of coefficient of friction at different stages such as initial, stabilized, steady state and unsteady state from friction evolution curves; observation of wear mechanisms at different loading conditions and conclusions drawn from outcomes of the experiments.

2.1.4 Finite Element Method (FEM) models

Modeling contact problems in finite element method is a tedious process due to high stress gradients at contact area which increases the number of elements and computational time. Researchers (R. Rajasekaran, D. Nowell, 2006; A. Cruzado et al., 2013; C. Gandiolle and S. Fouvry, 2015; M. Luke et al., 2016) modelled the contact configuration during fretting process using finite element method packages like ANSYS and ABAQUS. A. Cruzado et al. (2013) worked on finite element simulation of wear and fatigue life of thin steel wires. Square shape eight node linear brick elements (Figure 2.9) were used for meshing and more fine elements were used at contact of two wires. C. Gandiolle and S. Fouvry (2015) modeled the crack nucleation and propagation during fretting with plasticity effect using ABAQUS 6.1 software. A 2D fretting fatigue test was modelled with linear triangular type element CPE3, except at contact area where linear quadrilateral elements type CPE4R was used (Figure 2.10).

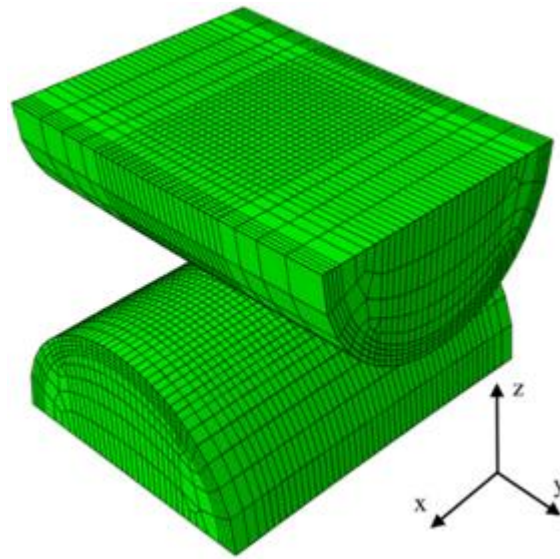


Figure 2.9: Finite element mesh details of fretting wear test (Cruzado *et al.*, 2013)

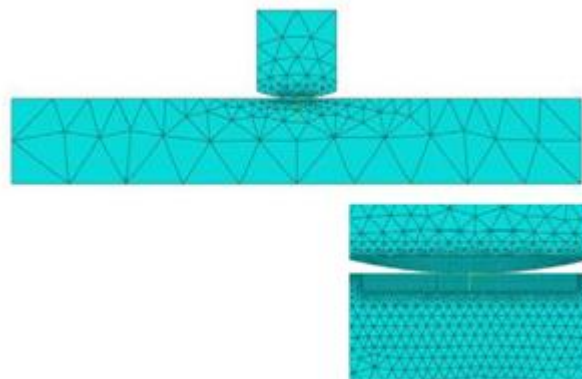


Figure 2.10: Abaqus model of the fretting test (C. Gandiolle and S. Fouvry, 2015)

Giovanni Strafellini *et al.*, conducted experiments and finite element analysis (ANSYS software) to study temperature evolution in Pin-on-Disc Tribotesting using pin made of low metallic friction material sliding against disk made of Pearlitic Cast Iron. The experiments were conducted at room temperature (12 °C). Cylindrical pins of diameter 18 mm and 23 mm were used for the experiments. Both the pins were of 10mm length. Two Chrome – Alumina type Thermo-couples were inserted in the pin at two different locations at 4 mm and 6 mm from the contact interface. Temperature profile was observed for different sliding distances of 377 m, 565 m, 754 m and 1884 m. The temperature data showed steep rise when the sliding distance increased to 1884 m. The temperature data computed using ANSYS showed comparatively higher

values (Figure 2.11). This higher temperature data is attributed to insulated pin and disc boundaries.

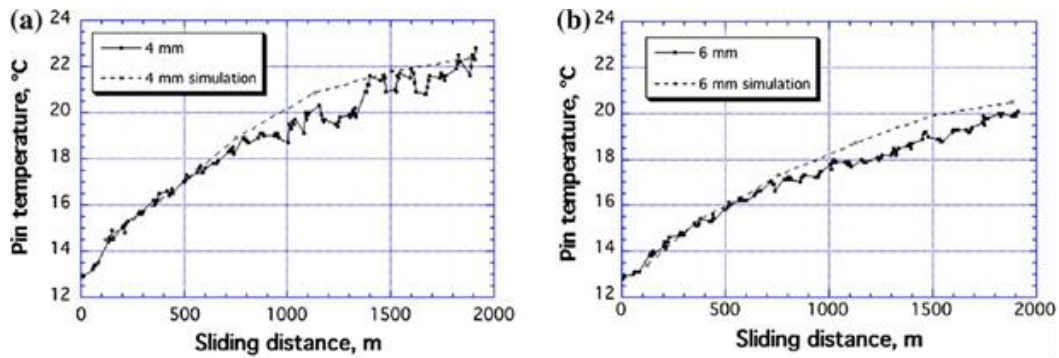


Figure 2.11: Comparison of experimental Observation and FEA- computed temperatures of Pin at (a) 4 mm and (b) 6 mm distance from the sliding surface

Kennedy et.al, conducted experiments to study effect of contact temperature on wear during pin on disk tribotesting. They used 2 cm long pin of diameter 1 cm disk of diameter 10 cm and 1.5 cm thickness for Finite Element Analysis (FEA). The pin was considered to be made of 4340 grade alloy steel. The disk was considered to be made of zirconia. The heat flux of pin and disk is 25104 w/m^2 . Convection coefficient of the disk $14.23 \text{ w/m}^2 \text{ K}$. From Finite Element Analysis maximum contact pin bottom surface temperature was obtained as $59.987 \text{ }^\circ\text{C}$. The pin top surface temperature was $0 \text{ }^\circ\text{C}$. The maximum temperature at the disk contact surface is $37.606 \text{ }^\circ\text{C}$. All other surfaces of pin and disk were insulated. They conducted experiments on pin-on- disk apparatus for verification of FEA data.

Giovanni Straffelini and Alberto Molinari (2010) conduct experiments in dry sliding condition by using pin on disk equipment to understand the tribological characteristics of three different materials (Fe-0.2%C, Ti-6%Al-4%V and Al-7072). They compared practical temperature changes and theoretical steady and unsteady state temperature changes with calculated transition variation of these three materials. They identified theoretical variation of contact surface flash temperature with varying the

sliding speed (0.2 m/s to 1 m/s). The experiment was conducted at room temperature at 1 MPa contact pressure test was conducted for maximum 6000 seconds. In this test they used 6 mm diameter pin and height of the pin is 26 mm and the disk was made of SAE 52100 steel with a hardness of 66 HRc. The low sliding speed (0.2 m/s to 0.6 m/s) the surface contact temperature was low (100 °C). They increased the sliding velocity (0.8 m/s to 1 m/s) and surface temperature increased (130 °C - 151 °C). Due to increase the sliding velocity (0.6 m/s to 1 m/s) surface oxidation is more. The wear rate and coefficient of friction decreased in case of iron oxide for Fe- material. In case of Al and Ti material wear rate and coefficient of friction decreased.

Matteo Federici et.al. (2017) they conducted the experiment by using pin on disk machine to understand the tribological behavior of gray cast iron material pin coated with ceramic and that of uncoated pin and disk in dry sliding condition. The experiments were conducted at room temperature diameter of pin and length of pin are 6 mm and 10 mm respectively. The diameter of disk is 140 mm thickness of disk is 15 mm applied normal load is 1 N/mm² and sliding velocity is 1.57 m/s. They conducted the experiment for maximum duration of 10 minutes. They used High Velocity Oxygen Fuel (HVOF) coating method. The sliding pin and disk transition temperatures are calculated and they measured the surface temperature of pin and disk by using K-type thermocouple. Thermocouple is pasted at two location above the disk at 6.5 mm and 9 mm along longitudinal axis of the pin. The observed data is verified with the contact temperature value obtained through Finite element analysis in steady state condition with different theoretical approaches. Finally, this research work measures the rising contact temperature at contact interface by using Kennedy approach theoretically with different contact condition.

L.Wang et.al. (2010) conducted tribological experiment by using ball on disk equipment; they studied effect of varying temperature (25 °C to 450 °C) on Al 7475 Alloy disk whose diameter is 45 mm and thickness is 5 mm. Hot work steel ball of 6mm diameter sliding against the disk at applied load of 2 N. They performed the Finite element simulation by using DEFORM 3D software. The Finite element simulation applied adiabatic boundary condition during the extrusion process of Al

7475 material during the simulation. Increase in plastic deformation was observed. Ball on disk contact interface friction increased resulting in increase of contact temperature. From Finite element simulation they calculated coefficient of friction value with varying sliding distance. It shows material deformation increases with increasing contact temperature, stress and strain change at the contact point. The friction coefficient oscillates and increases. From the experiment the observed the friction coefficient increases with increase in the contact temperature.

C.R. Raghavendra et.al. (2018) conducted the pin on disk experiment to measure the contact surface temperature they are used thermocouple to accrued the temperature value those values are compare with finite elemental module by using the develop the pin-on-disk model to Analysis of temperature field in dry sliding wear test by using ANSYS software (Figure 2.12). For this analysis there consider hollow pin at the contact surface material made of Al6061 aluminum hollow and disk made of harden steel the simulated the model there identified the heat flux generated due to friction and convective heat transfer coefficient are calculated Later the temperature distribution in pin and disk material are analyzed.

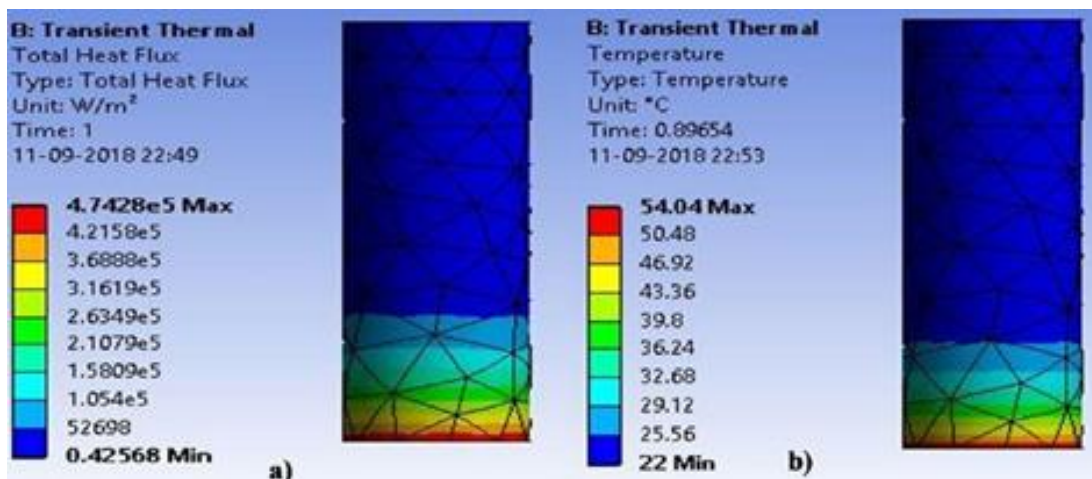


Figure 2.12 (a) total heat flux and (b) temperature variation due to friction shows the FEM analysis of pin model (C.R. Raghavendra et.al. (2018))

2.2 Problem Formulation

In spite of many theoretical, analytical and experimental studies carried out on the tribological and frictional behavior of different materials (steel, aluminum and composite materials), the study of literature showed that no experimental study was conducted on similar or like materials such as steel alloy on steel alloy, aluminum alloy on aluminum alloy as pin and disc to study the tribological characteristics and frictional behavior.

In this present study, the influence of sliding speeds and normal loads on the evolution of Pin temperature at the contact interface of fully sliding components has been studied. Experiments have been conducted at three different sliding speeds and normal loads. Pin and Disk were fabricated from the same material, SS304 alloy, and were used to carry out pin on disk rotary type fully sliding experiments to acquire temperature at two different locations. During Pin-on-disk experiments, the distribution of temperature along the length of the cylindrical pin was measured using two K-type thermocouples fixed along the longitudinal direction of the cylindrical pin at two different locations from the contact surface. One dimensional inverse heat transfer model was developed using Finite Difference Method and Beck's algorithm. Finite Element Analysis has been carried out to evaluate the pin temperature at the contact interface, which is compared with the experimental results, obtained from pin-on-disk experiments for SS304 alloy.

Cylindrical pins with radius 3mm, height 30 mm, thickness 6 mm and circular disk with thickness 8 mm and diameter 165 mm were fabricated to conduct full sliding experiments. Experiments were conducted at three different sliding speeds of 1 m/s, 2 m/s, and 3 m/s under normal load of 1 kg, 1.5 kg and 2 kg and two different wear tracks of diameter (60 mm and 120 mm) respectively. Experiments were conducted at 29 °C - 32 °C ambient temperature and 80 % - 86 % relative humidity.

2.3 Aim and objectives

The current research work focuses on the effect of sliding speeds, normal loads, and temperature rise at the contact interface of SS304 alloys subjected to full sliding experiments. Dry sliding experiments were conducted on Rotary Type Pin-on-Disk Tribometer and Finite Element Modelling was carried out using ANSYS Software. Cylindrical pins of radius 3 mm, height 30 mm, and circular disk of diameter 165 mm having flat surface were fabricated to simulate Hertzian contact configuration. Experiments were conducted at three different sliding speeds of 1 m/s, 2 m/s, and 3 m/s under normal load of 1 kg, 1.5 kg and 2 kg and two different wear tracks of diameter (60 mm and 120 mm) respectively. The following objectives have to be full filled as part of the proposed study:

The main objectives of this thesis are:

- To study the influence of normal load and sliding speeds on coefficient of friction in SS304 alloys during rotary type dry sliding experiments.
- To study the influence of rise in Contact Temperature on Coefficient of Friction from the contact interface.
- Finite element modelling (FEM) for estimation of temperature at contact interface in SS304 alloy during pin-on-disk rotary type sliding motion.

CHAPTER 3

DETAILS OF ROTARY-TYPE DRY SLIDING EXPERIMENTS

This chapter gives detail procedure of material selection, fabrication of cylindrical pin and circular disc specimens, measuring surface roughness and experimental setup. The methodology adopted for the present research work, which involves fabrication of specimens, conducting rotary-type dry sliding experiments, one dimensional inverse heat transfer model, finite element modeling, analysis of results and validation of experiment results.

3.1 Material

Stainless steels represent quite an interesting material family, both from a scientific and commercial point of view, owing to their excellent qualities in terms of strength and ductility, combined with corrosion resistance. The austenitic structure provides stainless steels (SS304) with good ductility and formability. Experiments were conducted with SS304 Alloy for studying friction properties at the contact interface. Table 3.1 shows the chemical composition of the SS304 Grade material while the physical and mechanical properties are listed in Table 3.2 (Caydas et al., 2012).

Table 3.1: Chemical Composition of Stainless Steel (SS304 grade)

Chemical Element	SS304 alloy
	Max (% mass)
Carbon	0.08
Manganese	2.00
Phosphorous	0.045
Sulphur	0.030
Silicon	0.75
Molybdenum	0.50
Copper	0.768

Chromium	18.00 - 20.00
Nickel	8.00 - 12.00
Nitrogen	0.10
Iron	67-71

Table 3.2: Properties of Stainless Steel (SS304 grade)

Mechanical properties	SS304 alloy
Tensile Strength (MPa)	515
Yield Strength (MPa)	206
Poisson's ratio	0.28
Young's Modulus (GPa)	210
Brinell Hardness (HRB)	87
Elongation (%)	41

Cylindrical pins and circular disks were fabricated from industrially produced Stainless Steel rods having a diameter of 170 mm and length of 150 mm. From the Stainless-Steel rods, 12 mm thick disks were cut along the length using a semi-automatic hack saw cutting machine with a depth of cutting at a rate of 2 mm/minute. After cutting 12 mm thick disks, Computer Numerical Controlled (CNC) lathe machine was used to reduce the thickness of the disks and obtain disks of thickness 8 mm and diameter 165 mm (Figure 3.1(a)). One disk was used for the fabrication of pins of cross-sectional area (6 mm × 6 mm) and length 30 mm (Figure 3.1 (b)). The contact end of the pin is milled into a semi-circular shape with of radius 3 mm. Before conducting the friction tests, Silicon Carbide emery paper was used to remove excess material from the surface of samples, then the pin and disk surfaces were cleaned by using (CH₃)₂CO solution to remove undesirable substances and degreasing. Soft lightweight cotton fabric was used to clean surfaces. Samples were then polished with Silicon Carbide emery paper (1000 grit) to ensure smoothness.

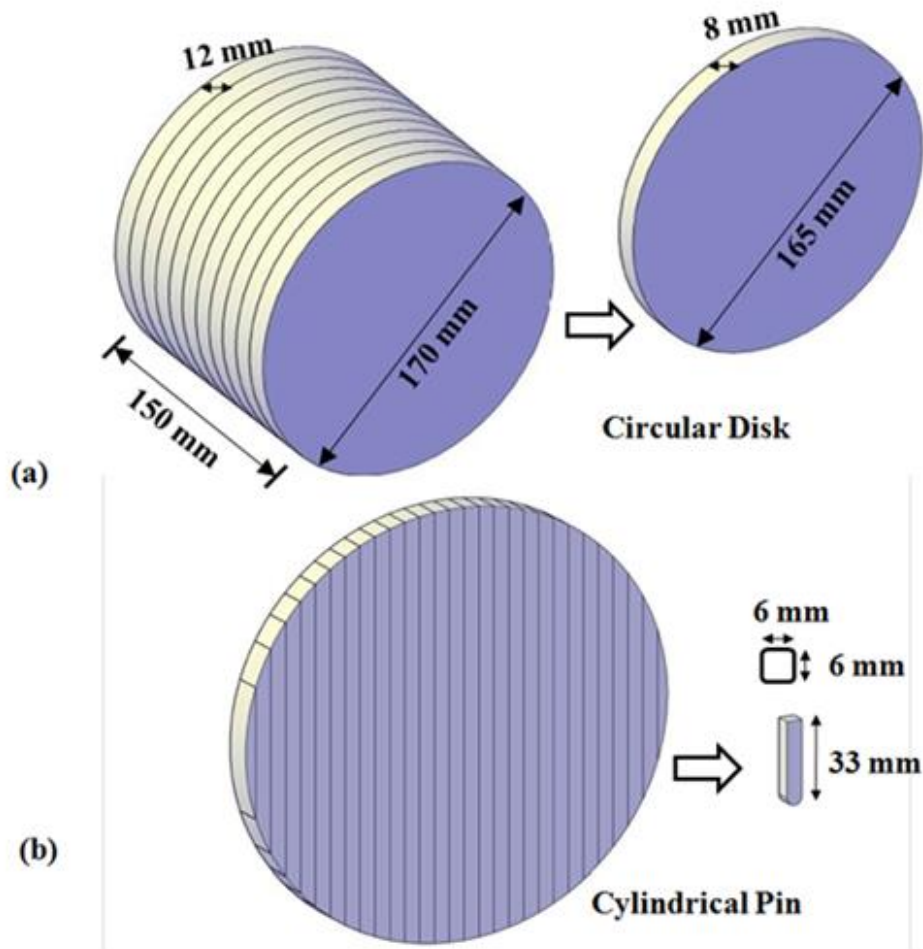


Figure 3.1: Schematic diagram of Stainless-Steel rod used for (a) Circular Disk and (b) Cylindrical Pin preparation

3.1.1 Measuring Surface Roughness (R_a)

A Roughness tester was used to determine surface texture or average surface roughness (R_a) values of the disk. Surface roughness is measured as the average deviation from the normal surface. The surface is rough if these deviations are substantial, and smooth if they are modest. Surface roughness of Stainless-steel pin and disk was measured at ten different points located uniformly along the diameter of the planned wear track at an angle of 36° as shown in the Figure 3.2 and their values are given in Table 3.3. The range of surface roughness (R_a) values of disk specimens was $0.10 \mu\text{m} - 0.18 \mu\text{m}$ for Stainless steel (SS304 grade)

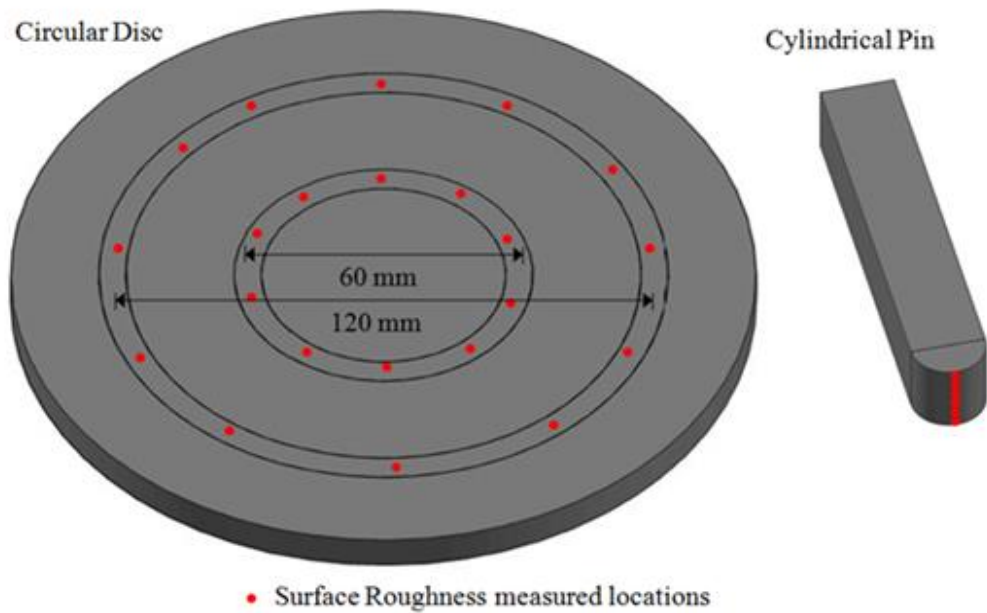


Figure 3.2: Schematic representation of surface roughness (Ra) measured at different location on pin and disk specimens

Table 3.3: Surface Roughness values of Stainless Steel (SS304 grade)

Sl.No	Surface Roughness (μm)
	SS304 alloy
1	0.10
2	0.18
3	0.14
4	0.12
5	0.11
6	0.13
7	0.15
8	0.16
9	0.11
10	0.12

3.2 Experimental Setup

Stainless steel alloy (SS304 grade) was used as cylindrical pins and the circular disks specimens to conduct experiments. Pin-on-disk tribometer was used for conducting full sliding experiments with cylinder on flat contact configuration under dry sliding conditions (Figure.3.3 and Figure.3.4). The stationary cylindrical pin is pressed against rotating disk under normal load using stationary held pin holder arrangement.

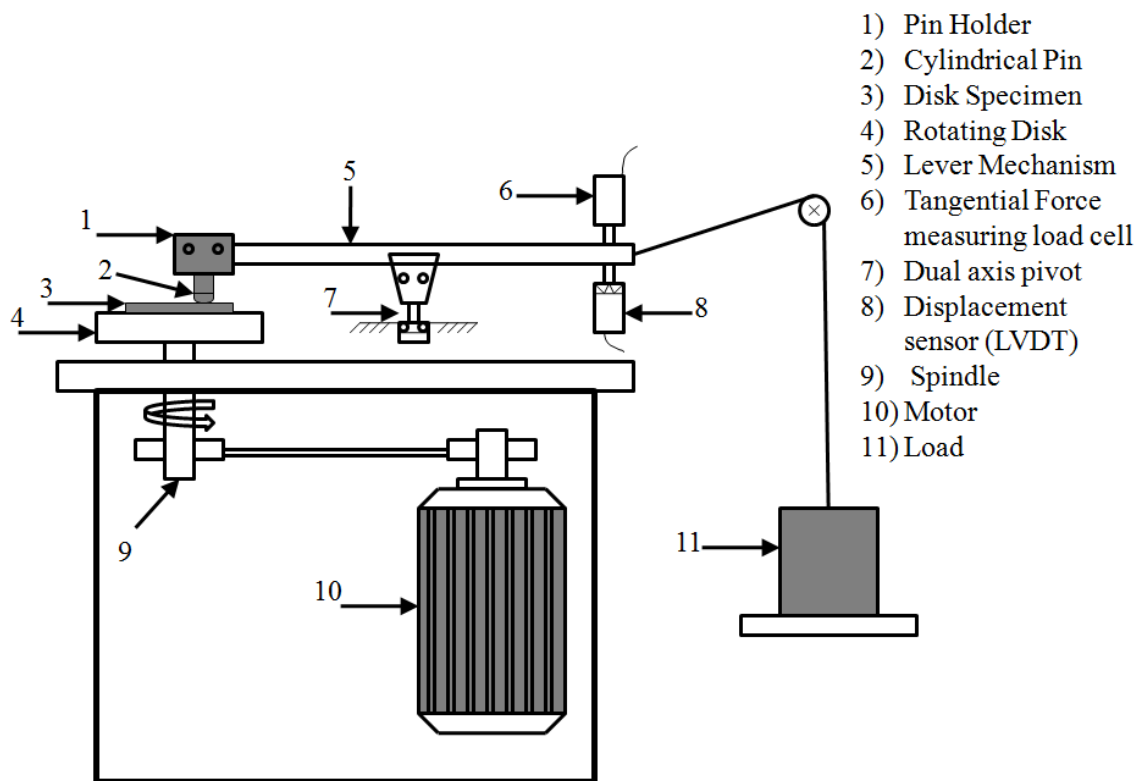


Figure 3.3: Schematic representation of pin-on-disk tribometer equipment.

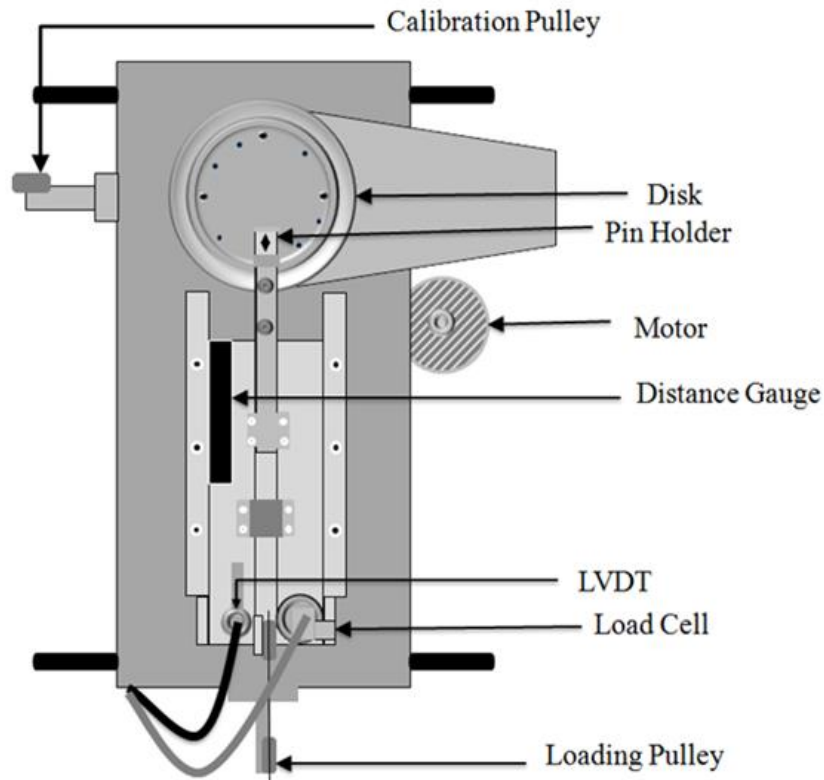


Figure 3.4: Top view of pin-on-disk tribometer equipment

Cylindrical pins with radius 3 mm, height 30 mm, thickness 6 mm and circular disk with thickness 8 mm and diameter 165 mm were fabricated to conduct full sliding experiments. The experimental parameters normal load [38] and sliding speed used for SS304 alloys are given in Table 3.4. Two wear tracks of diameter 60 mm and 120 mm was used for three different sliding speeds under three different normal loads. Experiments were conducted at 29 °C - 31 °C ambient temperature and 80 % - 86 % relative humidity. Schematic representation of pin specimen dimensions and disk specimen dimensions are shown in Figure. 3.5.

Table3.4: Experimental parameters used for dry sliding pin on disk experiments

Material	Normal load (kg)	Sliding speed (m/s)
SS304	1	1
	1.5	2
	2	3

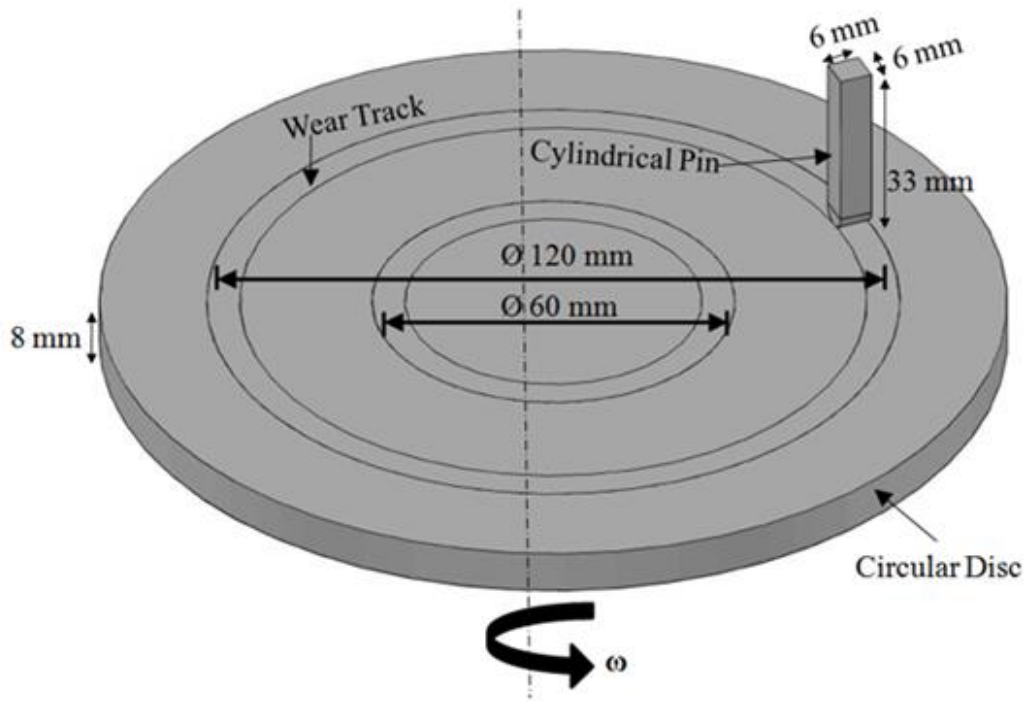


Figure 3.5: Schematic representation of Pin and disk specimen dimensions

The measurement of frictional force data is obtained by conducting the experiments. Pin-on-disk apparatus (Figure 3.6) was used to perform full sliding experiments. To and fro movement of the cylindrical pin can be avoided by fixing the pin properly on the pin holder arm. All the data measuring sensors (shear traction) are synchronized at the beginning of the experiments, and data is collected at a sampling rate of 300 samples per minute. The tangential load is measured by using a horizontal load cell. The acquired tangential load (Q) data is used to compute the coefficient of friction for a specific time.

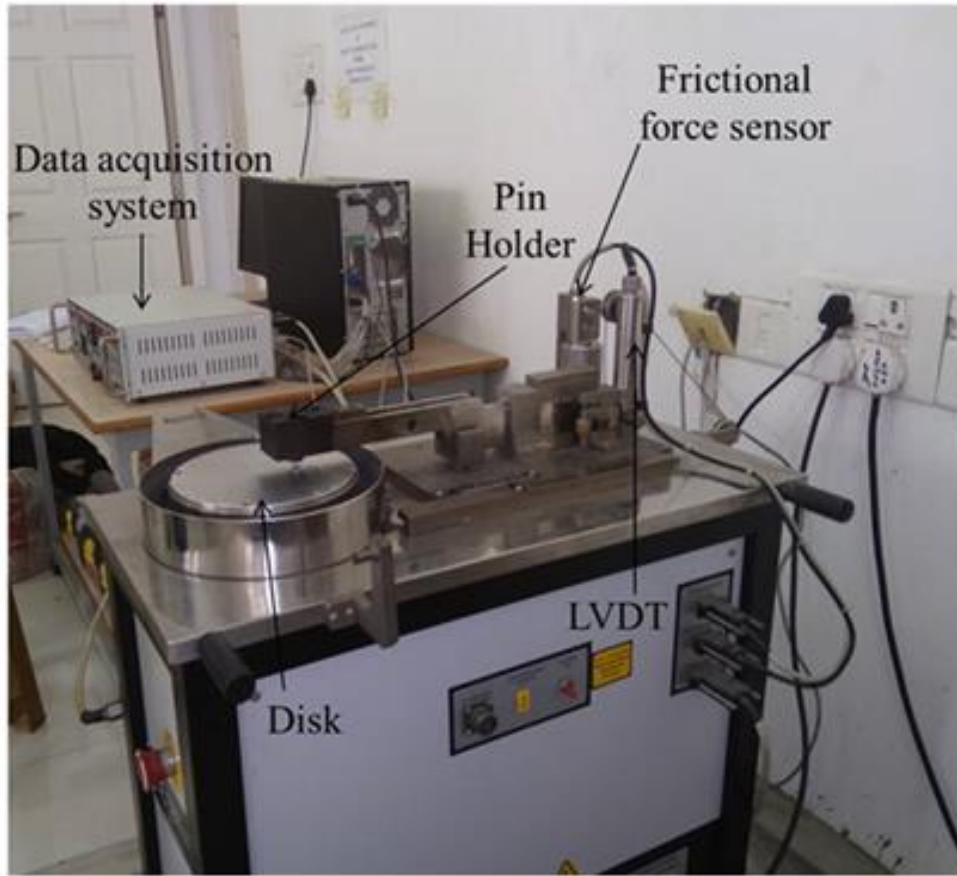


Figure 3.6: Pin-on-disk tribometer used for friction test

Total wear depth (H) is obtained from Pin-on-disk tribometer. The wear volume was determined by multiplying the total wear depth (H) by the region of contact. A wear volume is calculated based on equation (3.1) by deriving the contact volume as a function of time. Equation (3.1) was derived based on few assumptions: (i) the wear rate of pin and disk are the same, (ii) the wear is uniform along the length of the pin (Figure 3.7). Here, R = radius of cylindrical pin, L = width of pin and d = wear track diameter [Straffelini, G et.al,(2016)].

$$\text{Total wear volume (H)} = (Bh\pi d) + \left(\left[\frac{\pi R^2}{2} - R^2 \left(\theta + \frac{\sin(2\theta)}{2} \right) \right] L \right) \quad (3.1)$$

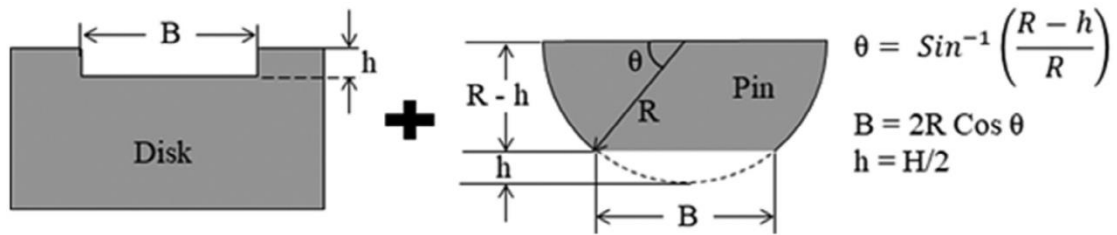


Figure 3.7: Schematic representation of a weary disk and pin used to measure total wear volume

3.3 Identification of Optimum location for pasting thermocouples through Finite Element Analysis

3.3.1 Finite element model

Finite Element Analysis was performed to observe the stress variation at 9 different locations along the longitudinal axis of the pin with and without hole from the contact interface for normal load of 10 N. The three-dimensional finite element analysis was performed using ANSYS software. Solid 226 element was used for all the configurations of the cylindrical pin. Solid 226 element has twenty nodes; it was used to simulate plane element with five degrees of freedom at each node. Solid 226 element is suitable for conduction studies and convection studies of three-dimensional transient heat transfer problems. After meshing, the model consists of 604352 nodes and 596752 elements that is adequate for the present system. Element size for cylindrical pin is 0.25 mm

3.3.2 Boundary condition and application of pressure

For the nodes on the bottom surface of the flat plate, all degrees of freedom is restricted and rigidly constrained from translating in the x, y and z directions. For the nodes on the top surface of cylindrical pin uniform pressure of 0.28 N/mm² is applied. Figure 3.8 and Figure 3.9 show the contour plot of von Mises stress for the applied normal load of 10 N. As it is clear from the figures 3.8 and 3.9 that induced stress is higher at contact zone which is marked by red color. From the contour plot of von Mises stress it was observed that the pin with hole of 1.5 mm diameter and 3 mm depth at 2 mm, 3 mm location showed uneven distribution of stresses from the contact interface but at 4 mm, 5 mm, 6 mm, 7 mm, 8 mm, 9 mm and 10 mm showed even distribution of stresses from the contact interface. It is very clear from the results that

4 mm and 7 mm locations are best suited for pasting thermocouples. Finite Element Analysis gives the best solution to find the optimum location for pasting thermocouples.

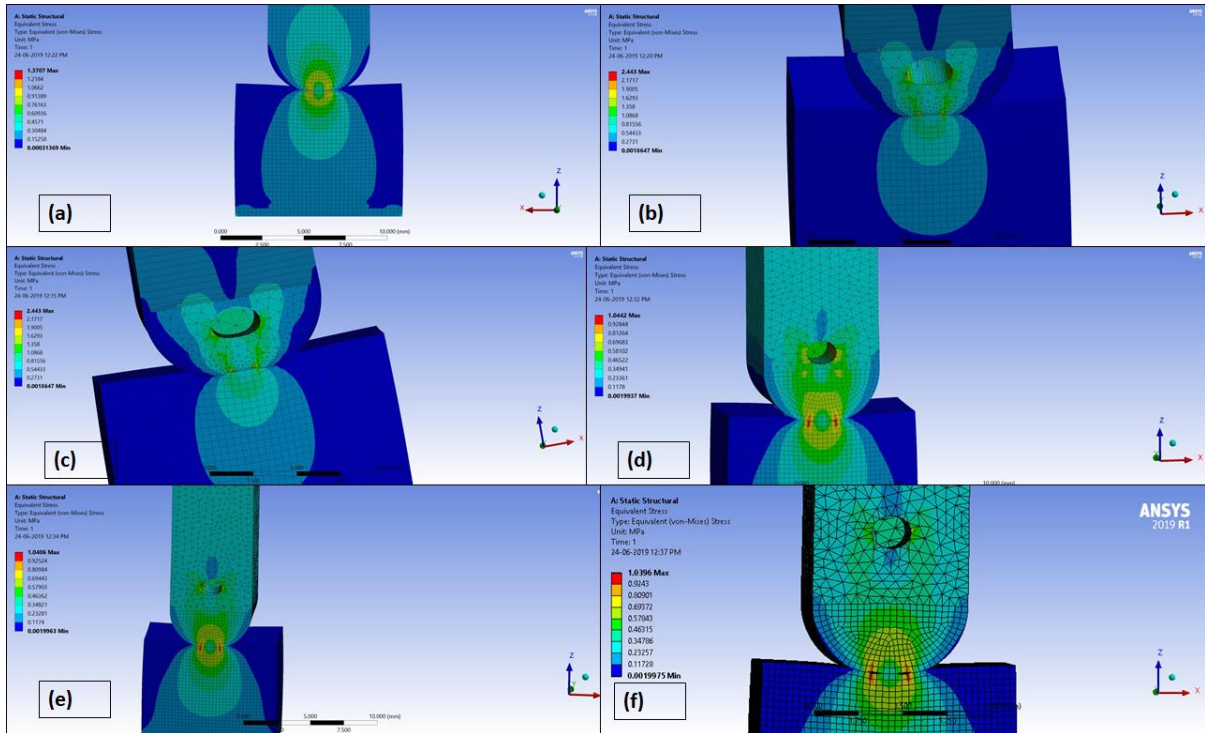


Figure 3.8: von Mises stress distribution over solid cylinder-flat for the pin with hole (2 mm, 3 mm, 4 mm, 5 mm and 6 mm) and with-out hole

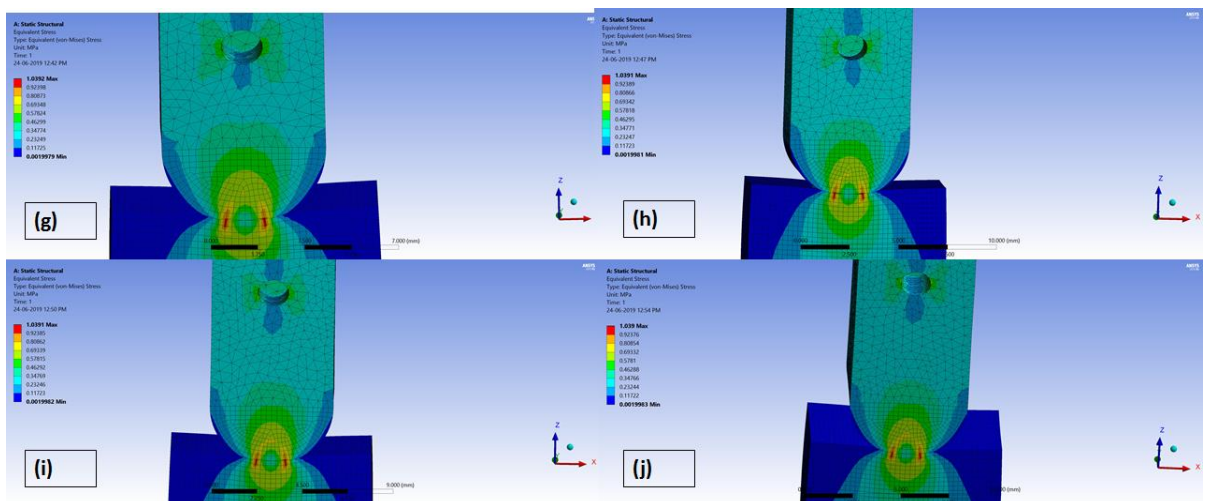


Figure 3.9: von Mises stress distribution over solid cylinder-flat for the pin with hole (7 mm, 8 mm, 9 mm, and 10 mm)

From the finite element analysis results, it was very clear that 4 mm and 7 mm locations are best suited for pasting thermocouples. Two perpendicular faces of the cylindrical pin specimen were drilled to a depth of 3 mm with 2.0 mm diameter drill bit. The drill locations are 4 mm (point 'a' in Figure 3.10) and 7 mm (point 'b' in Figure 3.10) from the cylindrical contact interface.

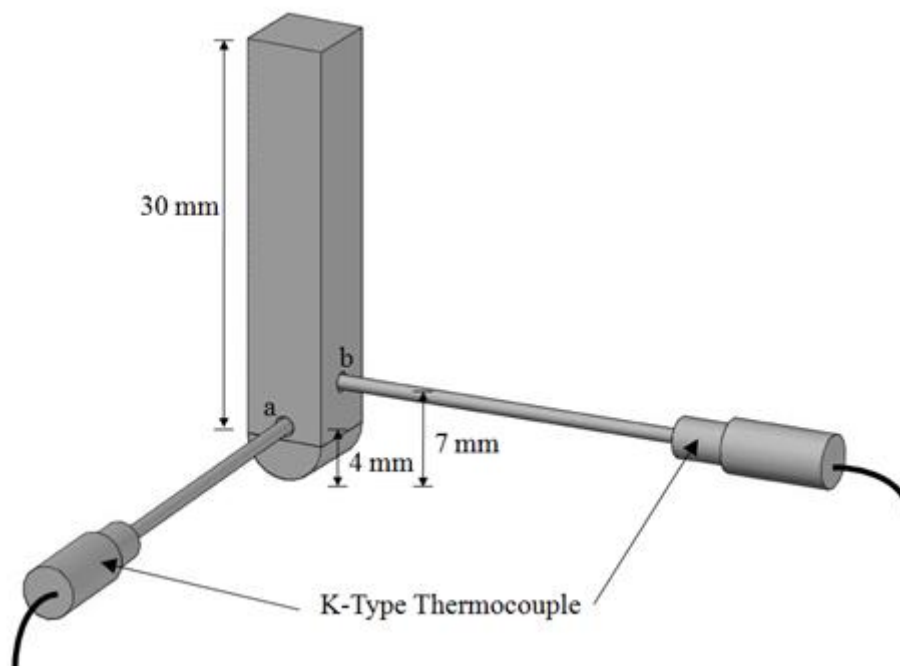


Figure 3.10: Schematic representation of temperature measurement points with K- Type thermocouples in pin specimen

The thermocouples were inserted in the drilled holes to measure temperature at mid-section of the pin. The temperature data was measured at 5 data samples per second with accuracy of 0.0001 °C. The measured temperatures at 4 mm location and 7 mm location are given in Figure 3.11.

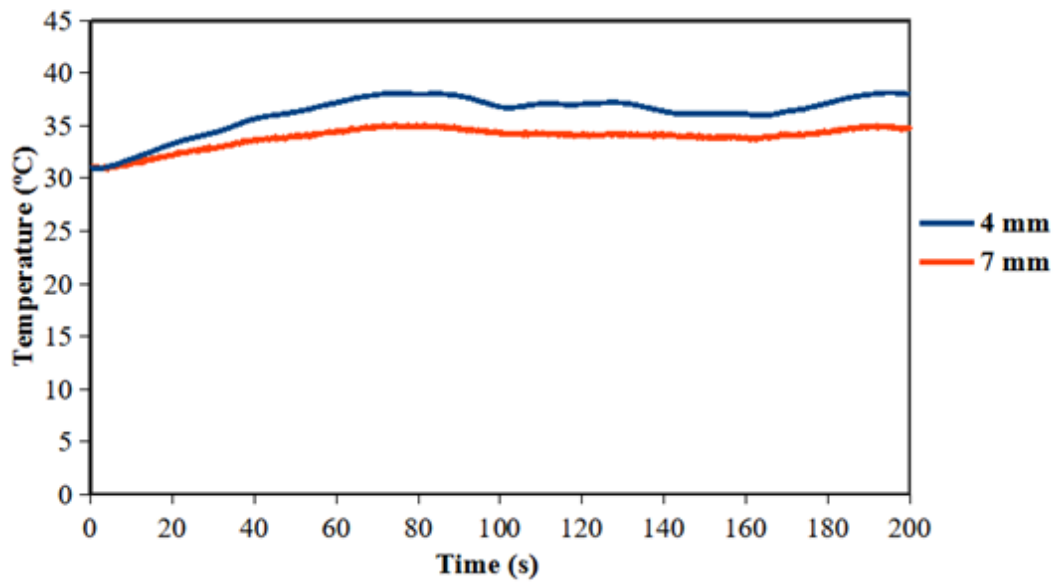


Figure 3.11: Temperatures measured at 4 mm and 7 mm locations using thermocouples from contact interface during dry sliding experiments on SS304 alloy

CHAPTER 4

ONE DIMENSIONAL INVERSE HEAT TRANSFER MODEL AND FINITE ELEMENT MODELING

This chapter focuses on one dimensional inverse heat transfer model and finite element modeling performed on cylindrical pin and circular disc specimens made of stainless steel of SS304 grade.

4.1 Mathematical modelling to estimate surface temperature

For the pin on Disk tests, a one-dimensional transient heat conduction equation is solved to determine the interfacial heat flux as well as the pin surface temperature. Eq.(4.1) shows the governing equation,

$$\frac{\partial^2 T}{\partial x^2} = \frac{1}{\alpha} \frac{\partial T}{\partial t} \quad (4.1)$$

Subjected to boundary condition,

$$\text{At } x = 0 \text{ (at the pin and Disk contact), } q = -k \frac{\partial T}{\partial x} \quad (4.2)$$

$$\text{At } x = L, T = T_{meas} \text{ (at 7 mm from interface),} \quad (4.3)$$

$$\text{At } t = 0, T = T_i \quad (4.4)$$

where q is the surface interfacial heat flux between the pin and Disk (W/m^2), k is the thermal conductivity of the pin (W/mK), T_{meas} is the measured temperatures from the experiments, T_i is the initial condition of the pin. The initial temperature T_i is considered as 30°C . Two K-type thermocouples are inserted at 4 mm and 7 mm location from the pin-Disk interface to measure the experimental temperatures. The thermocouple location at 7 mm from the pin-Disk interface is considered as $x = L$ boundary condition.

The governing equation along the boundary conditions, eqns. [4.1 - 4.4], are solved using Implicit finite difference method. To estimate the heat flux, 'q', and surface

temperature at the pin and Disk interface, a popularly known Beck's non-linear estimation inverse method (Beck, 1970) is used. For the estimation of unknown parameter 'q', a suitable initial value of 'q' is assumed that is kept constant for a definite number of subsequent time steps 'u' and 'j<u' is introduced which is integer subsequent future time steps (Chen et al., 2014). By solving the eqns. [4.1-4.3], temperature distribution is calculated for the initially assumed value of 'q'. The sensitivity coefficient at each step is calculated according to eqn.[4.5] where the assumed value of 'q' is changed by a small value 'εq', where 'ε' value is 1e-5 and a new temperature distribution is calculated using 'q+εq'. With the available information of sensitivity coefficient X_i^{p+j-1} , the Δq^p value is calculated to correct the initially assumed value of heat flux 'q'. The estimation process is continued till the convergence criteria in eqn.(4.8) is satisfied.

$$X_i^{p+j-1} = \frac{\partial T}{\partial q} = \frac{T_{est,i}^{p+j-1}(q^p + \varepsilon q^p) - T_{est,i}^{p+j-1}(q^p)}{\varepsilon q^p} \quad (4.5)$$

$$\Delta q^p = \frac{\sum_{j=1}^u \sum_i^m (T_{meas,i}^{p+j-1} - T_{est,i}^{p+j-1}) X_i^{p+j-1}}{\sum_{j=1}^u \sum_i^m (X_i^{p+j-1})^2} \quad (4.6)$$

$$q_{corr}^p = q^p + \Delta q^p \quad (4.7)$$

$$\frac{\Delta q^p}{q^p} \leq 10^{-5} \quad (4.8)$$

Where i is the location of sensor, m is the number of sensor position, p is the iteration number, u is the future time steps (u =20). The flowchart of the estimation process is represented as shown in the Figure 4.1.

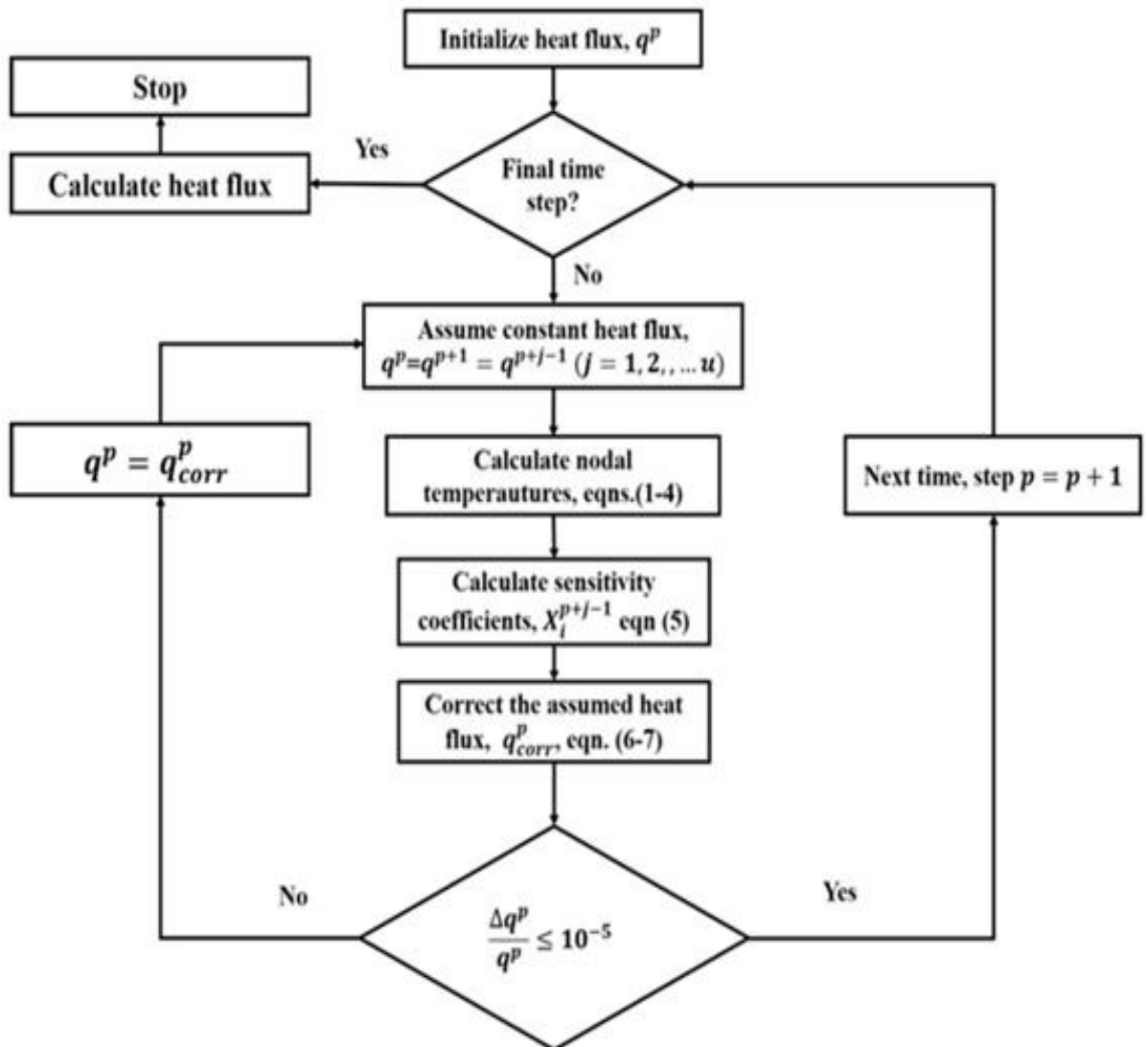


Figure 4.1: Flowchart of the heat flux estimation process (Chen, et al 2014, Sun Z et al 2011)

4.2 Finite Element Modeling

4.2.1 Pin and Disk Geometric Parameters and Material Properties

The material considered for finite element analysis is SS304 alloy is illustrated in figure 4.2 and figure 4.3. Table 4.1 gives the geometric parameters and material properties. The manufacturer has given the material properties shown below. The commercial package AutoCAD is used to model the geometries of cylindrical pin and circular disk.

Table 4.1: Geometric parameters and engineering properties of cylindrical pin and Circular disk.

Description		Value
Cylindrical Pin	Radius	3 mm
	Width	6 mm
	Height	30 mm
Circular disk	Diameter	165 mm
	Thickness	8 mm
Wear Track	Track 1	Ø 60 mm
	Track 2	Ø 120 mm
Thermal conductivity ($\text{W m}^{-1} \text{ } ^\circ\text{C}^{-1}$)		22
Specific heat ($\text{J kg}^{-1} \text{ } ^\circ\text{C}^{-1}$)		700
Density (kg/m^3)		7200

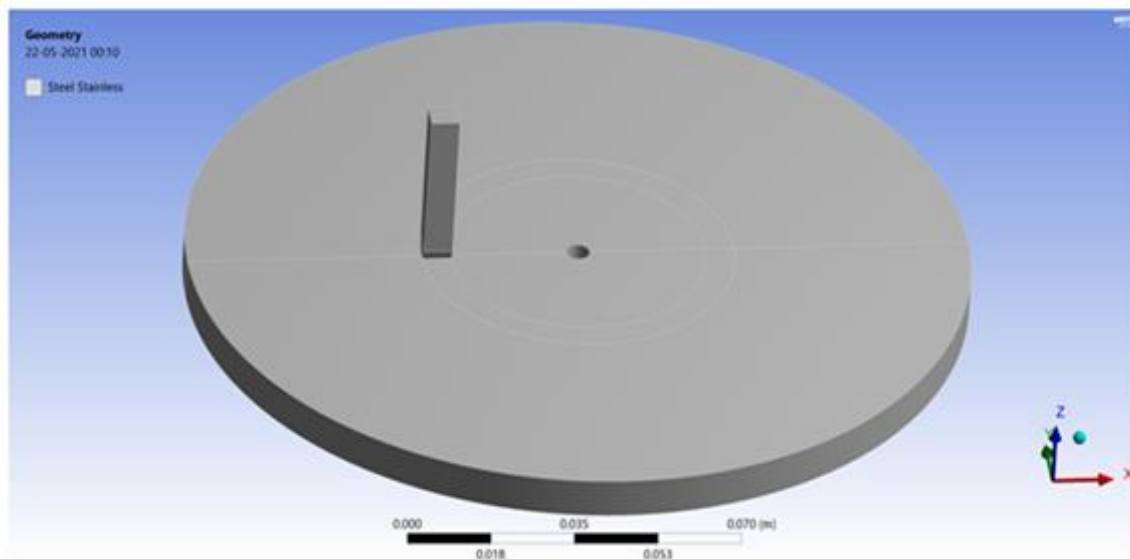


Figure 4.2: Geometry of pin-on-disk finite element model (60 mm Track)

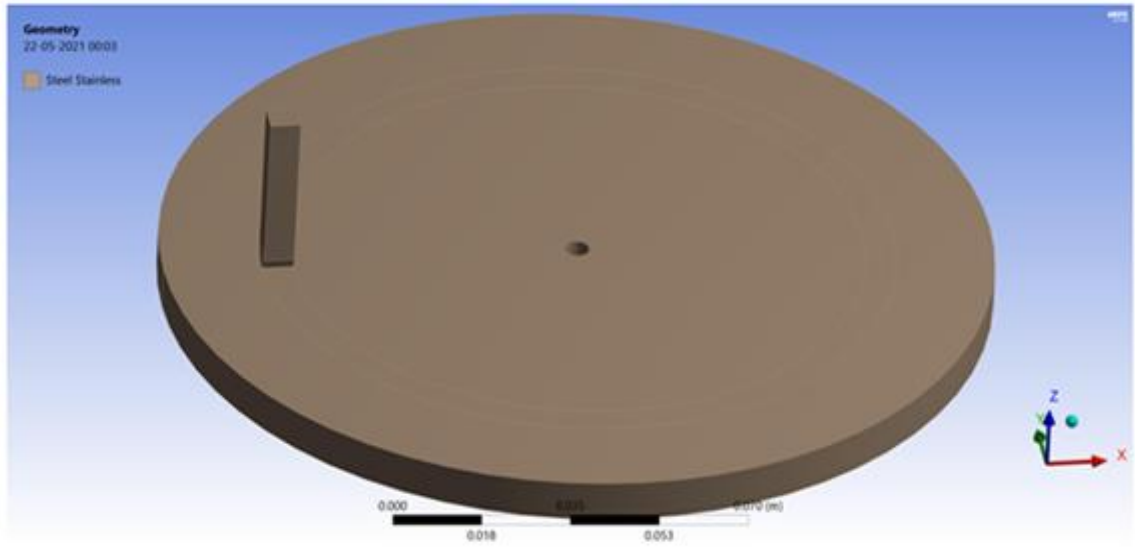


Figure 4.3: Geometry of pin-on-disk finite element model (120 mm Track)

4.2.2 Meshing Parameter, Boundary Conditions, and Loading

Pin on disk models were analyzed by employing Transient Thermal analysis and finite element models were developed in ANSYS 2020 R2 Workbench. For modeling and meshing pin on disk models, SOLID90 elements were considered for solid models and surface elements TARGE174 and CONTA170 were considered to study temperature. SOLID90 element consists of 8 nodes along model's outer surface, 8 nodes along the model's inner surface, and 4 nodes at model's mid-thickness (Figure 4.4). MultiZone method was to perform meshing. The smoothing parameter and the Span angle center were both set to medium. The element size of 1.0 mm was considered at cylindrical pin and circular disk contact interface. The simulation was carried out for a duration of 200 s. Mesh quality was determined using Fourier number (F_0) (Straffelini, et al. (2016), Day (2014)).

$$F_0 = \frac{\alpha \Delta T}{\Delta x^2} \quad (4.9)$$

where α is the thermal diffusivity of the material considered, Δt is the time increment of the FE simulation and Δx is the element size along the direction of the heat flux.

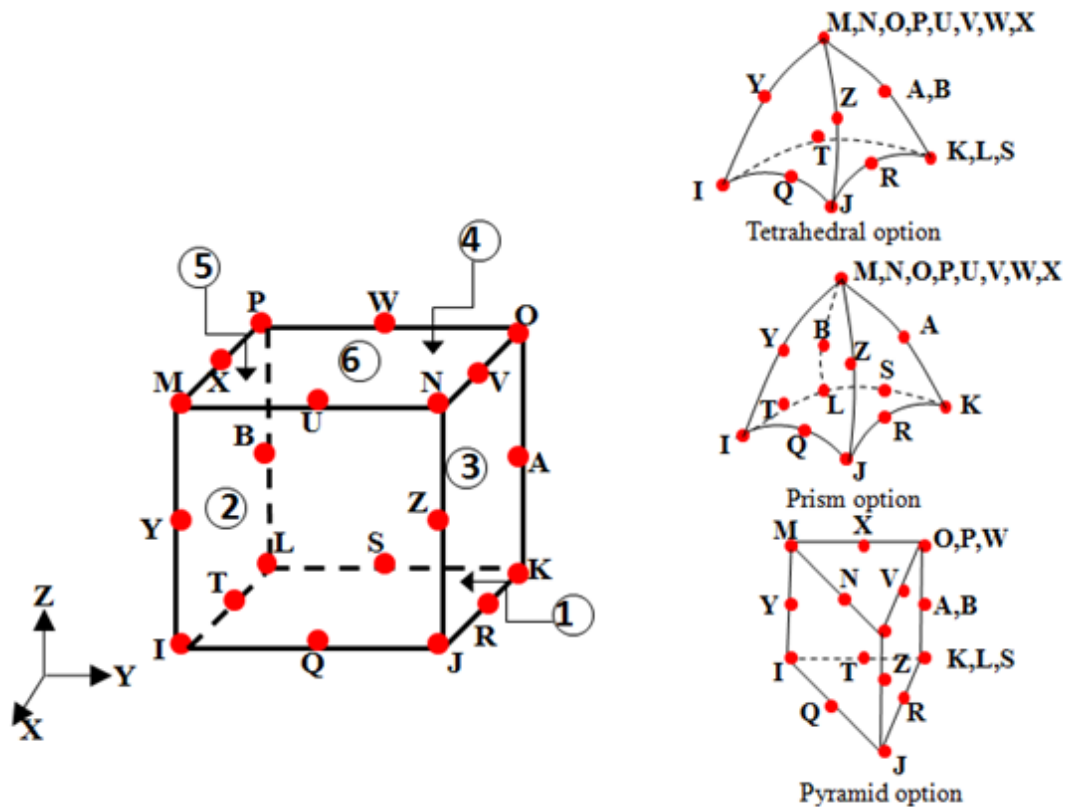


Figure 4.4: Element (SOLID90) considered for finite element analysis(ANSYS Workbench Manual)

The most significant region of the model in the present study was the pin and disk at the contact interface. Therefore, Element size of the cylindrical pin at the contact region was decreased to ensure proper distribution of temperature at the contact interface. From literature (Day, 2014), for 3D heat analysis the value of Fourier number (F_0) must be less than 0.17. The Fourier number (F_0), calculated with Eqn. (4.9), was equal to 0.066. As a result, the mesh quality evaluated was appropriate for describing the thermal behaviour of the friction material. Figure 4.5 and Figure 4.6 show the pin-on-disk model meshing in ANSYS 2020 R2. In order to prevent computational and convergence issues, the element size was chosen of comparable dimensions in the vicinity of the pin–Disk contact. Mesh Details of pin-on-disk finite element models has been given in Table 4.2.

Table 4.2: Mesh Details of pin-on-disk finite element models

Wear Track	Dimensions of Wear Track (mm)		No. of total nodes	No. of total elements
	Diameter	Width		
Track 1	60	6	336183	109154
Track 2	120	6	220609	82332

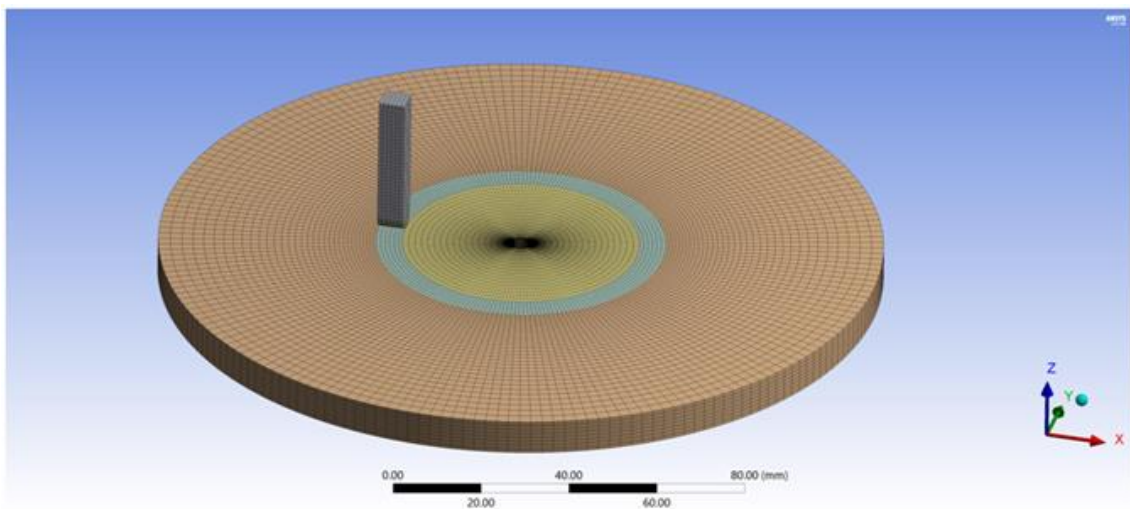


Figure 4.5: Solid element mesh of the Pin-on-disk model (60 mm Track)

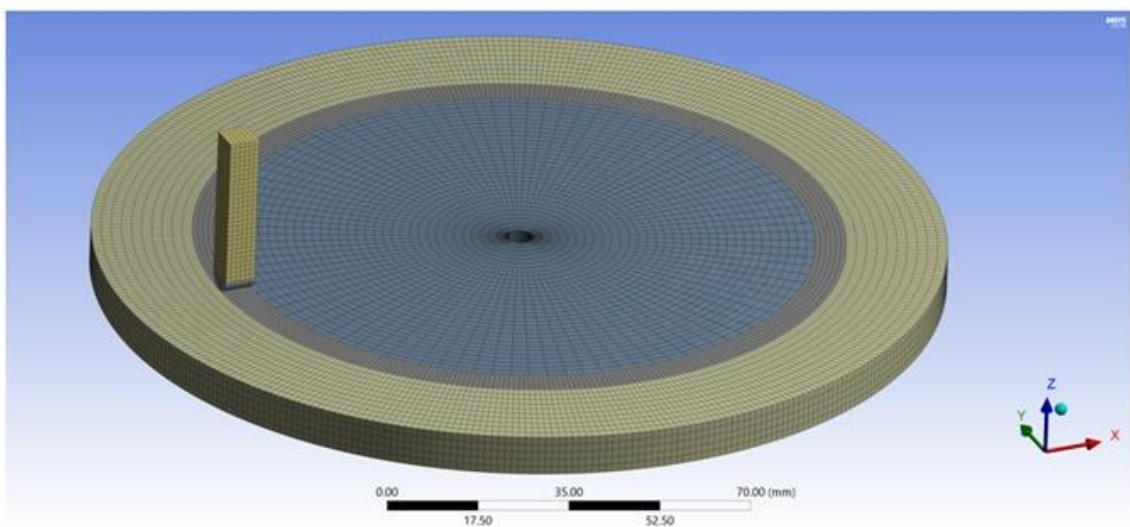


Figure 4.6: Solid element mesh of the Pin-on-disk model (120 mm Track)

Figure 4.7 depicts a schematic representation of the Pin-on-Disk model for understanding the boundary conditions (heat convection coefficient) employed in the Finite Element simulation. The convection coefficient and the ambient temperature considered for the analysis are given in Table 4.3. Load was applied in the form of a thermal flux to the Disk wear track, therefore assuming that the temperature throughout the wear track on the disk is uniform.

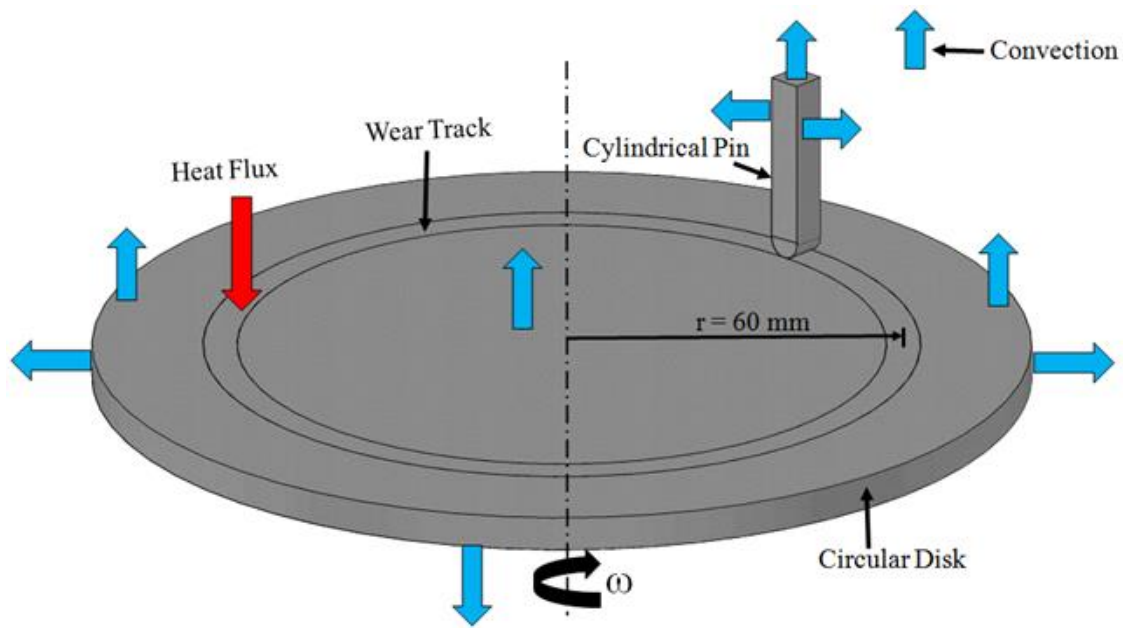


Figure 4.7: Schematic representation of Boundary Conditions considered for Pin-on-disk model

Table 4.3: Values of Convection Coefficient applied to various surfaces of pin on disk model and Ambient Temperature used in the study (Sagar, 2016)).

	Top surface and side surface of the cylindrical pin	Top surface, bottom surface and side surface of the circular disk
Convection coefficient (W/m ² °C)	250	250
Ambient Temperature	30 °C	

CHAPTER 5

RESULTS AND DISCUSSION

5.1 Friction behavior

Friction coefficient depends on many parameters such as sliding speed, load, surface roughness and frictional heat etc. Sliding speed is one of the most important parameters in dynamic conditions. So tribological test was carried out on Pin on disk. Experimental were conducted at ambient temperature condition for maximum time duration of 200 s. The experiments were carried out with varying normal loads such as 1 kg, 1.5 kg and 2 kg with varying sliding speeds 1 m/s, 2 m/s, and 3 m/s with track diameter 60 mm and 120 mm respectively. Stabilization values of coefficient of friction at different sliding speed with different Normal load is given in table 5.1. Variation of coefficient of friction with respect to time at different sliding speeds and normal loads for 60 mm track diameter is as shown in figure 5.1 and figure 5.2. The present research work mainly focuses on the initial stabilization of friction coefficient of SS304 alloys.

Table 5.1: Coefficient of friction stabilization value at different sliding speeds with different Normal loads

Normal Load (kg)	Sliding Speed (m/s)	Coefficient of friction(μ) stabilization value at 60 mm track diameter	Coefficient of friction(μ) stabilization value at 120 mm track diameter
1	1	0.0044	0.0068
	2	0.0025	0.0039
	3	0.0021	0.0024
1.5	1	0.0063	0.0069
	2	0.0043	0.0053
	3	0.0036	0.0038
2	1	0.0064	0.0072
	2	0.0055	0.0059
	3	0.0041	0.0019

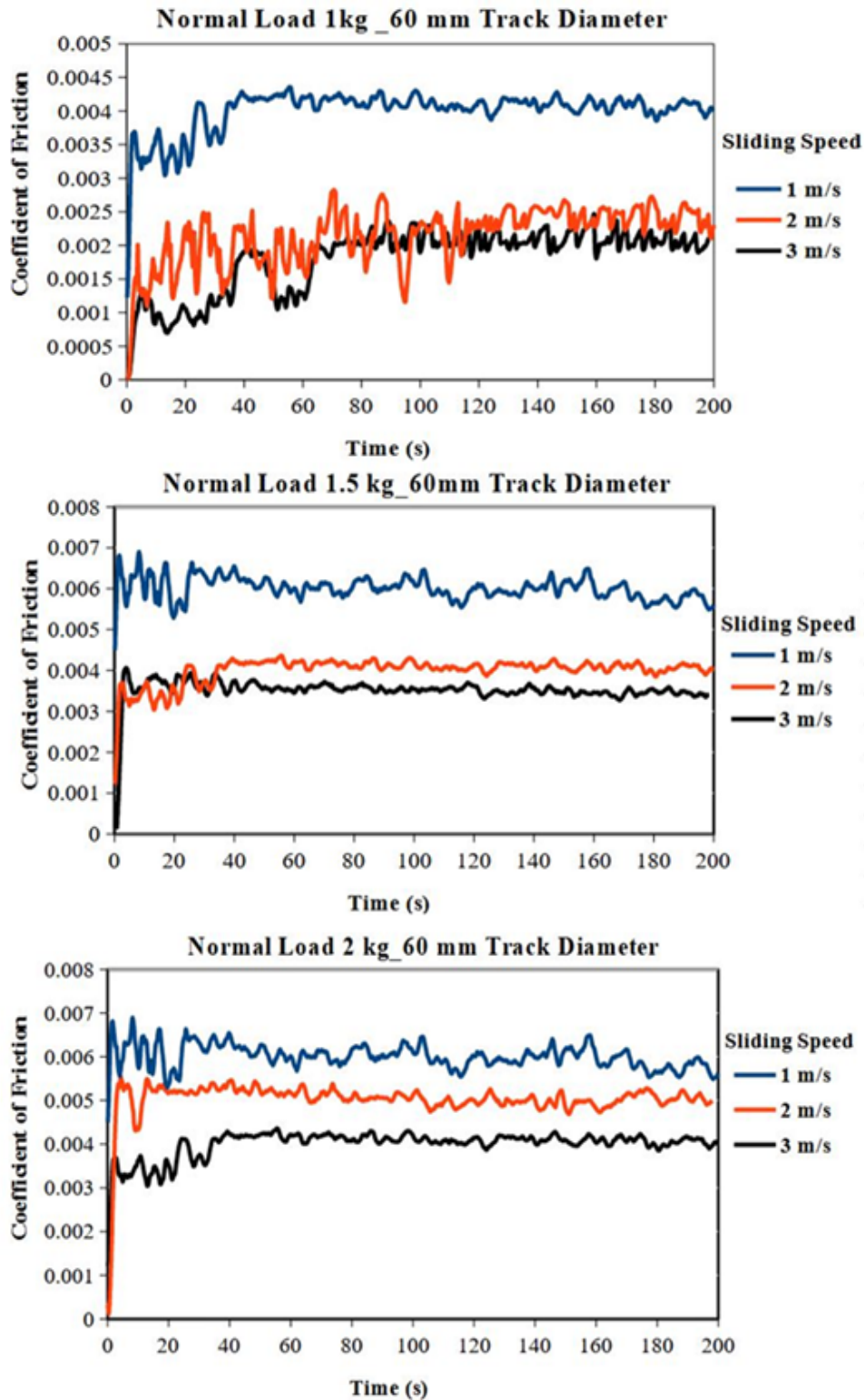


Figure 5.1: Variation of coefficient of friction with respect to time at different sliding speeds and normal loads for 60 mm track diameter

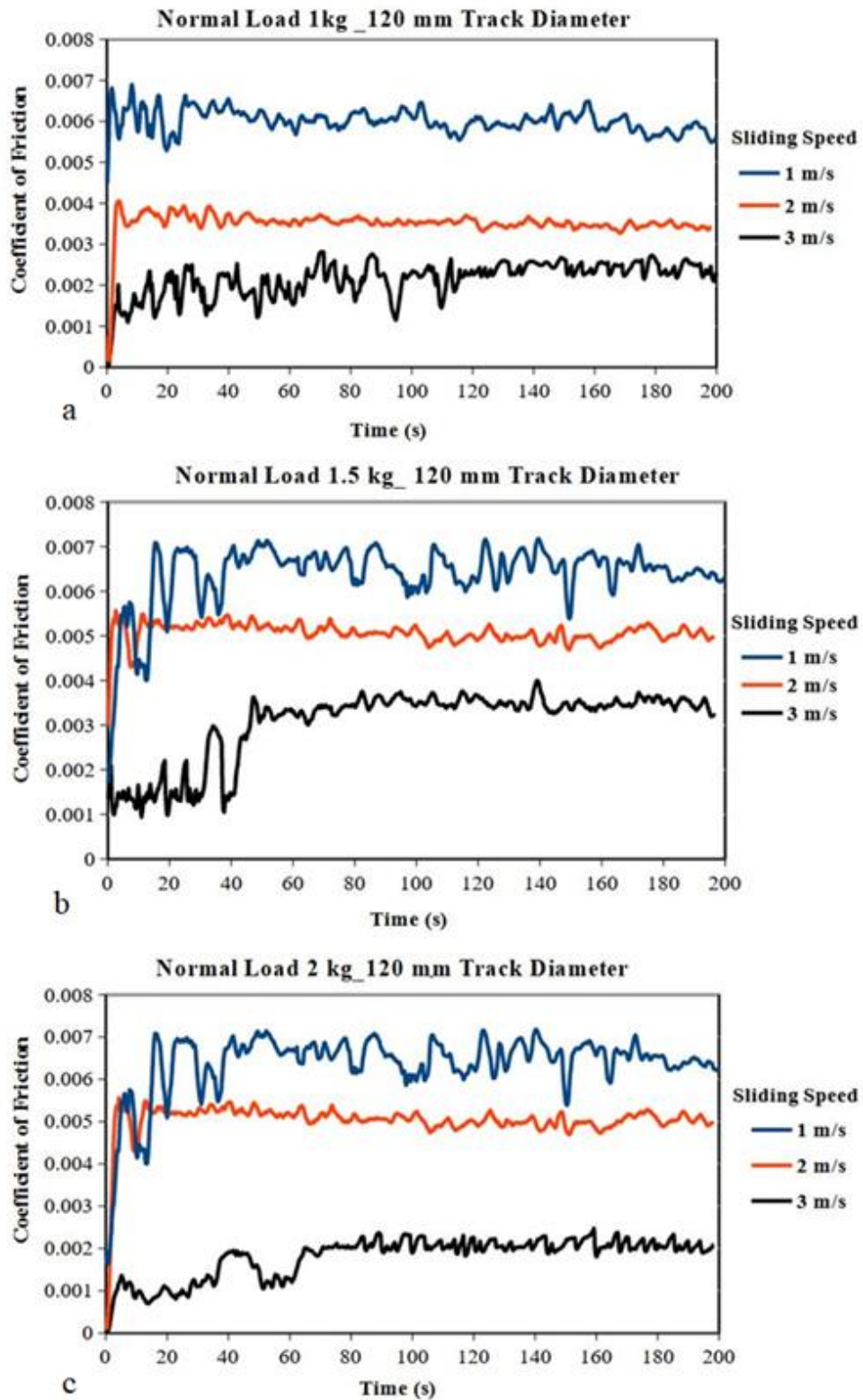


Figure 5.2: Variation of coefficient of friction with respect to time at different sliding speeds and normal loads for 120 mm track diameter

From figure 5.1 at normal load 1 kg (figure 5.1(a)) the coefficient of friction value increased drastically for the time duration of 5 s to 40 s at a sliding speed of 1m/s. This is due to the strong agreement with surface aspirates. After a period of 40 s friction coefficient was stabilized and its value is $(\mu) = 0.0044$ (Table 5.1). For a Sliding speed of 2 m/s friction coefficient increased initially.

During the experiment most of the surface aspirates gone to the outer track area of disk surface. however, some of the surface aspirates in irregular shape still exist between pin and disk these asperities act as third body due to this resign the undulation higher during 5 s to 115 s. After a subsequent time, the surface asperities become flat. Due to this at time duration of 115 s the coefficient was stabilized at $(\mu) = 0.0025$. Similar observation was observed initially for a sliding speed of 3 m/s. From the experimental observation for a time duration 5 s to 72 s the undulation was more due to the third body interaction. For the sliding speed of 3 m/s friction coefficient was stabilized at $(\mu) = 0.0021$.

Normal loads at 1.5 kg (figure 5.1 b) and 2 kg (figure 5.1 c) for a Sliding speed of 1 m/s, 2 m/s and 3 m/s the coefficient friction was raised initially and the undulation was observed after 5 s to 47 s due to the third body interaction. While increasing the sliding speed which implies the surface aspirates melting in small contact of element which results in the initiation of thermal process for the slow relaxation at the contact point for that reason pin and disk track surface changes from stick to slip condition.

Based on this condition while increasing the normal loads and sliding speeds the friction coefficient was stabilized. From the experimental observation the friction coefficient was stabilized at $(\mu) = 0.0067$, 0.0038 and 0.0042 for a sliding speed of 1 m/s, 2 m/s and 3 m/s respectively. Worn surfaces of wear track 60 mm diameter for three different normal loads and sliding speeds is as shown in figure 5.3.

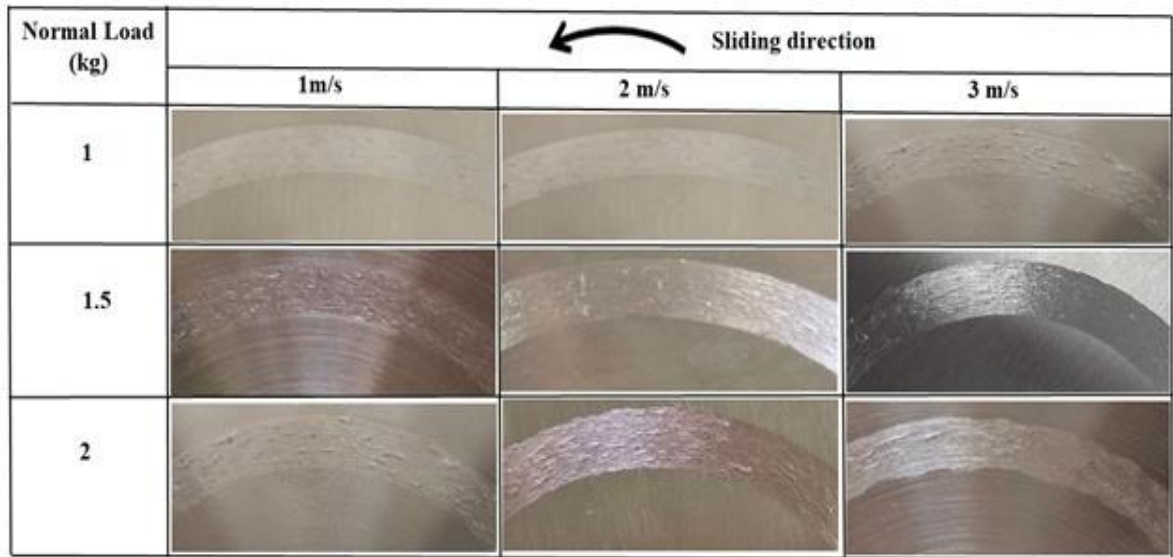


Figure 5.3: Worn surfaces of wear track 60 mm diameter for three different normal loads and sliding speeds

Figure 5.2 shows the variation of coefficient of friction with variation of time duration for different sliding speed at 120 mm track diameter. Normal load at 1kg (Figure 5.2 a) with sliding speed 1 m/s coefficient of friction was increase gradually. after 5 s weak surface asperities removal of the sliding track contact area due to this resign after 5 s to 28 s small undulation was observed. After 28 s friction coefficient was stabilized at the value of $(\mu) = 0.0068$ (Table 5.1). Sliding speed at 2 m/s similar trend was observed friction coefficient was stabilized at the value of $(\mu) = 0.0038$.

For sliding speed 3 m/s there slight increase in coefficient of friction. After 5 s to 121 s undulation was high due to the surface asperities acting like a roller between the contact. Friction coefficient was stabilized at the value of $(\mu) = 0.0022$.

Normal load at 1.5 kg (figure 5.2 b) with sliding speed 1 m/s coefficient of friction was increased. After 7 s to 178 s for a long-time duration undulation is high because abrasion plays major contribution with hard particles present between the contact surface. Friction coefficient was stabilized at the value of $(\mu) = 0.0067$. Sliding speed at 2 m/s friction coefficient similar trend was observed starting few second after 19 s friction coefficient was stabilized at the value of $(\mu) = 0.0058$.

For sliding speed 3 m/s coefficient of friction was increase initially. After 5 s to 51 s high influencing adhesion due to the iron-oxide layer with surface asperities contaminants mating contact. Friction coefficient was stabilized at the value of (μ) = 0.0038.

Normal loads at 1.5 kg (figure 5.2b) and 2 kg (figure 5.2 c) with sliding speeds 1 m/s and 2 m/s coefficient of friction was increased similar tread was observed. Normal loads 2 kg with sliding speeds 1 m/s and 2 m/s Friction coefficient was stabilized at the values are (μ) = 0.0071 and 0.0053. Normal loads 2 kg with sliding speeds 3 m/s coefficient of friction was increased because of strong adhesion bonded with active surface asperities. After 7 s Friction coefficient was stabilized at the value of (μ) = 0.0022. Worn surfaces of wear track 120 mm diameter for three different normal loads and sliding speeds is as shown in figure 5.4.

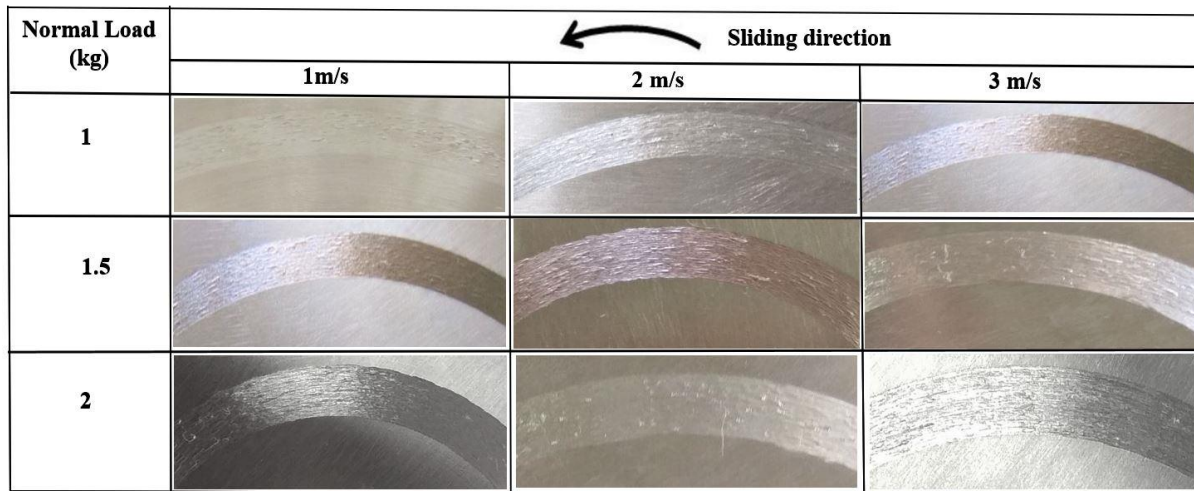


Figure 5.4: Worn surfaces of wear track 120 mm diameter for three different normal loads and sliding speeds

5.2 Wear behavior

Wear test was performed using pin on disk tribometer before conducting experiment the pin and disk surface was cleaned with acetone solution. Pin and disk weight was measured before the experiment by using digital weighing balance machine with accuracy of 0.001 gm. Figure 5.5 shows the variation of wear volume with varying time at different sliding speed with track diameter of 60 mm.

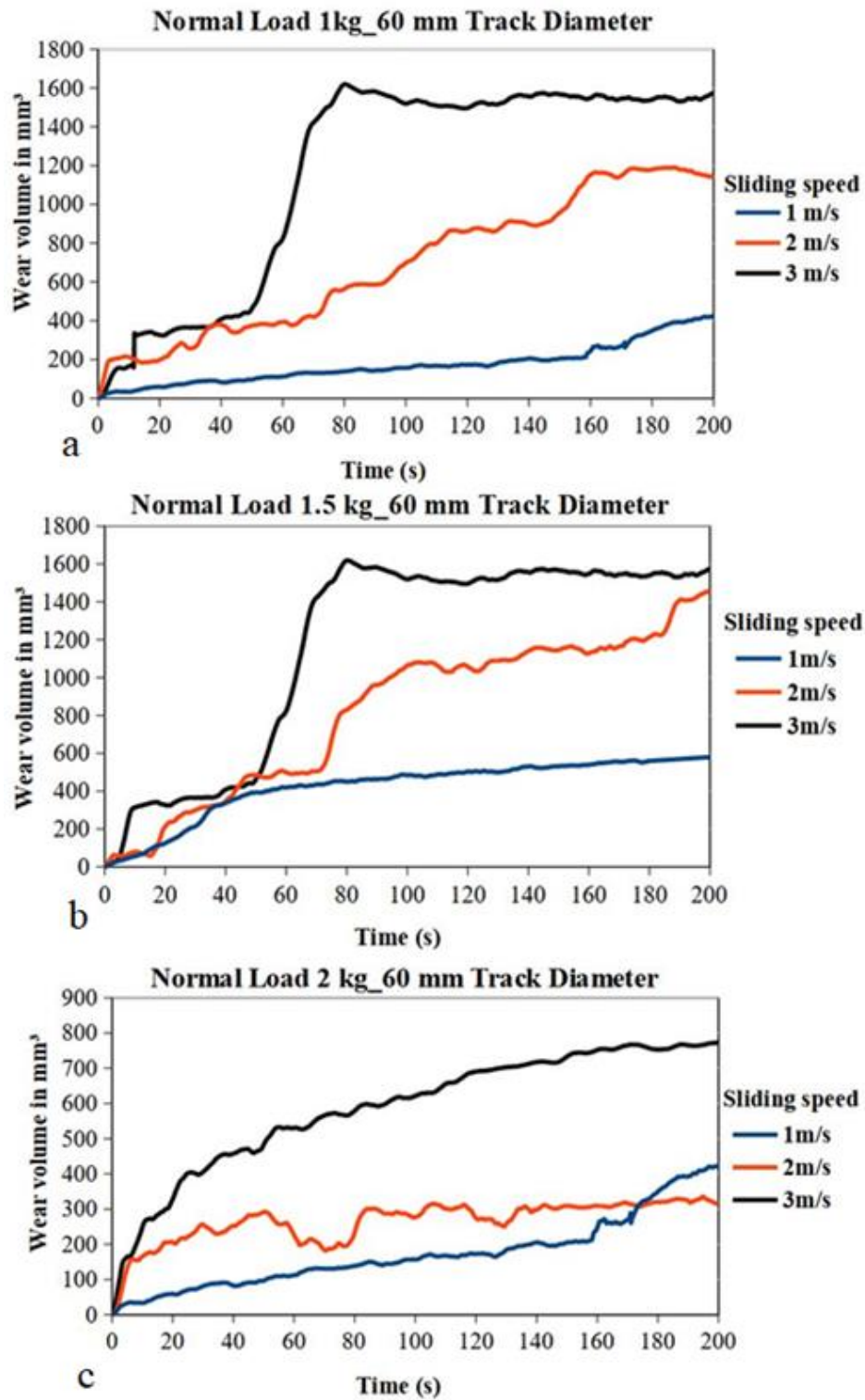


Figure 5.5: Variation of wear volume with varying time at different sliding speeds and normal loads for track diameter of 60 mm

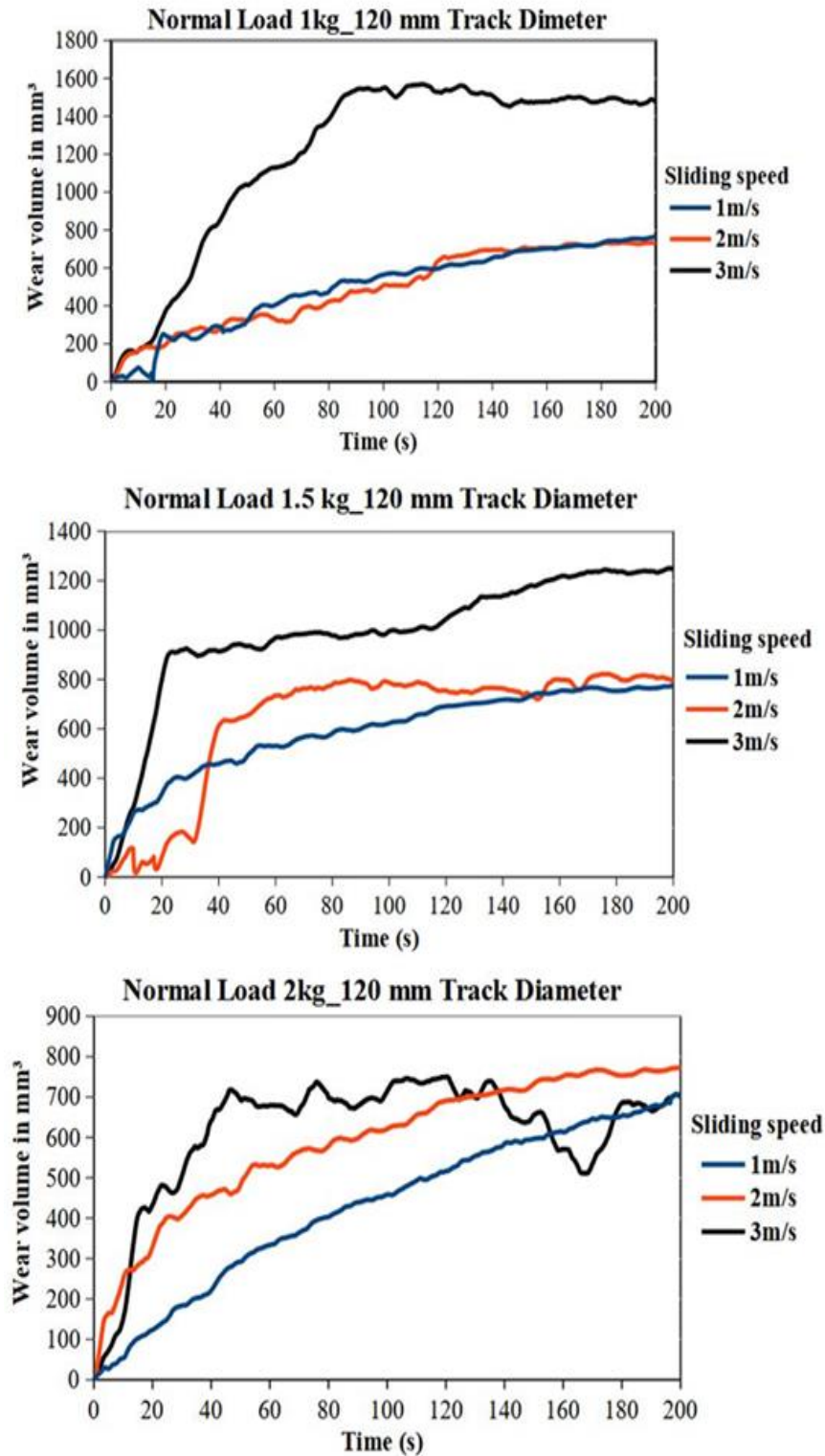


Figure 5.6: Variation of wear volume with varying time at different sliding speeds and normal loads for track diameter of 120 mm

Table 5.2: Comparison of wear volume stabilization value at different Normal loads and different sliding speeds with 60 mm and 120 mm track diameter

Normal Load (kg)	Sliding Speed (m/s)	Wear volume stabilization value (mm ³) at 60 mm track diameter	Wear volume stabilization value (mm ³) at 120 mm track diameter
1	1	380	580
	2	980	620
	3	1600	1400
1.5	1	500	670
	2	903	600
	3	1620	950
2	1	390	690
	2	290	880
	3	769	778

Wear volume was measured with varying normal loads 1 kg (Figure 5.5 a), 1.5 kg (Figure 5.5 b) and 2 kg (Figure 5.5 c) also varying sliding speeds of 1 m/s, 2 m/s and 3 m/s. At a normal load of 1 kg (Figure 5.5 a) with a sliding speed of 1 m/s wear volume increased gradually due to remove the Fe-oxide layer and wear grooves. Sliding speed of 1 m/s maximum wear volume is 380 mm³ (Table 5.2) was observed. Sliding speed of 2 m/s wear volume increased 74 s after couple of time duration wear volume increases rapidly due the abrasive wear with active contact surface aspirates. Sliding speed of 2 m/s maximum wear volume is 980 mm³ was observed. After 165 s wear volume was stabilized. Sliding speed of 3 m/s wear volume increased after 51 s wear volume increased drastically due the increase the sliding speed with strong abrasive bond with pin and disk contact track surface roughness with active contact surface aspirates. Sliding speed of 3 m/s maximum wear volume is 1600 mm³ was observed with time duration of 78 s. After 81 s wear volume was stabilized.

Normal load of 1.5 kg (Figure 5.5 b) with sliding speed of 1 m/s, 2 m/s and 3 m/s wear volume is similar trend was observed. sliding speed of 1m/s maximum wear volume is 500 mm³ was observed. sliding speed of 2 m/s wear volume increase with increase sliding speed. After 110 s wear volume was stabilized. Sliding speed of 2 m/s maximum wear volume 903 mm³ was observed.

Normal load of 2 kg (Figure 5.5 c) with sliding speed of 1 m/s, 2 m/s and 3 m/s wear volume increased gradually due to remove the Fe-oxide layer and weak surface asperities. Sliding speed of 1m/s maximum wear volume is 390 mm³ was observed. The Sliding speed of 2 m/s wear volume increased till 50 s after few second wear volume get the undulation due to the micro level pit formation or wear depress more between the mating surface. After 140 s wear volume was stabilized the maximum wear volume is 290 mm³ was observed. The Sliding speed of 3 m/s wear volume increased drastically because of higher load with high sliding speed surface asperities get fatigue. After 185 s wear volume was stabilized the maximum wear volume is 780 mm³ was observed.

Figure 5.6 show the variation of wear volume with varying time at different sliding speed with track diameter of 120 mm. applying normal load 1 kg (Figure 5.6 a),1.5kg, (Figure 5.6 b) and 2 kg (Figure 5.6 c) with sliding speed of 1 m/s,2 m/s and 3 m/s wear volume was observed.

Normal load 1 kg with sliding speed 1m/s initially wear volume was gets mild undulation till 18 s due to hard roughness of the disk surface after 20 s wear volume was increase gradually due to removal of iron oxide layer with good agreement contact surface. Normal load 1 kg with sliding speed 1m/s wear volume 580 mm³ was observed. At sliding speed 2 m/s wear volume was increase gradually due to good agreement with track surface contact. Normal load 1 kg with sliding speed 2 m/s wear volume 620 mm³ (Table 5.2) was observed. At sliding speed 3 m/s wear volume was increase rapidly due the higher sliding speed at sliding speed 3 m/s wear volume 1400 mm³ was observed within the 95 s. After few second wear volume stabilized.

Normal load of 1.5 kg with sliding speed of 1 m/s, 2 m/s and 3 m/s wear volume it was observed. Sliding speed of 1 m/s maximum wear volume is 670 mm³. Sliding speed of 2 m/s wear volume gets mild undulation till 35 s due to roughness hardness of the contact surfaces After few second wear volume was increases due formation of chipping. wear volume was stabilized After 41 s Sliding speed of 2 m/s maximum wear volume 600 mm³ was observed. Sliding speed 3 m/s wear volume was increase rapidly due the higher sliding speed at sliding speed 3 m/s wear volume 950 mm³ was observed within the 22 s.

Normal load of 2 kg with sliding speed of 1 m/s, 2 m/s and 3 m/s wear volume it was observed. sliding speed of 1 m/s wear volume increases gradually maximum wear volume is 690 mm³. At sliding speed of 2 m/s wear volume increases due to increase sliding speed with Normal load and also similar trend was observed at sliding speed 1 m/s and 2 m/s. sliding speed of 2 m/s the maximum wear volume is 880 mm³. At Sliding speed 3 m/s wear volume was increase heavily due the higher sliding speed at sliding speed 3 m/s. after 18 s to 180 s more undulation in wear volume because of the removal of material wear debris is formed due to the abrasion and adhesion induced ploughing occur in the contact surface. After 180 s wear volume stabilized. Sliding speed 3 m/s maximum wear volume is 771 mm³ was observed.

5.3 Analysis of worn-out disks track surface

Pin and disk surface was examined by using optical microscope image before and after contacting experiment. The damage disks track surface is shown in figure 5.7 and figure 5.8. However, pin on disk experiment was carry out such as 60 mm and 120 mm track diameter with different normal load such as 1 kg, 1.5 kg and 2 kg and different sliding speed (1 m/s, 2 m/s and 3 m/s) All the experiment was conducted maximum time duration at 200 s with ambient temperature at 32 °C with relative humidity 84% at dry sliding condition.

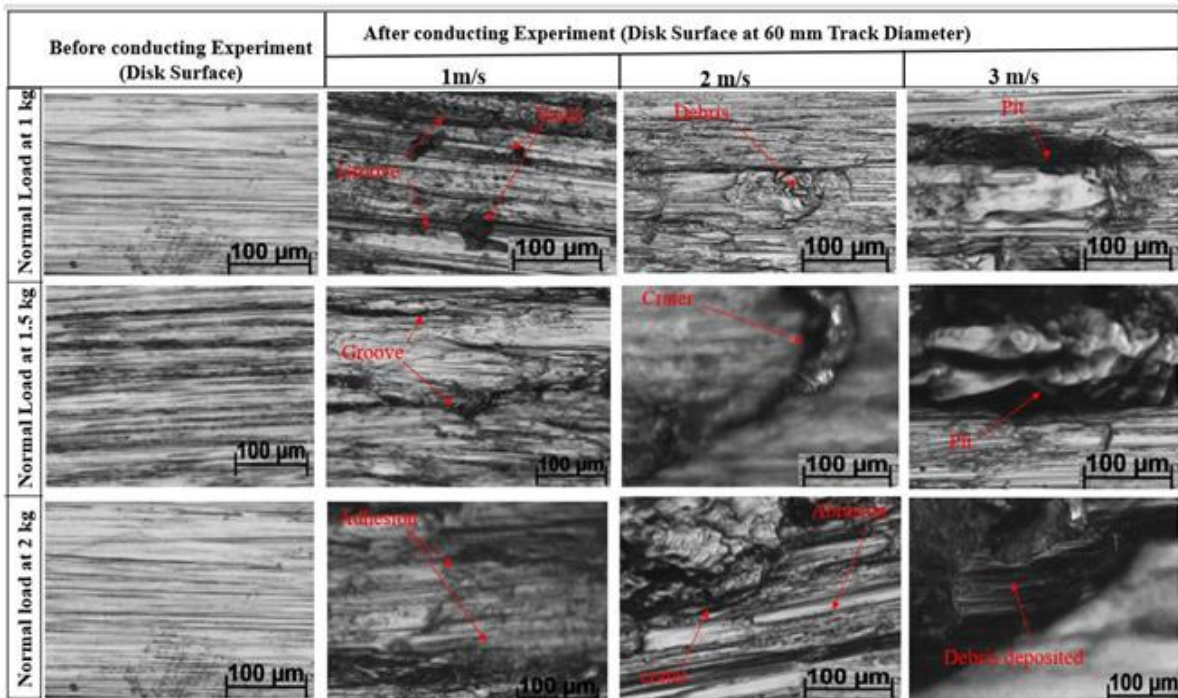


Figure 5.7: Optical microscopy image for damage disks at 60 mm track surface

Figure 5.7 shows Optical microscopy image was taken for damage disks at 60 mm track surface show in as normal load at 1 kg,1.5 kg and 2 kg with the sliding speed 1 m/s initially 5 s duration removal of Fe-oxide layer due to that wear grooves formed after 5 s metallic adhesion dominating. Normal load 1 kg with sliding speed 2 m/s and 3 m/s due to increase the sliding speed with load maximum strain accumulated at the contact surface aspirates due to that aspirate detached to the track surface due to that wear debris formation was more at wear track. At the sliding speed 3 m/s small pit formation was more due to the detached surface aspirates.

Normal load 1.5 kg with sliding speed 2 m/s due to increase load with sliding speed crater on the wear track surface. At the sliding speed 3 m/s small pit formation was observed.

Normal load 2 kg with sliding speed 2 m/s due to increase load with sliding speed crater and abrasion was more on the wear track surface. At the sliding speed 3 m/s with increase load due to that heat generation with heat addition was more due to that

surface aspirates were melting and striking on deposited to the track surface due to heat dissipation.

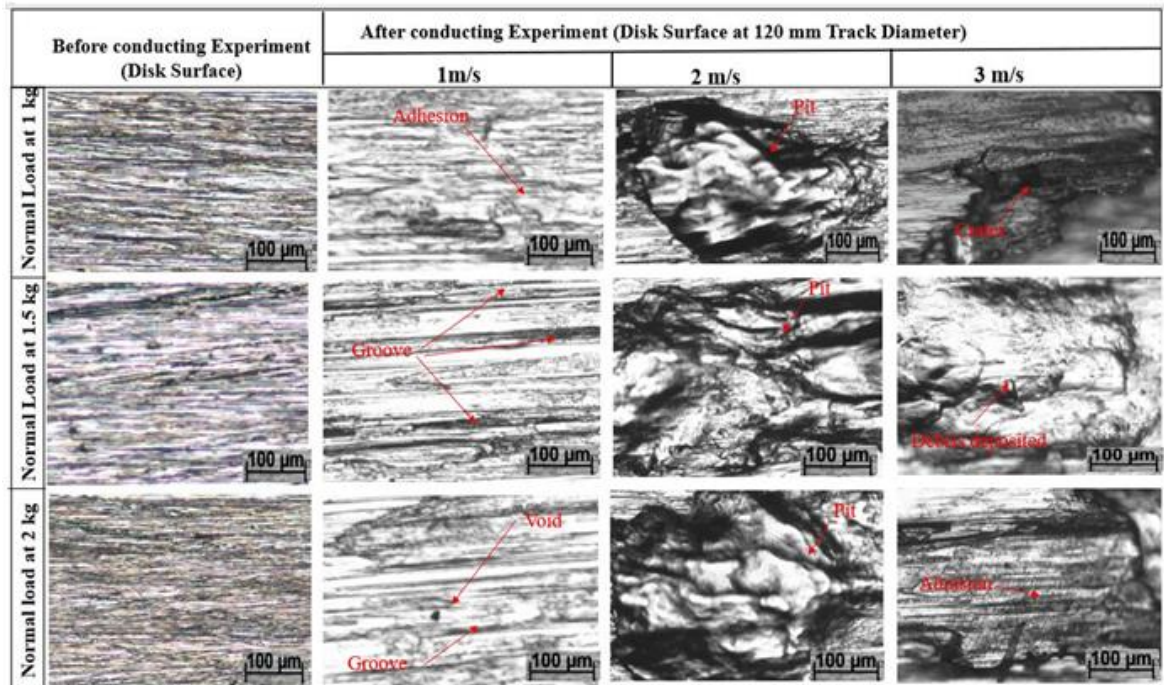


Figure 5.8: Optical microscopy image for damage disks at 120 mm track surface

Figure 5.8 shows that wear damage disks at 120 mm track surface with different normal load such as 1 kg, 1.5 kg and 2 kg with different sliding speeds (1 m/s, 2 m/s and 3 m/s). At a normal load 1 kg, 1.5 kg and 2 kg with sliding speed for 1 m/s initially 7 s time duration removal of Fe-oxide layer due to that wear grooves formed after 7 s metallic adhesion dominating and few locations of the contact surface void formation was observed. Normal load 1 kg with sliding speed 2 m/s pit formation was more due to increase sliding speed with increase the track diameter (120 mm). As the sliding speed increase 3 m/s crater with metal deposited on the track surface was observed.

Normal load 1.5 kg with sliding speed 2 m/s, the track surface aspirates was melting and pit formation was more due to increase sliding speed with increase load at a track diameter (120 mm). As the sliding speed increase 3m/s wear debris melting due to frictional heat generation with metal deposited on the track surface was observed.

Normal load 2 kg with sliding speed 2 m/s, the track surface asperities were melting and pit formation was more due to increase sliding speed with increase load at a track diameter (120 mm). As the sliding speed increase 3 m/s metal abrasion more on the track surface was observed.

5.4 Variation of coefficient of friction over sliding distance

Experiments were conducted to measure co-efficient of friction and temperature. For all full sliding experiments, the constant normal load of 1 kg and three different sliding speeds of 1 m/s, 2 m/s and 3 m/s were considered. The co-efficient of friction was measured and plotted against sliding cycles/sliding distance. During initial full sliding cycles (Figure 5.9), there is no metallic contact between pin and disk due to the presence of oxide and nitride layers in the contact interface [Wu et al.,2015].

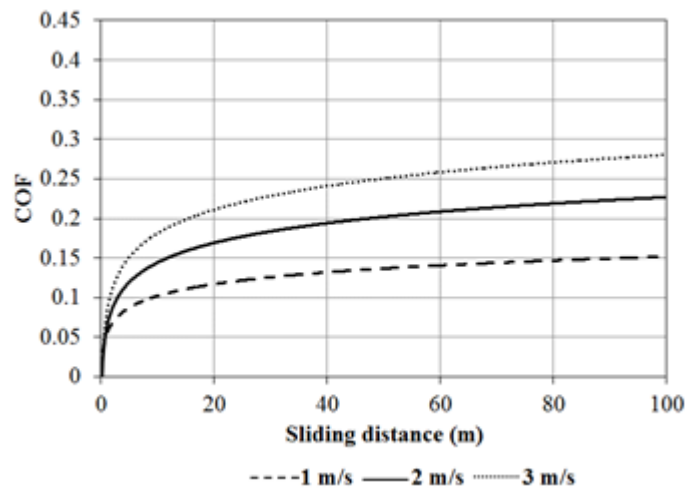


Figure 5.9: Coefficient of friction vs. sliding distance

Due to flattening of asperities, the adhesion is more because of increase in real area of contact [Douglas et al.,1995]; as a result, there is more atomic interaction [Sharma et al.,2001]. Further flattening of asperities provides stabilized coefficient of friction as shown in Figure 4 and the same trend was observed for sliding speeds of 1 m/s, 2 m/s and 3 m/s; the corresponding stabilized values of coefficient of friction are 0.15, 0.22 and 0.28 respectively. The decrease in coefficient of friction for lower sliding speed (1 m/s) at the stabilized stage was mainly due to formation of less wear debris and the presence of inactive contacts. The wear debris acts like roller or spherical balls at the contact interface, enhancing the motion between the sliding components and reduces

the coefficient of friction [Aditya et al.,2014]. The increase in stabilized coefficient of friction at higher sliding speeds (2 m/s and 3 m/s) is mainly due to increase in real contact area and formation of micro welding between wear debris and asperities [Gwidon et al.,2005]. In Figure 5.9, there is no variation in coefficient of friction for various sliding speeds at a sliding distance of 1.4 m and the corresponding coefficient of friction is observed as 0.06. Observation of single valued coefficient of friction is mainly due to the presence of oxide and nitride layer formation on the metallic surface. The formation of oxide and nitride layers affect the direct metallic contact leads to poor coordinate covalent bond strength in adhesion effect [Murthy et al.,2017].

5.5 Variation of temperature over sliding distance

Full sliding experiments were conducted at room temperature of 30 °C for three different sliding speeds of 1 m/s, 2 m/s and 3 m/s. The rise in contact temperature was measured from two K-type thermocouples located at 4 mm and 7 mm from the contact interface. The evolution of contact temperature data was plotted against the sliding distance (Figure 5.10). From Figure 5.2, stabilization of temperature data is observed over sliding distance. This trend is similar to the trend shown by coefficient of friction over sliding distance as observed from Figure 5.2. For lower sliding speed of 1 m/s, the temperature at interface increases with increase in sliding distance and the stabilized contact temperature is determined as 40 °C. For higher sliding speeds of 2 m/s and 3 m/s, the values of stabilized contact temperature are observed as 42 °C and 60 °C respectively. There is no significant difference in stabilized contact temperature at the sliding speeds of 1 m/s and 2 m/s and difference in stabilized contact temperature is observed to be 2 °C. Each sliding cycle, the cylindrical pin covers sliding distance of 376.8 mm. For sliding speeds of 1 m/s and 2 m/s, the pin covers sliding distances of 376.8 mm per second and 753.6 mm per second respectively. Area of contact is hidden at a particular moment of rotation and remaining wear track length is exposed to environmental conditions. Heat generated at the contact interface during sliding is dissipated due to conduction and convection heat transfer. For higher sliding speed of 3 m/s, heat generated during sliding is not

dissipated quickly because of less time interval between successive sliding cycles. Wear debris is more and melted during higher sliding speeds. This effect increases coefficient of friction at the contact interface. For lower sliding speed of 1 m/s, undulation is not observed in temperature vs. sliding distance. This is due to free movement of wear debris.

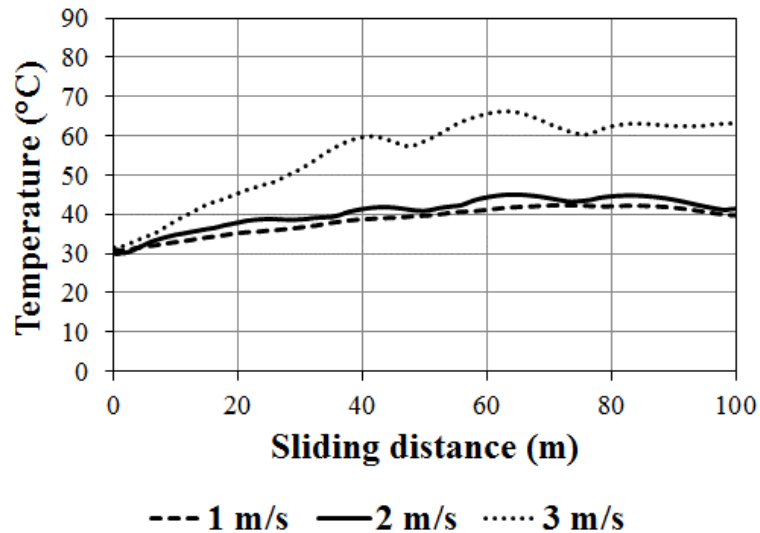


Figure 5.10: Temperature vs. sliding distance

5.6 Variation of temperature over sliding speeds and normal loads

Dry sliding experiments were carried out at an ambient temperature of 30 °C for three different sliding speeds of 1 m/s, 2 m/s, and 3 m/s under normal load of 1 kg, 1.5 kg, and 2 kg using two different wear tracks of diameter (60 mm and 120 mm) respectively. K-type thermocouples were pasted to the cylindrical pins at 4 mm and 7 mm distances from the contact interface to measure the temperature rise caused by friction. The rise in temperature at the contact interface was estimated using inverse heat transfer method.

The measured temperature data using K-type thermocouples at 4 mm and 7 mm locations from the contact interface was taken as base data, for MATLAB programming, to estimate heat flux and temperature distribution in pin specimen at contact interface for three different sliding speeds and normal loads. The temperature data was measured at time interval of 0.2 s, so the required parameters were estimated

at time step size of 0.2 s. Figure 5.11 and Figure 5.12 show the estimated heat flux and contact interface temperatures in SS304 alloy.

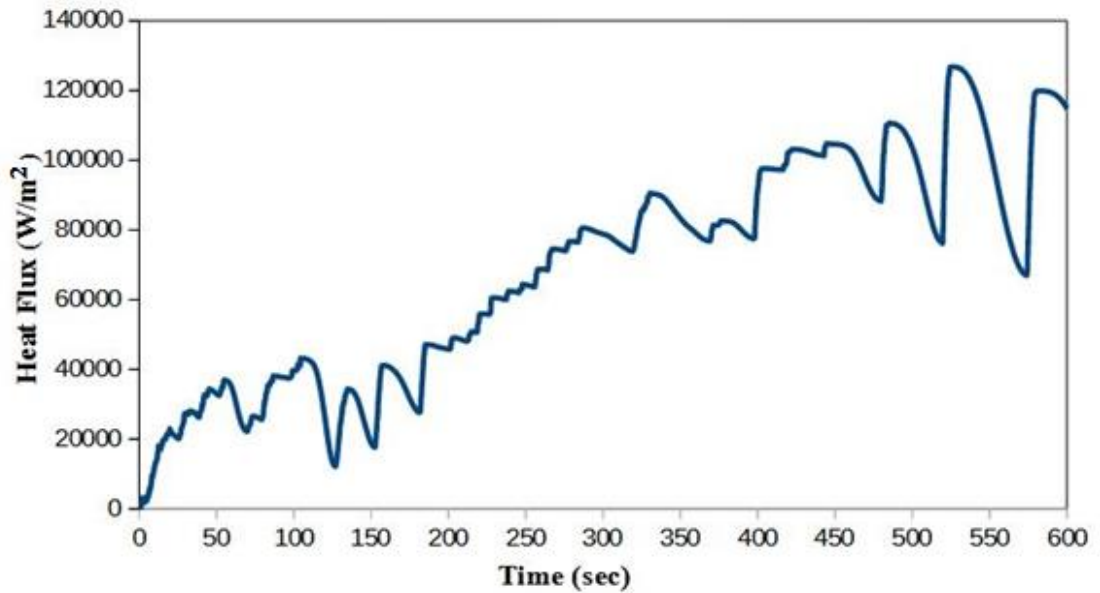


Figure 5.11: Estimated heat flux at contact interface of SS304 alloy

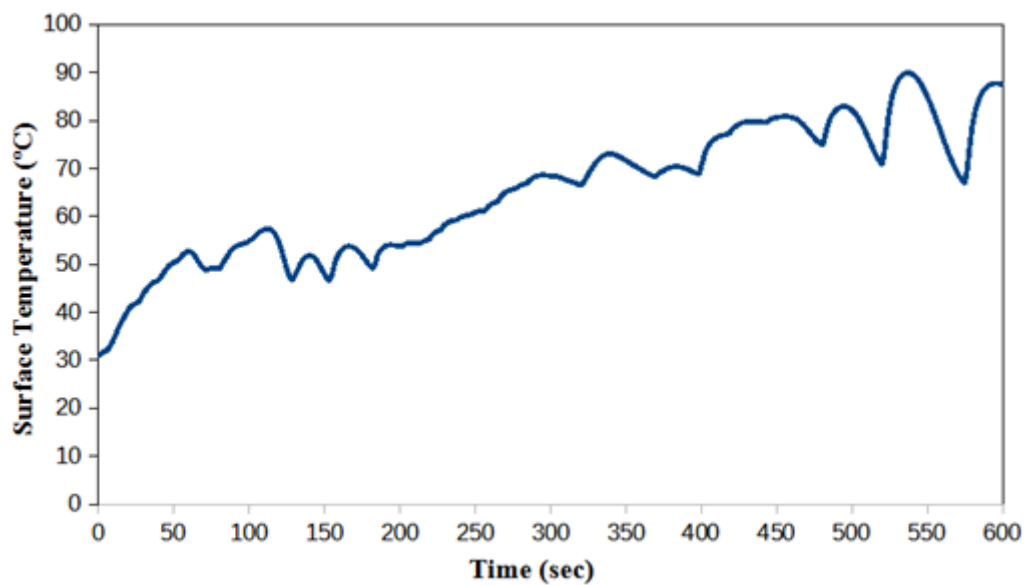


Figure 5.12: Estimated surface temperature at contact interface of SS304 alloy

When two metals are in contact and subjected to friction, heat is generated at the contact interface which plays a vital role in the field of tribology. When these two

metal bodies slide against each other, the friction between two surfaces develops high contact stress which leads to plastic deformation of contact surface and there by generates frictional heat (Johnson, 1985). The estimated heat flux at contact interface in SS304 alloy is given in Figure 5.11. The estimated surface temperature at contact interface of the pin specimen is given in Figure 5.12. From Figure 5.11 and Figure 5.12, for SS304 alloy, it is observed that for time interval of 0 s to 200 s of sliding there is slight increase in heat flux and surface temperature. This is because at the beginning of the experiment the contact at the surface is a line contact as the time progresses the contact will change from line contact to area contact. For time interval of 200 s to 350 s of sliding, it is observed that there is increase in heat flux and surface temperature values linearly without any undulations due to the fact that there is a transition in area of contact (which means area of contact at the interface increases and also geometry of the pin changes from cylinder to flat due to wear). For time interval of 350 s to 600 s of sliding, the increase in heat flux represents the increase in coefficient of friction between pin and disk specimen. The stable heat flux represents the stabilized friction coefficient. The pin contact surface temperature is important to understand the friction process at contact surfaces. The variation in heat flux and evolution of surface temperature at the contact interface with respect to time for time interval of 200 s of sliding considering different sliding speeds (1 m/s, 2 m/s, and 3 m/s) under normal loads (1 kg, 1.5 kg, and 2 kg) for two different tracks (60 mm and 120 mm) is shown in Figure 5.13 and Figure 5.14 respectively.

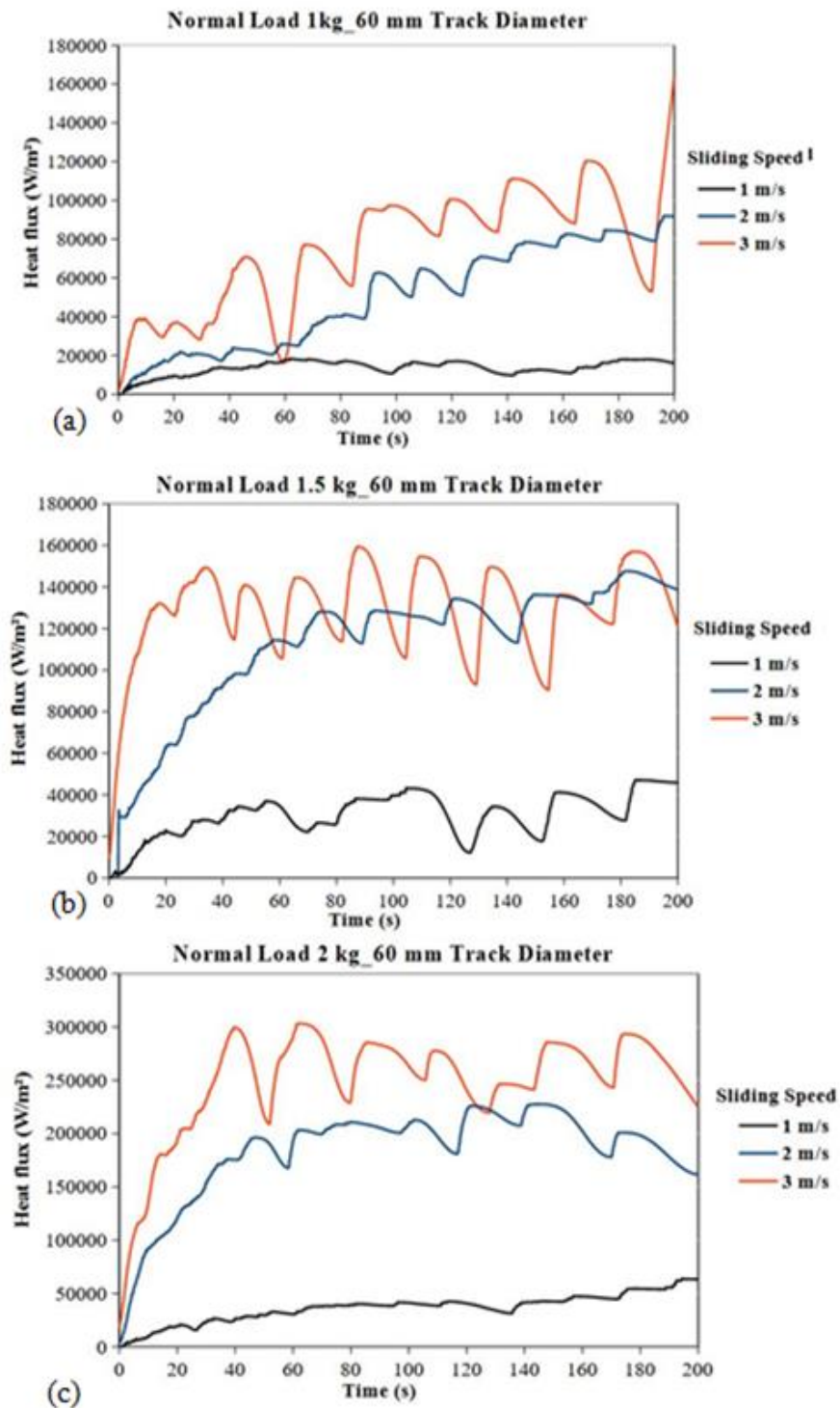


Figure 5.13: Variation of heat flux with respect to time (60 mm track diameter) for three different sliding speeds 1 m/s, 2 m/s, and 3 m/s under normal load of (a) 1 kg (b) 1.5 kg and (c) 2 kg

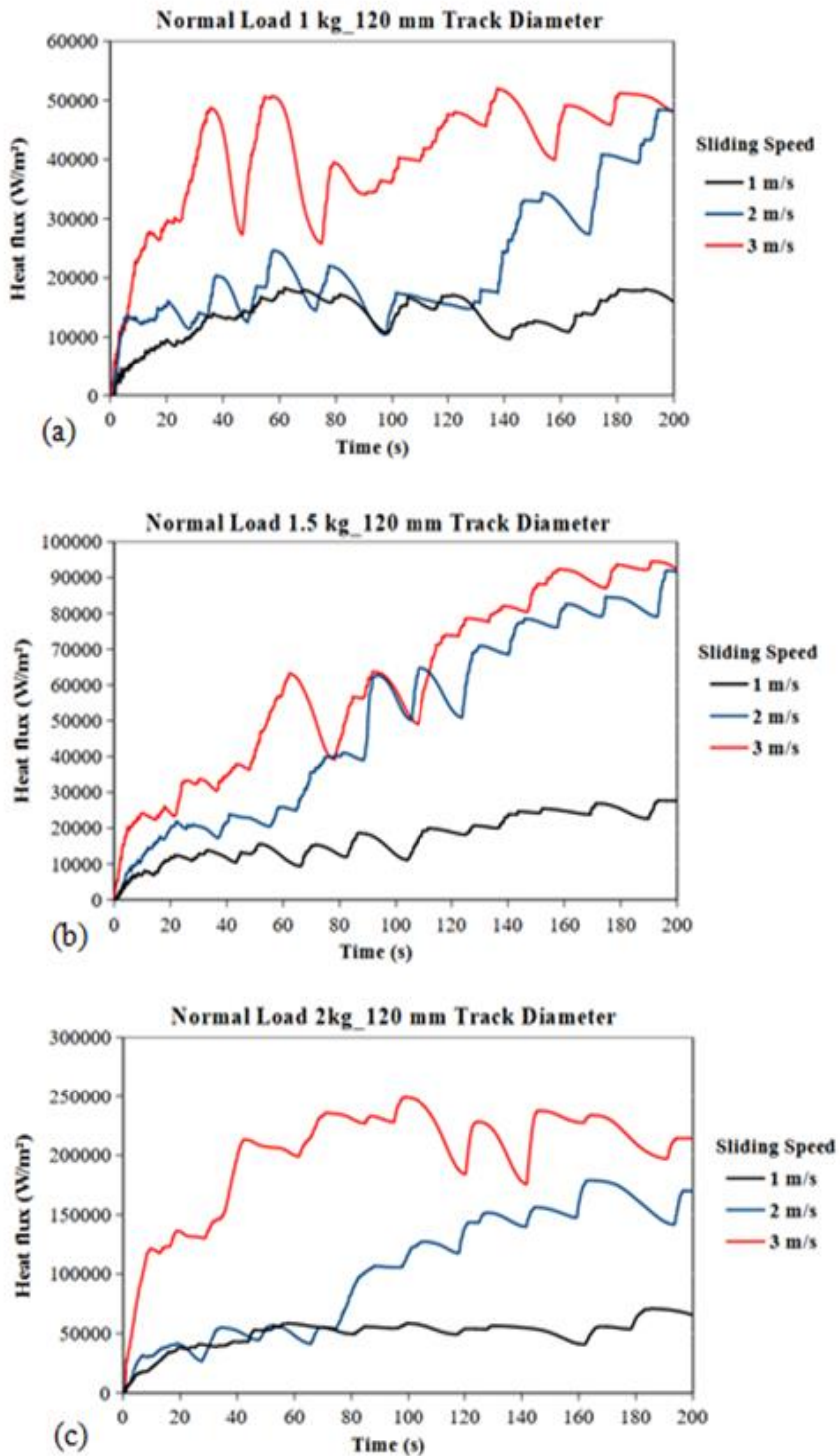


Figure 5.14: Variation of heat flux with respect to time (120 mm track diameter) for three different sliding speeds 1 m/s, 2 m/s, and 3 m/s under normal load of (a) 1 kg (b) 1.5 kg and (c) 2 kg

Figures 5.13 and 5.14 shows the variation in the maximum surface temperature and heat flux values estimated at surface of the pin, with respect to time for track diameter 60 mm and 120 mm. From Figs 5.13 (a), 5.14 (a) and 5.13 (c), 5.14 (c) it is observed as the sliding speed increases from 2 m/s to 3 m/s, initially there is rise in heat flux values for time interval of 40 s due to removal of asperities but in case of sliding speed 1 m/s we observed lesser heat flux values. After 40 s of sliding, there is a lot of peaks and valleys in heat flux values at higher sliding speeds compared to lower sliding speed this is due formation of wear and debris during sliding, similar kind of trend was observed in 120 mm diameter track.

From Figures 5.13 (b) and 5.14 (b), it is observed that as the sliding speed increases from 2 m/s to 3 m/s temperature at the contact interface for lower sliding speed, there is stabilization in temperature values over a sliding distance and same trend was observed for all three normal loads (1 kg, 1.5 kg, and 2 kg). For lower sliding speed of 1 m/s, formation of peak and valley is not observed in temperature vs. time. Initially there are few spikes of high temperature (due to the chip formation) but soon afterwards the temperature becomes steady. During sliding, heat generated at the contact interface dissipates via conduction and convection heat transfer. The area of contact is hidden at a particular moment of rotation, while the length of the remaining wear track is in contact with the environment. Because the time interval between successive sliding cycles is short at higher sliding speeds, heat generated during sliding is not easily dissipated. Wear debris is greater and melts more at higher sliding speeds (Palanikumar et.al, 2019). The oscillations in the pin temperature data represent the dynamic nature of oxide generation and degradation, as well as the associated continuous fluctuation in real surface emissivity.

The maximum surface temperature estimated by inverse heat transfer method at pin surface, maximum temperature obtained at 4 mm location and 7 mm location through thermocouple while conducting dry sliding experiments for three different sliding speeds under three normal loads at sliding time of 200 s are presented below in Table 5.3 and Table 5.4.

Table 5.3: Temperature values obtained by conducting experiment for track diameter 60 mm

Track Diameter 60 mm		Experimental obtained max temperature (200 s)		
		Surface Temperature (°C)	Temperature (°C) at 4 mm location	Temperature (°C) at 7 mm location
Normal Load (kg)	Sliding Speed (m/s)			
1	1	41.13	39.97	34.61
	2	81.17	59.21	43.63
	3	99.60	72.86	55.21
1.5	1	53.83	42.41	37.73
	2	113.31	78.69	54.49
	3	131.91	99.38	73.03
2	1	69.99	54.80	43.92
	2	140.44	99.45	67.85
	3	202.94	141.88	94.89

Table 5.4: Temperature values obtained by conducting experiment for track diameter 120 mm

Track Diameter 120 mm		Experiment obtained max temperature (200 s)		
		Surface Temperature (°C)	Temperature (°C) at 4 mm location	Temperature (°C) at 7 mm location
Normal Load (kg)	Sliding Speed (m/s)			
1	1	42.13	37.97	34.61
	2	57.78	44.25	37.98
	3	76.48	66.30	55.01
1.5	1	88.18	66.15	47.77
	2	88.15	65.14	47.77
	3	81.17	59.21	46.25
2	1	58.05	45.36	37.97
	2	127.11	86.26	56.55
	3	179.88	132.38	88.77

5.7 Finite Element Analysis results

ANSYS 2020 R2 Workbench was used for numerically simulating the sliding process. A finite element model was created and then simulated under conditions that were comparable to those found in the experiments. A transient thermal model was developed since the challenge involves a variety of highly interacting mechanical and thermal phenomena such as friction, temperature, and wear. The heat generated by friction (mechanical work) serves as a cause of the thermal issue.

The heat flux values estimated by inverse heat transfer method for a time interval of 200 s had been assigned to wear track as input and the corresponding temperature at the contact interface has been simulated. Figure 5.7 to 5.16 and Figure 5.16 to 5.25 shows the evolution of temperature at pin surfaces for 60 mm diameter track and 120 mm diameter track. The maximum temperature is observed at the base of the cylindrical pin, as seen in figure 5.15 - 5.23 and Figure 5.24 - 5.32. The temperature of the nodes at the pin's axis is higher than at its radius due to convection with atmospheric air. This is also the reason why the temperature at the pin's outer surface is lower than that in the pin's radius (Raghavendra, C.R et al., 2019). The maximum surface temperature obtained at pin surface, maximum pin temperature obtained longitudinally at 4 mm location and 7 mm location while conducting dry sliding experiments for three different sliding speeds under three normal loads at sliding time of 200 s is presented in below table 5.5 and table 5.6.

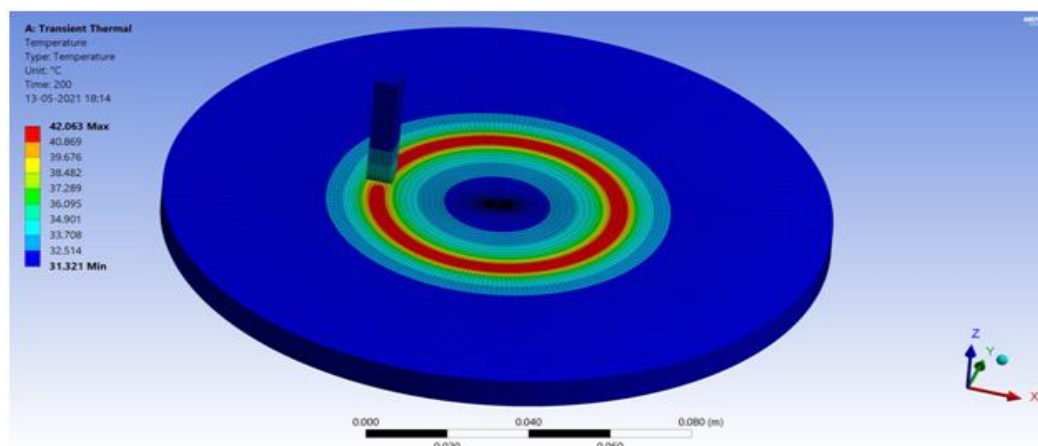


Figure 5.15: Temperature distribution between pin and disk over 200 s of sliding for a 60 mm diameter track using a Finite Element model (1 kg, 1 m/s).

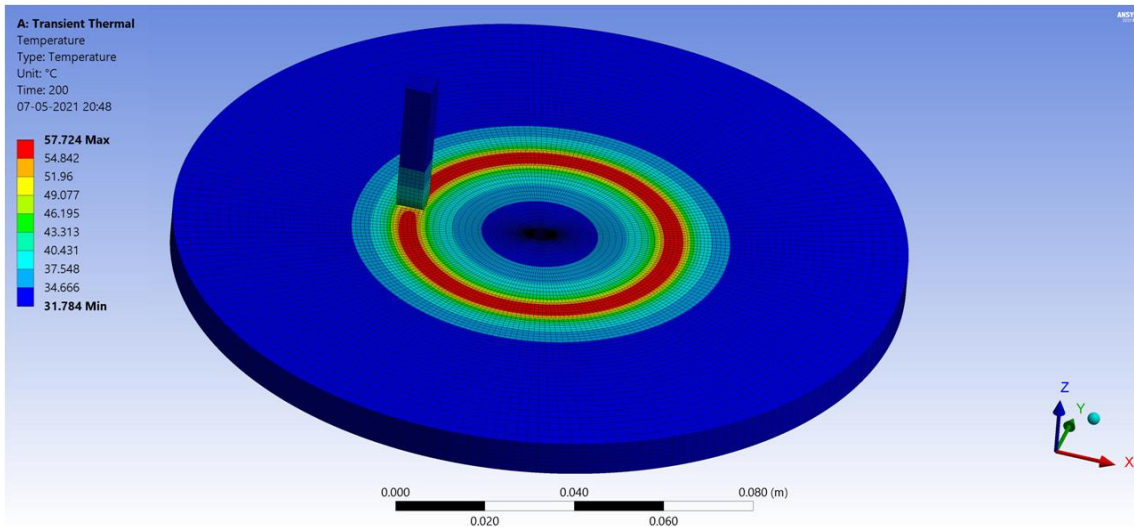


Figure 5.16: Temperature distribution between pin and disk over 200 s of sliding for a 60 mm diameter track using a Finite Element model (1 kg, 2 m/s).

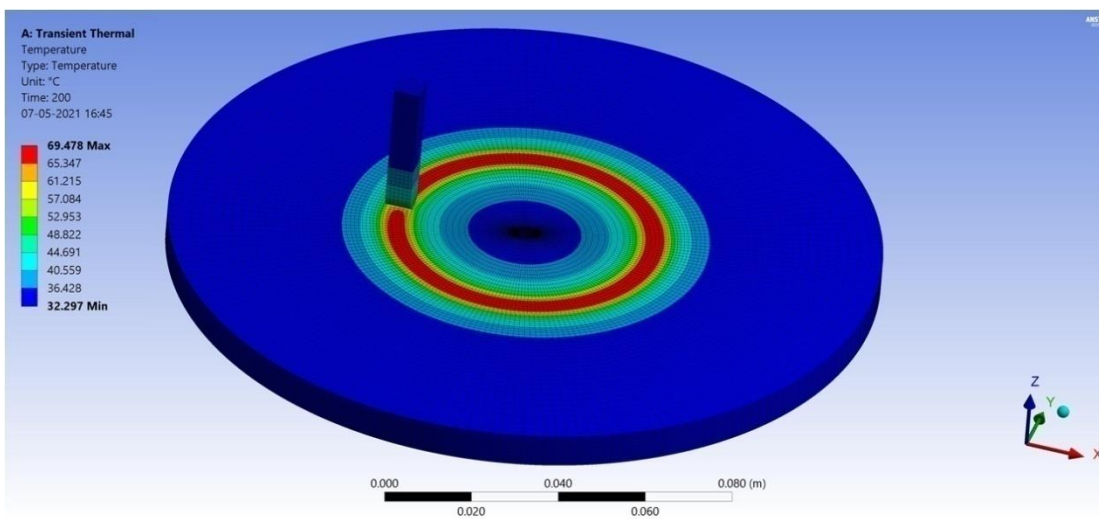


Figure 5.17: Temperature distribution between pin and disk over 200 s of sliding for a 60 mm diameter track using a Finite Element model (1 kg, 3 m/s).

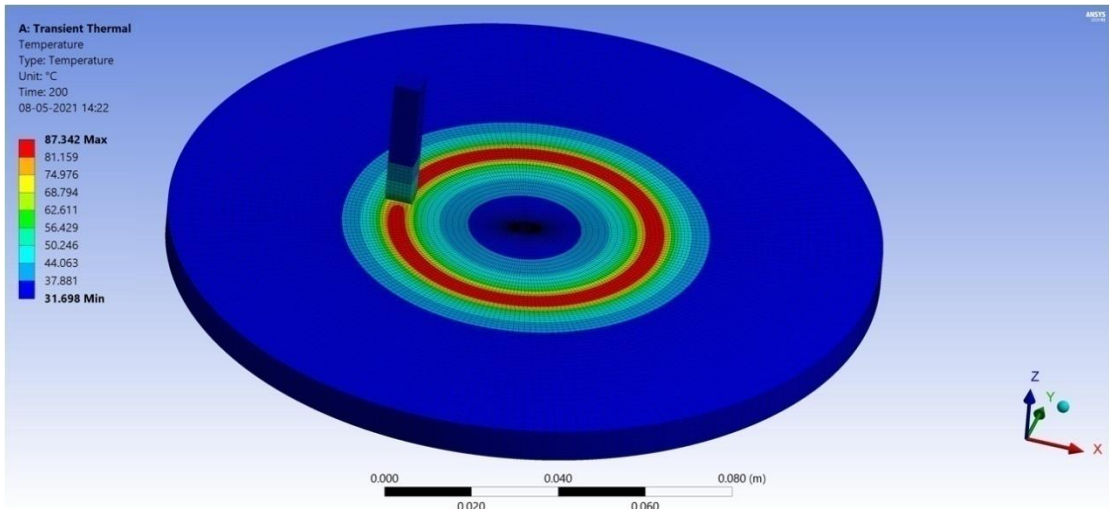


Figure 5.18: Temperature distribution between pin and disk over 200 s of sliding for a 60 mm diameter track using a Finite Element model (1.5 kg, 1 m/s).

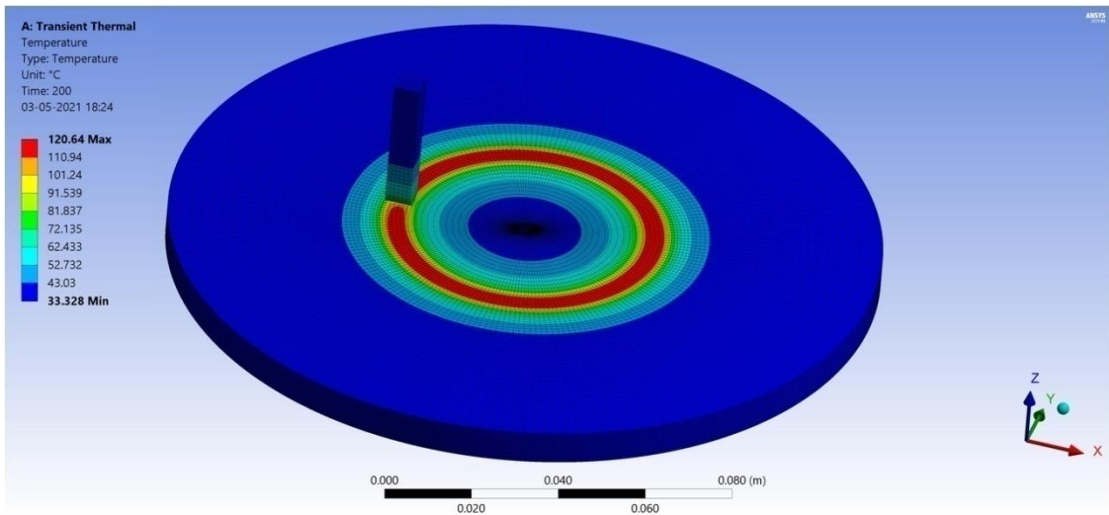


Figure 5.19: Temperature distribution between pin and disk over 200 s of sliding for a 60 mm diameter track using a Finite Element model (1.5 kg, 2 m/s).

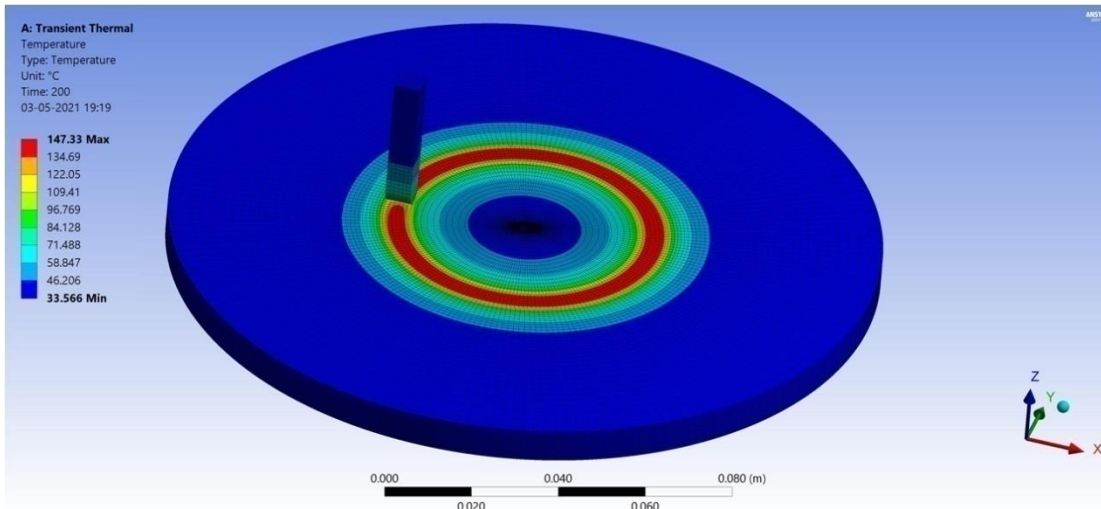


Figure 5.20: Temperature distribution between pin and disk over 200 s of sliding for a 60 mm diameter track using a Finite Element model (1.5 kg, 3 m/s).

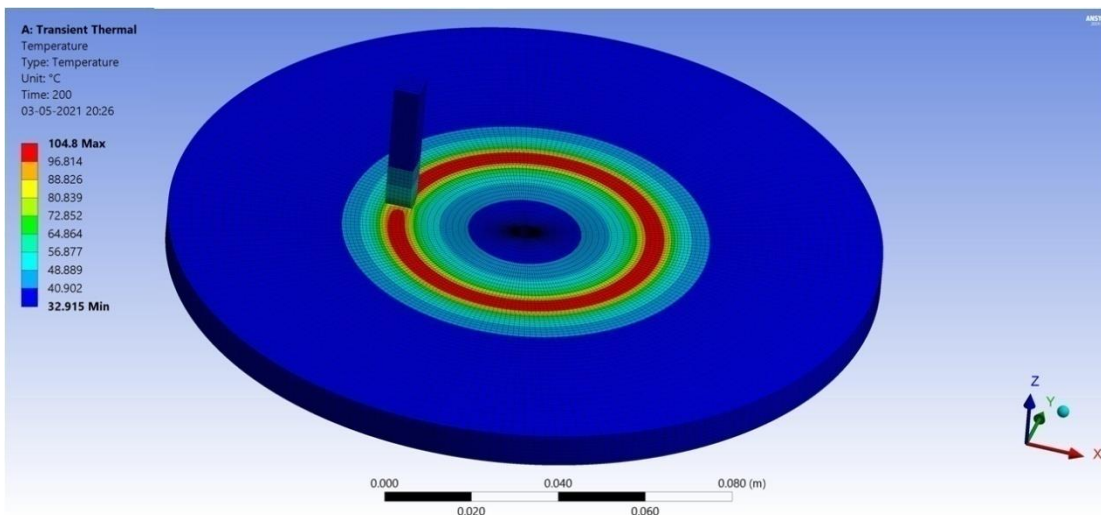


Figure 5.21: Temperature distribution between pin and disk over 200 s of sliding for a 60 mm diameter track using a Finite Element model (2 kg, 1 m/s).

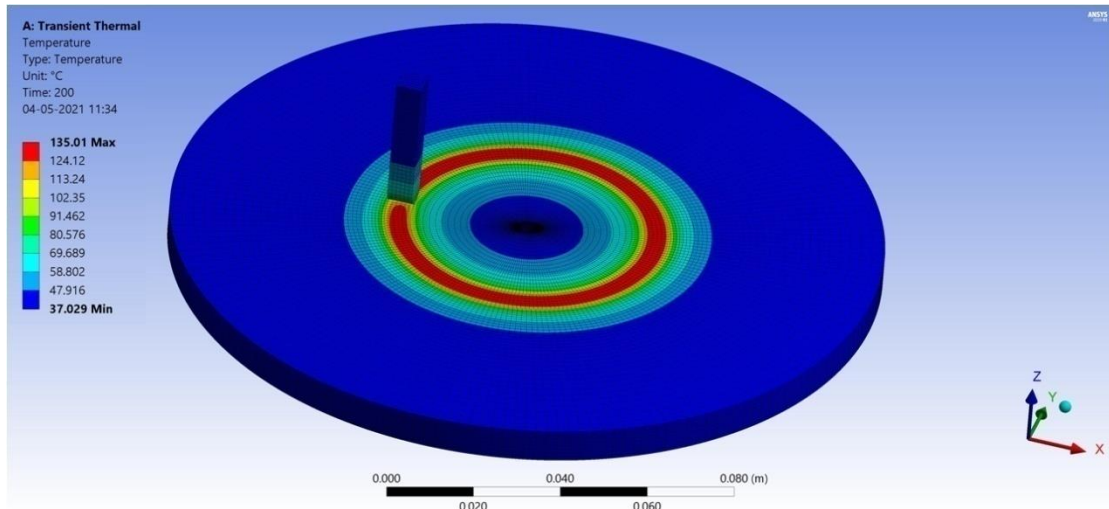


Figure 5.22: Temperature distribution between pin and disk over 200 s of sliding for a 60 mm diameter track using a Finite Element model (2 kg, 2 m/s).

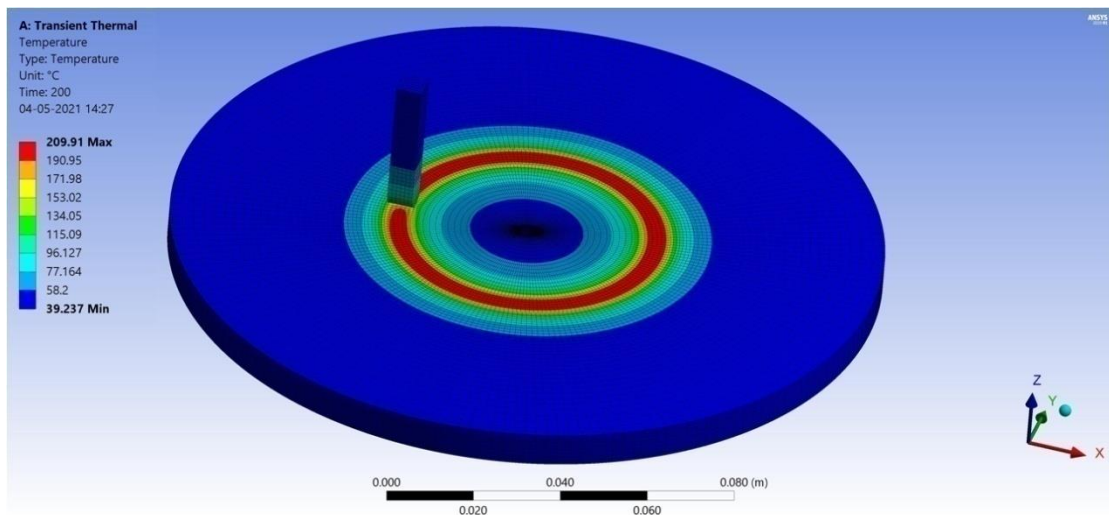


Figure 5.23: Temperature distribution between pin and disk over 200 s of sliding for a 60 mm diameter track using a Finite Element model (2 kg, 3 m/s).

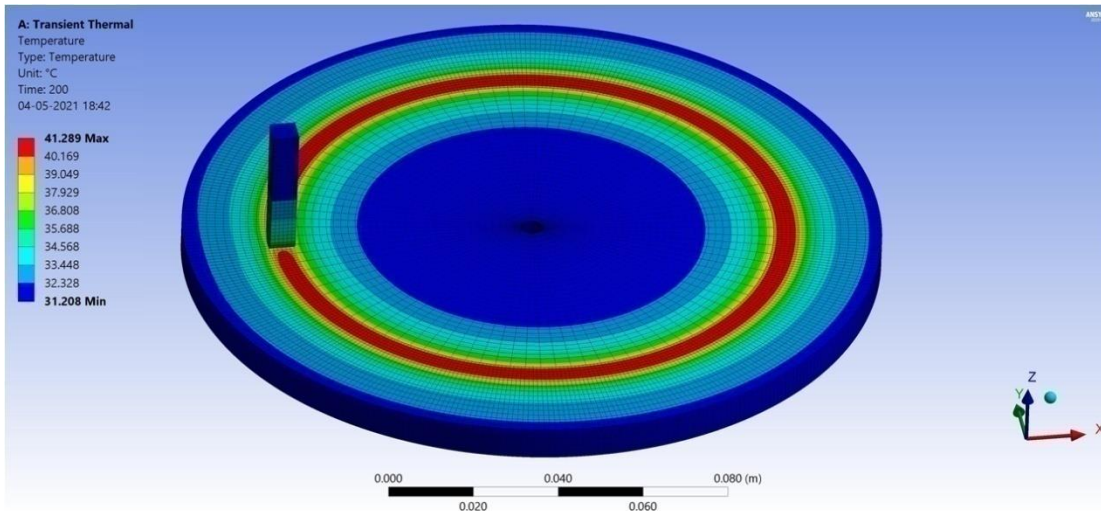


Figure 5.24: Temperature distribution between pin and disk over 200 s of sliding for a 120 mm diameter track using a Finite Element model (1 kg, 1 m/s).

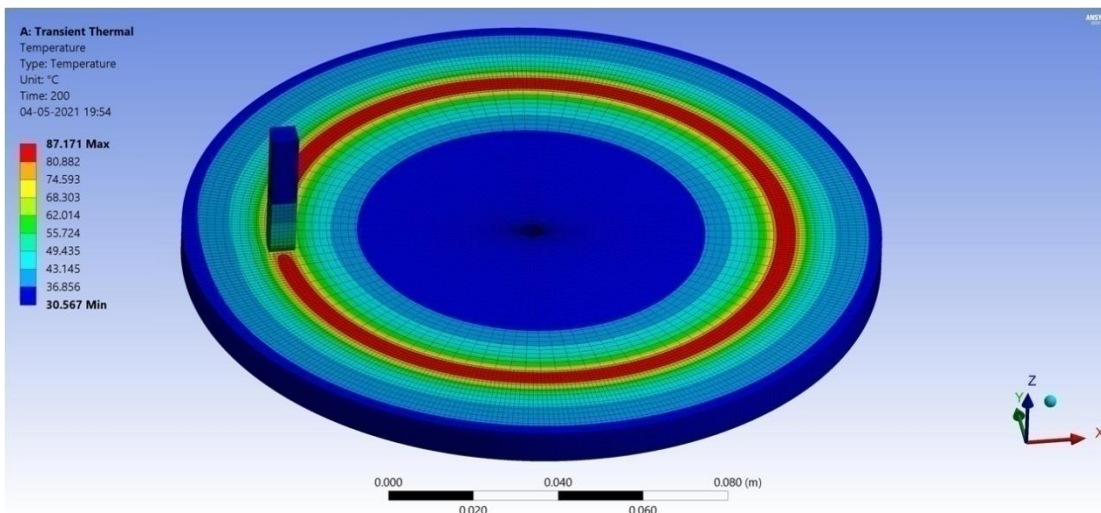


Figure 5.25: Temperature distribution between pin and disk over 200 s of sliding for a 120 mm diameter track using a Finite Element model (1 kg, 2 m/s).

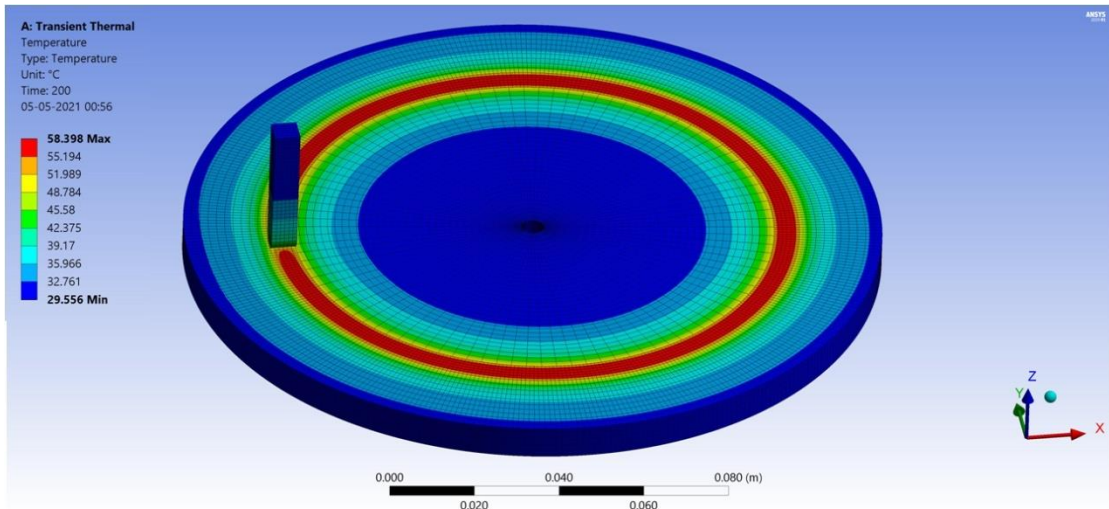


Figure 5.26: Temperature distribution between pin and disk over 200 s of sliding for a 120 mm diameter track using a Finite Element model (1 kg, 3 m/s).

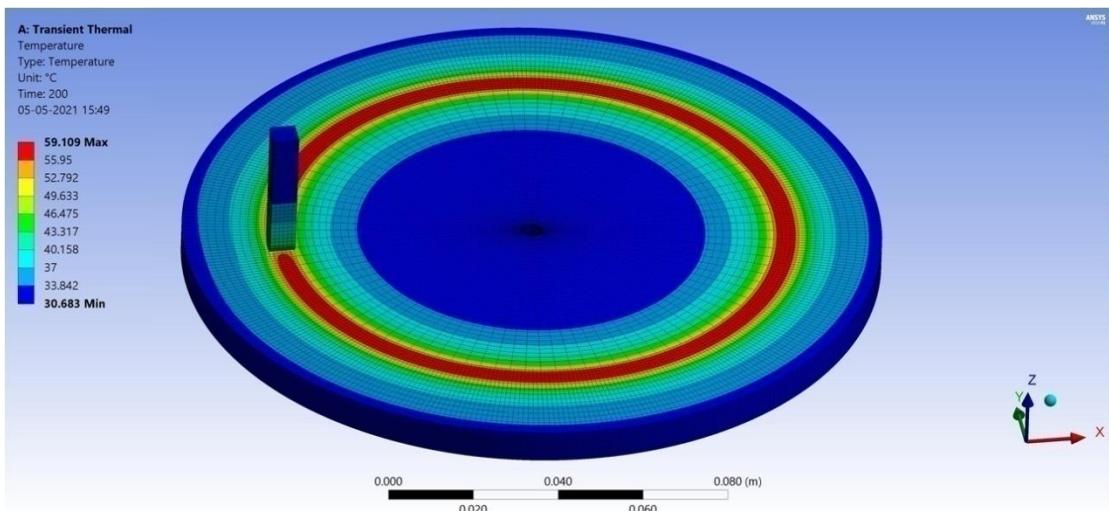


Figure 5.27: Temperature distribution between pin and disk over 200 s of sliding for a 120 mm diameter track using a Finite Element model (1.5 kg, 1 m/s).

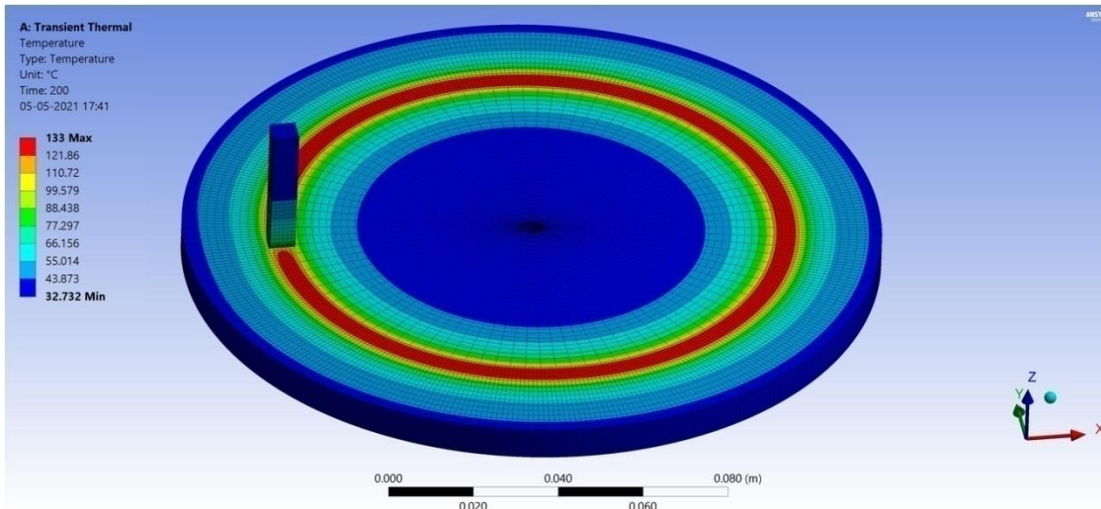


Figure 5.28: Temperature distribution between pin and disk over 200 s of sliding for a 120 mm diameter track using a Finite Element model (1.5 kg, 2 m/s).

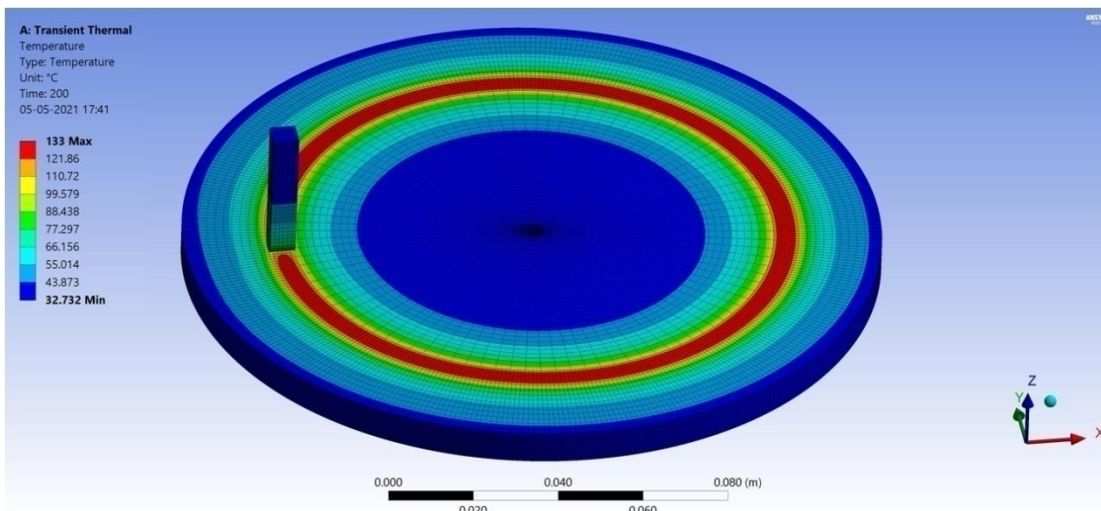


Figure 5.29: Temperature distribution between pin and disk over 200 s of sliding for a 120 mm diameter track using a Finite Element model (1.5 kg, 3 m/s).

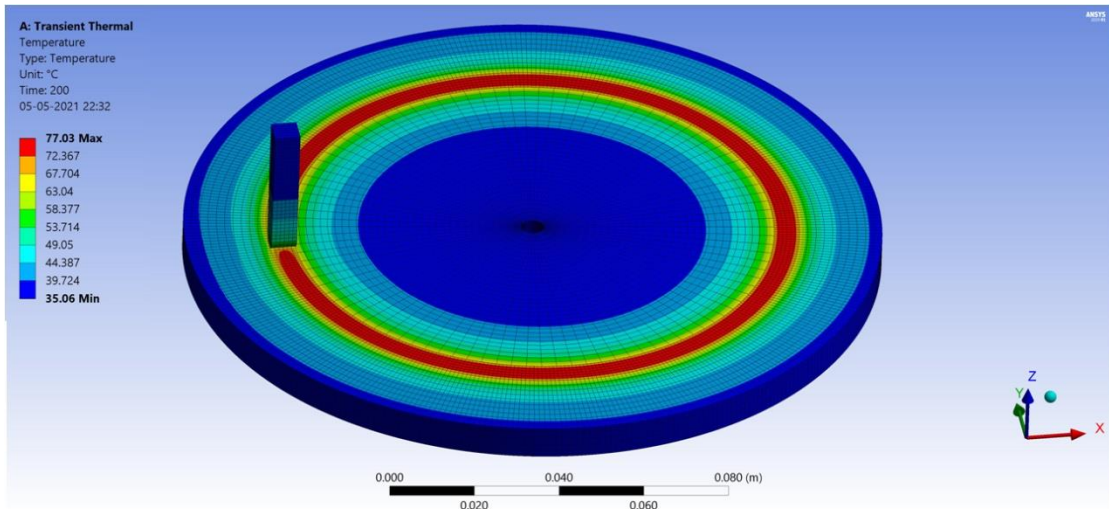


Figure 5.30: Temperature distribution between pin and disk over 200 s of sliding for a 120 mm diameter track using a Finite Element model (2 kg, 1 m/s).

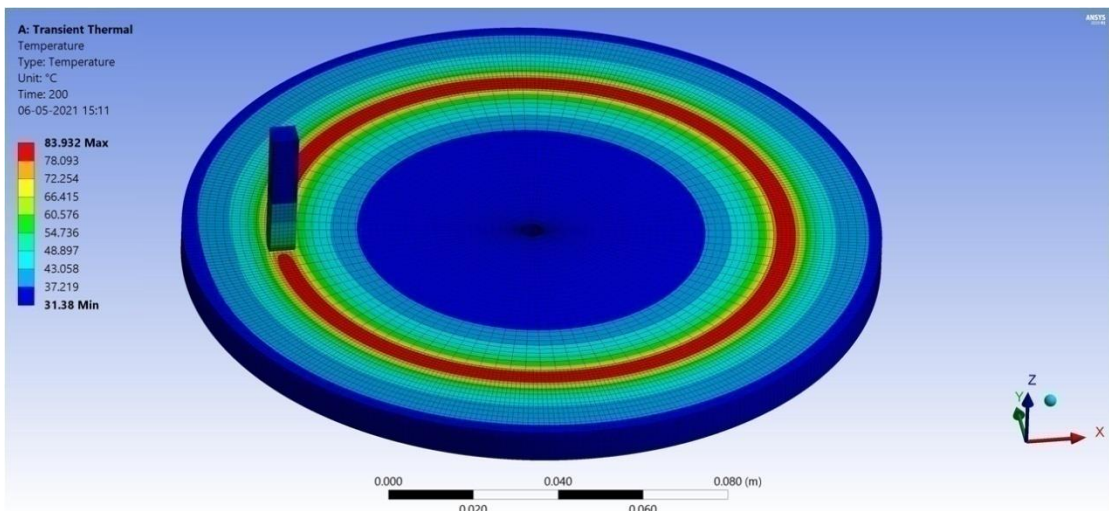


Figure 5.31: Temperature distribution between pin and disk over 200 s of sliding for a 120 mm diameter track using a Finite Element model (2 kg, 2 m/s).

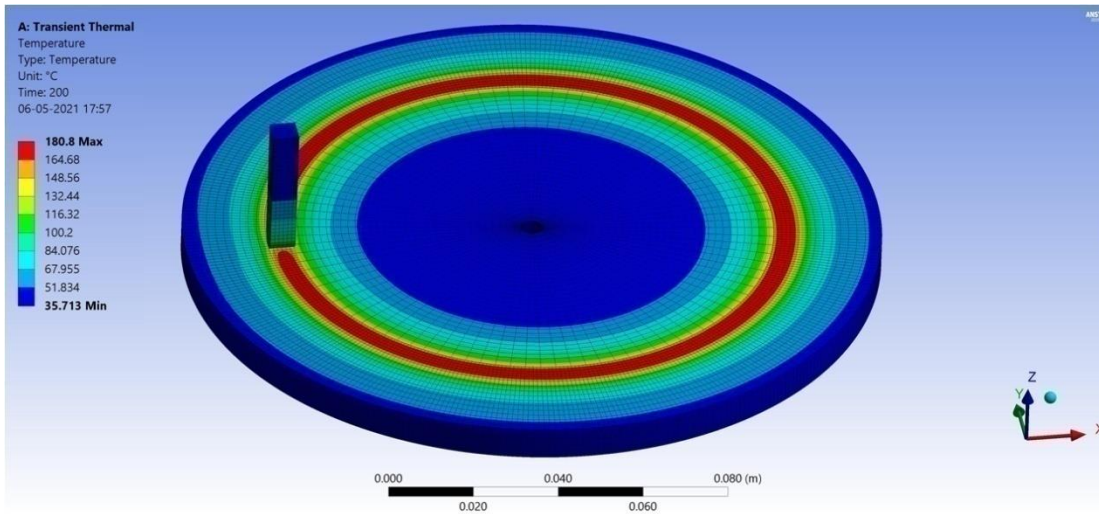


Figure 5.32: Temperature distribution between pin and disk over 200 s of sliding for a 120 mm diameter track using a Finite Element model (2 kg, 3 m/s).

Table 5.5: Temperature values obtained by finite element analysis for track diameter 60 mm at pin surfaces

Track Diameter 60 mm		Finite element analysis obtained max temperature (200 s)		
		Surface Temperature (°C)	Temperature (°C) at 4 mm location	Temperature (°C) at 7 mm location
Normal Load (kg)	Sliding Speed (m/s)			
1	1	42.069	38.61	35.96
	2	82.11	61.98	43.84
	3	104.08	66.65	55.07
1.5	1	57.72	47.42	39.36
	2	120.64	87.38	56.98
	3	135.01	100.89	76.25
2	1	69.47	55.02	44.72
	2	147.33	106.62	67.80
	3	209.91	148.85	98.04

Table 5.6: Temperature values obtained by finite element analysis for track diameter 120 mm at pin surfaces

Track Diameter 120 mm		Finite element analysis obtained max temperature (200 s)		
		Surface Temperature (°C)	Temperature (°C) at 4 mm location	Temperature (°C) at 7 mm location
Normal Load (kg)	Sliding Speed (m/s)			
1	1	41.29	37.42	34.61
	2	55.97	41.52	36.92
	3	77.03	62.63	54.63
1.5	1	89.45	65.49	49.57
	2	89.45	65.49	49.57
	3	83.92	61.25	41.52
2	1	58.38	46.17	36.39
	2	133.01	92.34	61.04
	3	180.08	139.78	88.47

5.8 Validation of finite element models against experiment results

Figures. 5.33 - 5.38, shows the comparison between the experimental curves of track diameter 60 mm and 120 mm, acquired by the pin-on-disk apparatus, and the curves obtained with the Finite element analysis (FEA). In Figures. 5.33 (b, c), 5.34 (b, c), 5.35 (b, c), 5.36 (b, c), 5.37 (b, c), and 5.38 (b, c), the finite element simulated temperature evolutions in the cylindrical pin at 4 mm and 7 mm locations from the sliding surface along the longitudinal axis are compared with the experimental values obtained through K-type thermocouples placed in the same position, was found to be in excellent agreement. The calculated Finite Element temperature evolutions and experimental surface temperature evolutions at the contact interface are presented in Figures. 5.33 (a), 5.34 (a), 5.35 (a), 5.36 (a), 5.37 (a), and 5.38 (a). Also, in this case good correlation was observed.

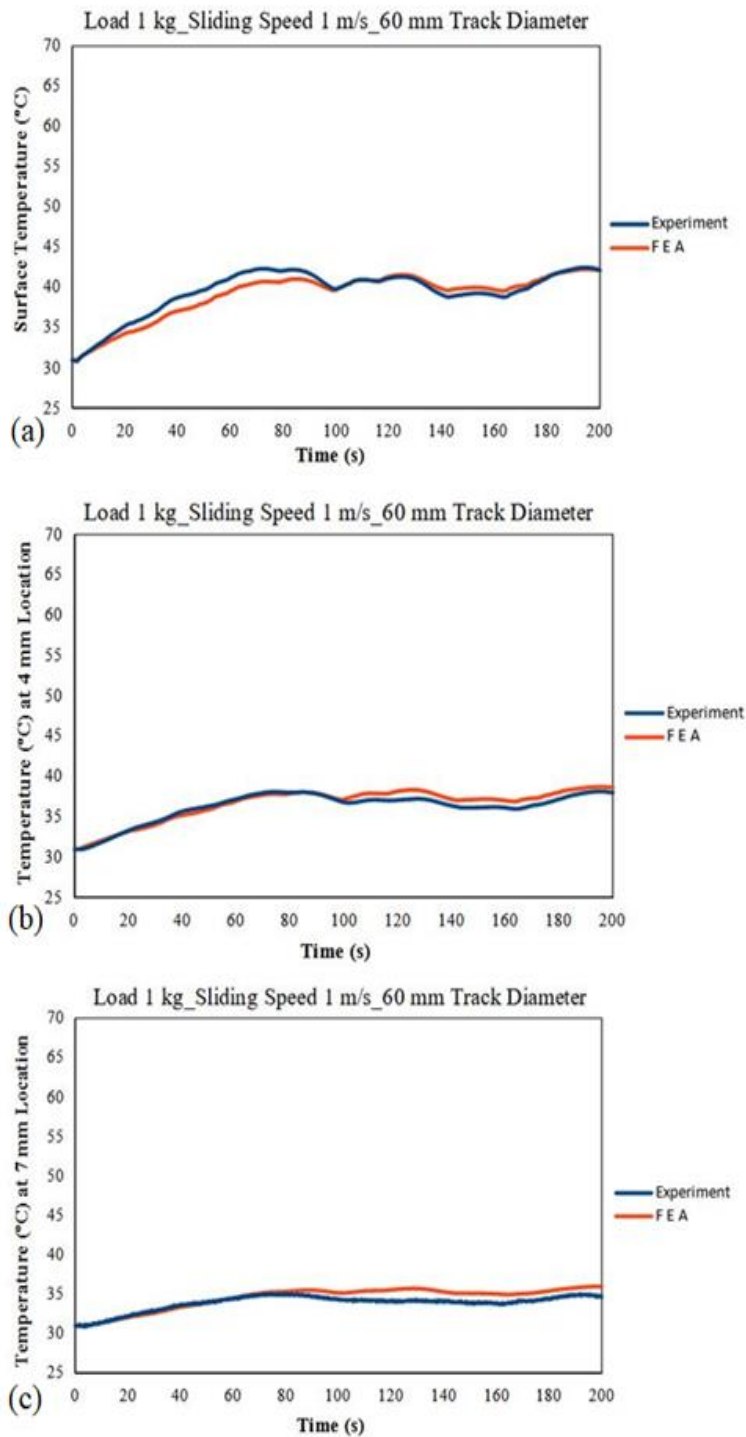


Figure 5.33: Temperature comparison between experimental and FE-simulated data (1 kg, 1 m/s) (a) evolution of the pin temperature at contact interface (b) Pin temperature evolution at 4 mm location (c) pin temperature evolution at 7 mm location for track diameter 60 mm.

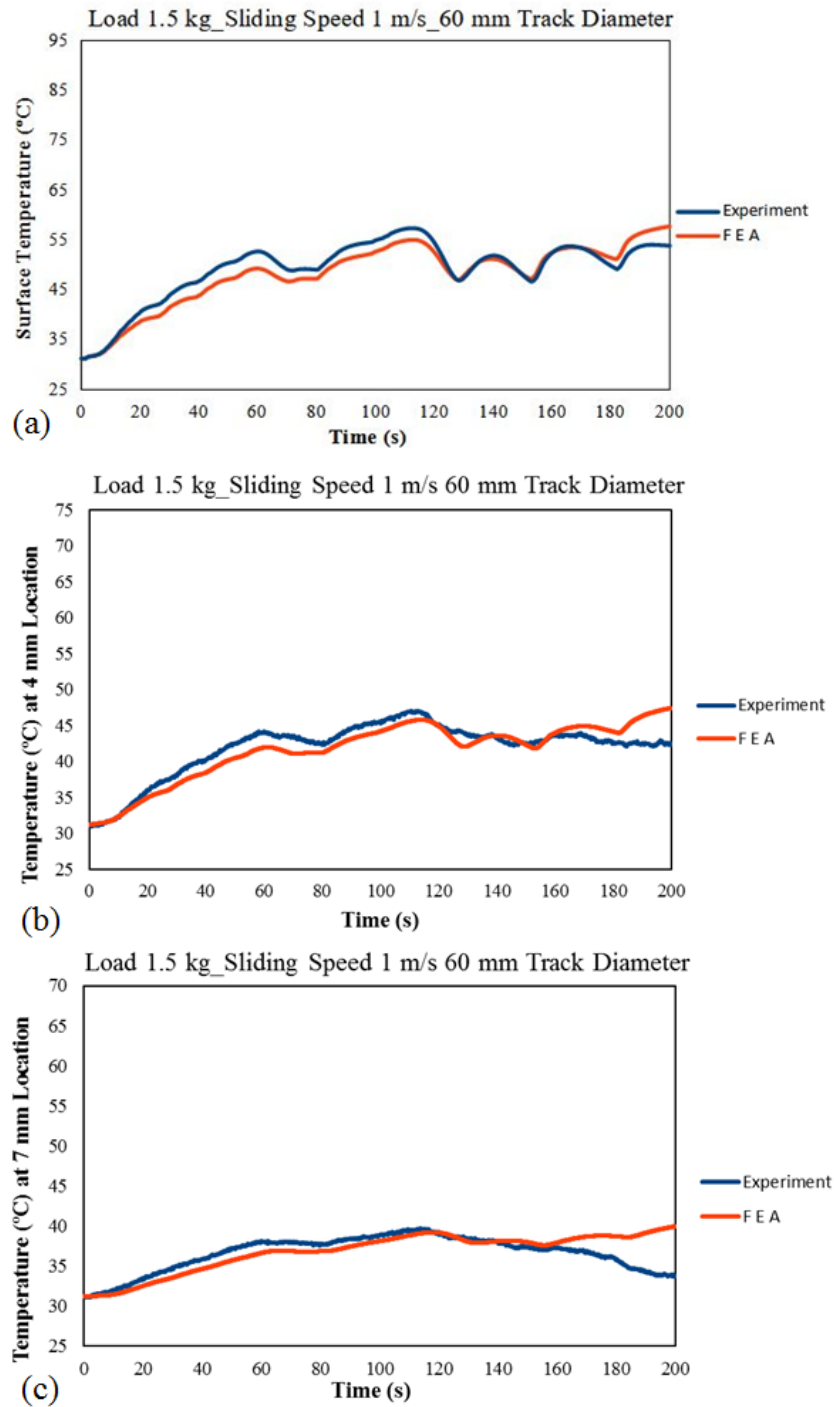


Figure 5.34: Temperature comparison between experimental and FE-simulated data (1.5 kg, 1 m/s) (a) evolution of the pin temperature at contact interface (b) Pin temperature evolution at 4 mm location (c) pin temperature evolution at 7 mm location for track diameter 60 mm.

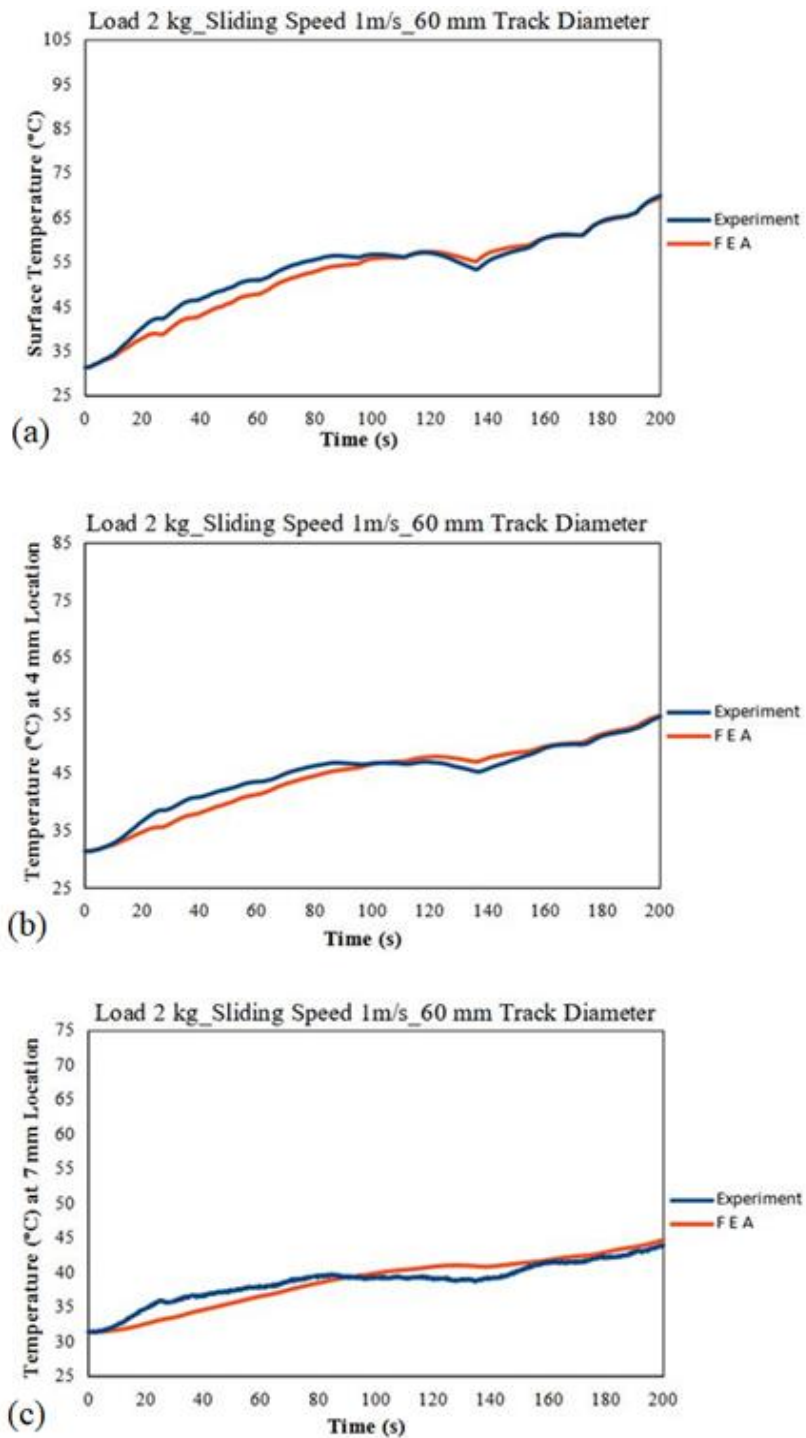


Figure 5.35: Temperature comparison between experimental and FE-simulated data (2 kg, 1 m/s) (a) evolution of the pin temperature at contact interface (b) Pin temperature evolution at 4 mm location (c) pin temperature evolution at 7 mm location for track diameter 60 mm.

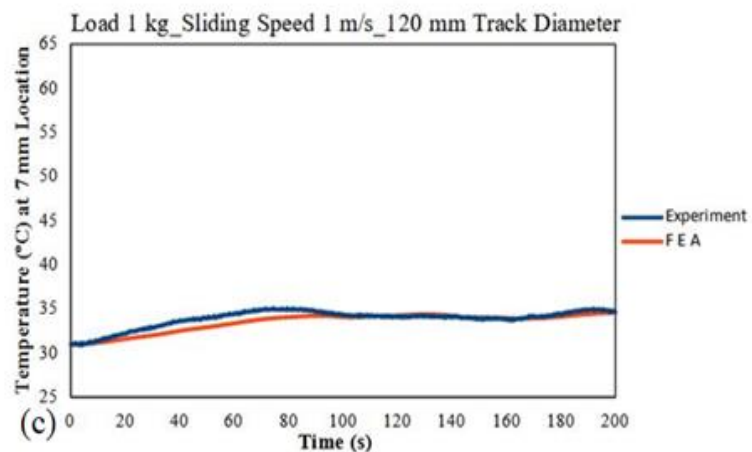
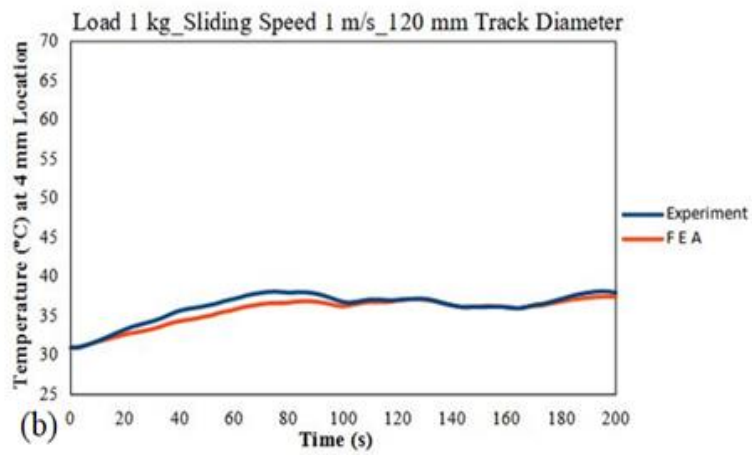
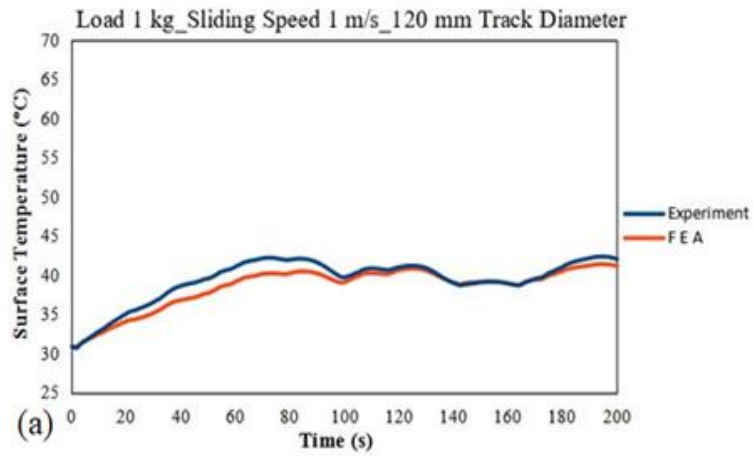


Figure 5.36: Temperature comparison between experimental and FE-simulated data (1 kg, 1 m/s) (a) evolution of the pin temperature at contact interface (b) Pin temperature evolution at 4 mm location (c) pin temperature evolution at 7 mm location for track diameter 120 mm.

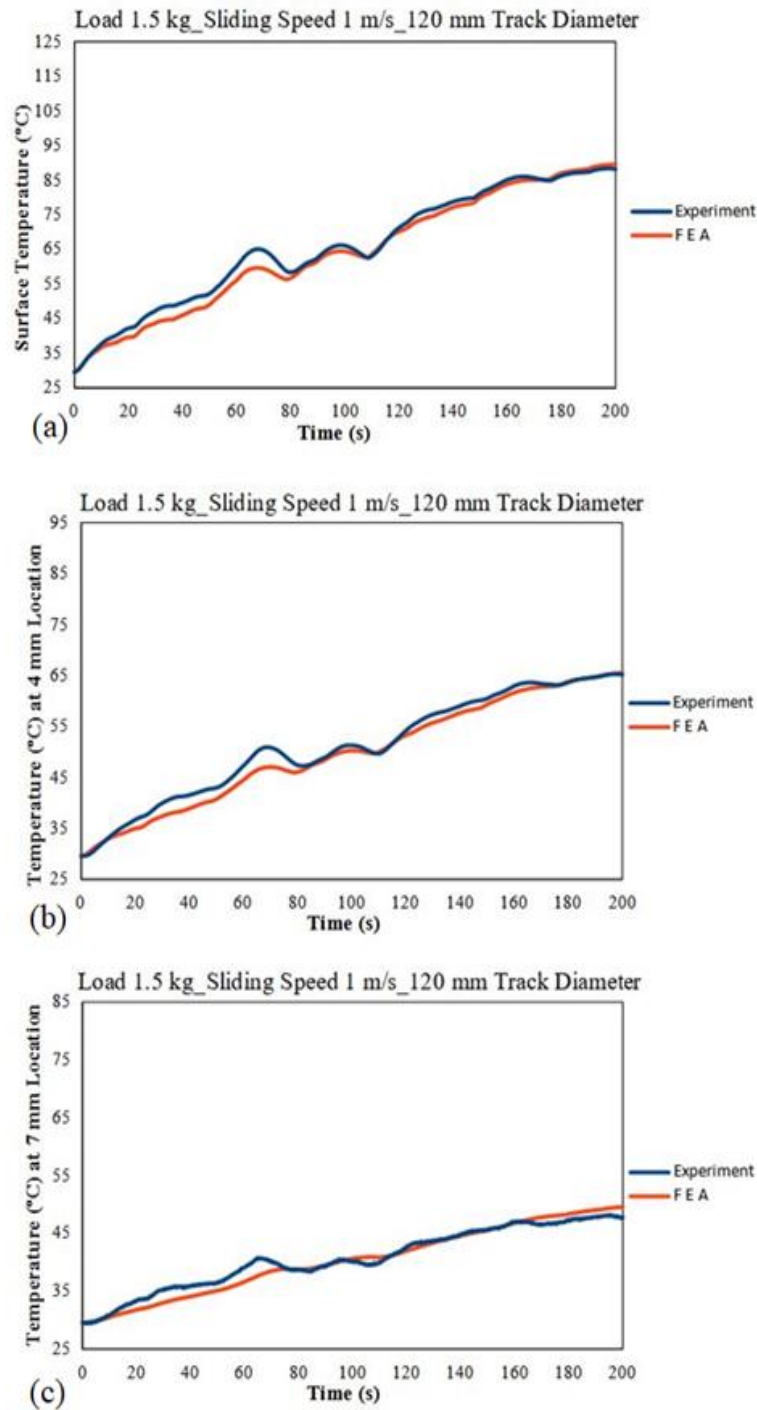


Figure 5.37: Temperature comparison between experimental and FE-simulated data (1.5 kg, 1 m/s) (a) evolution of the pin temperature at contact interface (b) Pin temperature evolution at 4 mm location (c) pin temperature evolution at 7 mm location for track diameter 120 mm.

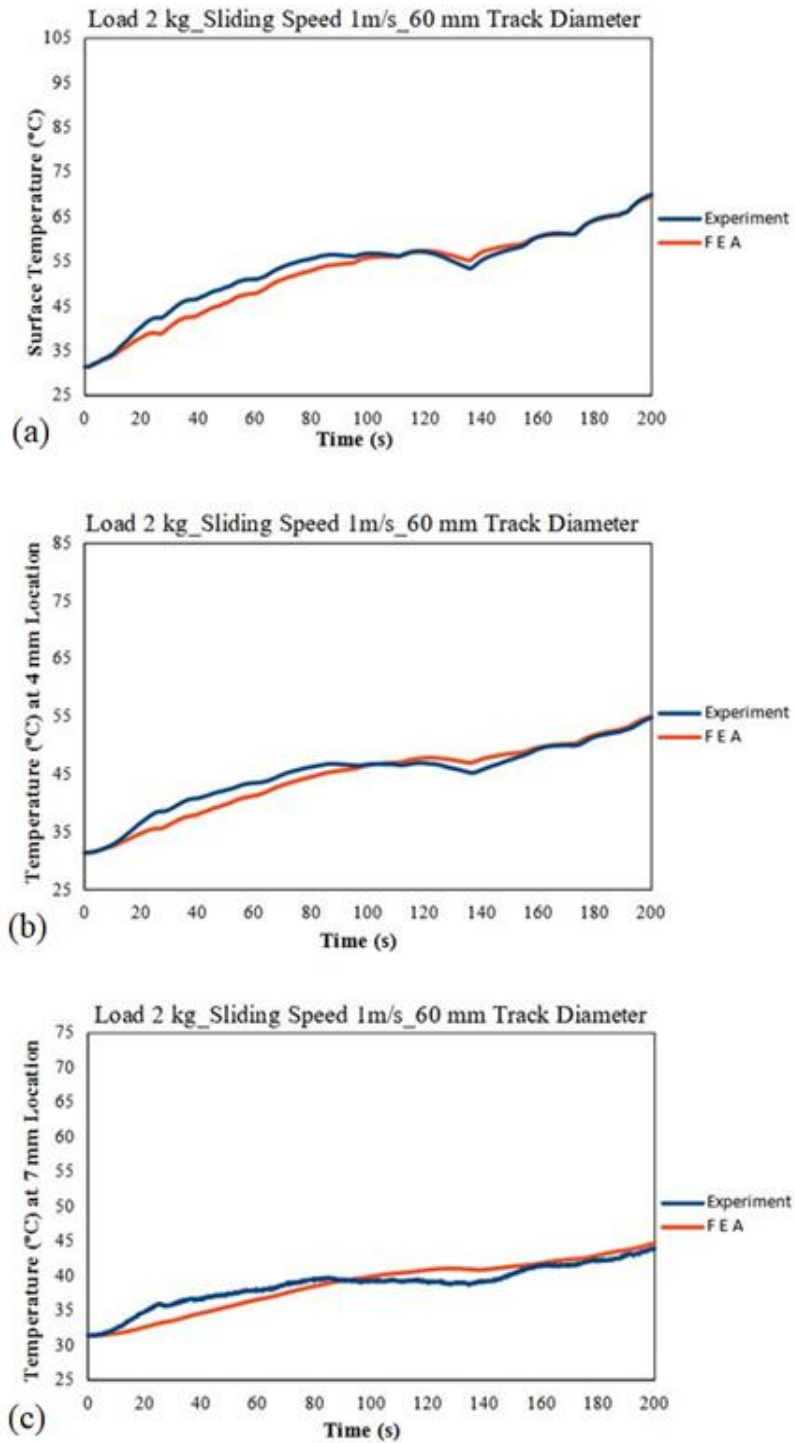


Figure 5.38: Temperature comparison between experimental and FE-simulated data (2 kg, 1 m/s) (a) evolution of the pin temperature at contact interface (b) Pin temperature evolution at 4 mm location (c) pin temperature evolution at 7 mm location for track diameter 120 mm.

Table 5.7: Comparison of maximum surface temperature between experiments and FEA for Track Diameter 60 mm

Track Diameter 60 mm		Maximum Surface Temperature (°C)		
Normal Load (kg)	Sliding Speed (m/s)	Experimental (°C)	Finite element analysis (°C)	Error (%)
	2	81.17	82.11	1.44
	3	99.60	104.08	4.33
1.5	1	53.83	57.72	6.73
	2	113.31	120.64	6.08
	3	131.91	135.01	2.29
2	1	69.99	69.47	0.74
	2	140.44	147.33	4.67
	3	202.94	209.91	3.32

Table 5.8: Comparison of maximum surface temperature between experiments and FEA for a Track Diameter 60 mm at 4mm location

Track Diameter 60 mm		Maximum Temperature (°C) at 4 mm Location		
Normal Load (kg)	Sliding Speed (m/s)	Experimental (°C)	Finite element analysis (°C)	Error (%)
	2	59.21	61.98	1.44
	3	72.86	66.65	4.33
1.5	1	42.41	47.42	6.73
	2	78.69	87.38	6.08
	3	99.38	100.89	2.29
2	1	54.80	55.02	0.39
	2	99.45	106.62	4.67
	3	141.88	148.85	3.32

Table 5.9: Comparison of maximum surface temperature between experiments and FEA for a Track Diameter 60 mm at 7 mm location

Track Diameter 60 mm		Maximum Temperature (°C) at 7 mm Location		
Normal Load (kg)	Sliding Speed (m/s)	Experimental (°C)	Finite element analysis (°C)	Error (%)
		1	1	34.61
	2	43.63	43.84	0.47
	3	55.21	55.07	0.25
1.5	1	37.73	39.36	4.14
	2	54.49	56.98	4.36
	3	73.03	76.25	4.22
2	1	43.92	44.72	1.78
	2	67.85	67.80	0.07
	3	94.89	98.04	3.21

Table 5.10: Comparison of surface temperature from experimental to FEA values for Track Diameter 120 mm

Track Diameter 120 mm		Maximum Surface Temperature (°C)		
Normal Load (kg)	Sliding Speed (m/s)	Experimental (°C)	Finite element analysis (°C)	Error (%)
		1	1	42.13
	2	57.78	55.97	3.23
	3	76.48	77.03	0.71
1.5	1	88.18	89.45	1.41
	2	88.15	89.45	1.45
	3	81.17	83.92	3.27
2	1	58.05	58.38	0.56
	2	127.11	133.01	0.07
	3	179.88	180.08	3.21

Table 5.11: Comparison cylindrical pin temperature 4 mm location from experimental to FEA values for Track Diameter 120 mm

Track Diameter 120 mm		Maximum Temperature (°C) at 4 mm Location		
Normal Load (kg)	Sliding Speed (m/s)	Experimental (°C)	Finite element analysis (°C)	Error (%)
		1	1	37.97
	2	44.25	41.52	6.16
	3	66.30	62.63	5.85
1.5	1	66.15	65.49	1.00
	2	65.14	65.49	0.53
	3	59.21	61.25	3.33
2	1	45.36	46.17	1.75
	2	86.26	92.34	6.58
	3	132.38	139.78	5.29

Table 5.12: Comparison of cylindrical pin temperature 7 mm location from experimental to FEA values for Track Diameter 120 mm

Track Diameter 120 mm		Maximum Temperature (°C) at 7 mm Location		
Normal Load (kg)	Sliding Speed (m/s)	Experimental (°C)	Finite element analysis (°C)	Error (%)
		1	1	34.61
	2	37.98	36.92	2.87
	3	55.01	54.63	0.69
1.5	1	47.77	49.57	3.63
	2	47.77	49.57	3.63
	3	44.25	41.52	6.16
2	1	37.97	36.39	4.34
	2	56.55	61.04	6.58
	3	88.77	88.47	0.03

The Tables 5.7, 5.8, 5.9, 5.10, 5.11 and 5.12 shows the experimental temperature values and Finite element simulated temperature values at contact interface, 4 mm location, 7 mm location in the cylindrical pin and their percentage of error values. An error of 6.16 % was noticed when compared with the values obtained from experiment. After 100 seconds of sliding, there is a discrepancy between the experimental and simulated data, due to an undesired third body interaction between the K-Type thermocouples and the cylindrical pin surface [Majcherczak et al., 2006]

CHAPTER 6

CONCLUSIONS

Rotary type full sliding experiments were conducted to study the coefficient of friction, evolution of Pin temperature at the contact interface of stainless steel (SS304) alloys at different loading conditions (normal load and sliding speed) and temperatures was studied in detail and the following conclusions were drawn:

1. Coefficient of friction stabilization value was increased at lower sliding speeds for the both wear (60 mm and 120 mm) track.
2. At higher sliding speeds Coefficient of friction stabilization value was decrease for both wear (60 mm and 120 mm) track.
3. Coefficient friction value was higher in 120 mm track comparatively 60 mm track with condition for similar loads with sliding speeds.
4. Wear volume decrease at lower sliding speed with lower normal load for both track surface. At Normal load with sliding speed increased Wear volume increase for both track surface.
5. Wear damage surface image was taken by using Optical microscope. At lower sliding speed with lower Normal load Wear damage was lesser in the both wear (60 mm and 120 mm) track surface. However normal load with sliding speed increases wear track surface damage higher at both wear track.
6. Wear damage was more at 60 mm track surface comparatively 120 mm track surface wear damage was lesser. At condition for similar loads with sliding speeds.
7. Full sliding experiments were conducted with three different sliding speeds of 1 m/s, 2 m/s and 3 m/s at constant normal load of 1 kg. For sliding speeds of 1 m/s, 2 m/s and 3 m/s, the stabilized values of coefficient of friction are observed to be 0.15, 0.22 and 0.28. For lower sliding speed of 1 m/s, wear debris acts as rollers or spherical balls and facilitates easy sliding of contact surfaces which leads to lower stabilized coefficient of friction (0.15). For higher sliding speeds, melting of wear debris and micro welding of wear

particles at the contact interface are found to be dominant resulting in higher stabilized coefficient of friction (0.22 and 0.28).

8. It is also observed that there is no variation in coefficient of friction for various sliding speeds at a sliding distance of 1.4 m and the corresponding coefficient friction is observed as 0.06. Observation of single valued coefficient of friction is mainly due to formation of oxide layer and nitride layer on the metallic surface.
9. For lower sliding speed of 1 m/s, the temperature at interface increases with increase in sliding distance and the stabilized contact temperature is determined as 40 °C. For higher sliding speeds of 2 m/s and 3 m/s, the values of stabilized contact temperature are observed as 42 °C and 60 °C respectively. There is no significant difference in stabilized contact temperature at the sliding speeds of 1 m/s and 2 m/s and difference in stabilized contact temperature is observed to be 2 °C.
10. A thorough calibration of the boundary conditions, particularly the heat convection coefficients, is necessary to create a valid FE model that agrees well with experimental data of the pin temperature evolutions.
11. The experimental values of pin-on-disk values are quite similar to the simulated values. This proves that the simulation approach for studying temperature rise caused by friction between two metals is accurate.
12. At higher sliding speeds and normal loads, pin contact profile changes from line contact to area contact at less time duration.
13. It is evident that this finite element analysis (transient thermal analysis) is effective in the investigation of material tribological characteristics.

6.1 Limitations of the study

- Validation of estimated contacted interface temperatures with experimentally measured contact interface temperatures can be considered for better reliability. Due to the lack of experimental facilities, the contact interface temperatures were not measured in the present study. The inverse heat transfer model used in this study to estimate temperature at the contact interface.

- The frictional heat can be estimated using tribological parameters (coefficient of friction and wear) instead of pure inverse heat transfer methods.
- The phase and chemical composition change of SS304 Stainless Steel alloys at higher temperatures can be conformed with SEM with EDX characterization.
- The effect of oxide layer thickness on coefficient of friction is not concentrated in this study.
- Experiments was carried out for the cylindrical pin specimen without ceramic coating to avoid convection and radiation.
- Data acquisition system used to obtain temperature samples per second is limited (5 sample/second).

6.2 Scope for future work

- The present study can be extended related to friction coefficient under full sliding conditions were used to obtain contact tractions for partial slip fretting conditions.
- Fretting studies can be carried out for coated and uncoated specimens.
- Composite Materials and Functionally Graded Materials (FGMs) can be used to conduct pin on disc tribometer experiments under both dry sliding conditions and wet sliding conditions.

REFERENCES

- ANSYS, Inc. ANSYS Workbench. Release 19.0: Theory guide.
- Adel Mahamood Hassan, Abdalla Alrashdan, Mohammed T. Hayajneh and Ahmad Turki Mayyas (2009). “Wear behavior of Al–Mg–Cu–based composites containing SiC particles.” *Tribology International*, 42, 1230–1238.
- Aditya A. Walvekar, Benjamin D. Leonard, Farshid Sadeghi, Behrooz Jalalahmadi, Nathan Bolander (2014). “An experimental study and fatigue damage model for fretting fatigue.” *Tribology International*, 79, 183–196.
- Ahmed A.D. Sarhan, E. Zalnezhad, M. Hamdi (2013). “The influence of higher surface hardness on fretting fatigue life of hard anodized aerospace AL7075-T6 alloy.” *Materials Science & Engineering, A* 560, 377–387.
- Anchalee Saengsai, Yuichi Otsuka, Yoshiharu Mutoh (2014). “Fretting fatigue behavior of SS304 stainless steel under pressurized hot water.” *Tribology International*, 79, 52– 58.
- Arora, P. R., M. S. D. Jacob, M. S. Salit, E. M. Ahmed, M. Saleem, and P. Edi (2007). “Experimental evaluation of fretting fatigue test apparatus.” *International Journal of Fatigue*, 29(5), 941 – 952.
- Beck, J.V., 1970. Nonlinear estimation applied to the nonlinear inverse heat conduction problem. *International Journal of heat and mass transfer*, 13(4), pp.703-716.
- Borut Cerne, Joze Duhovnik & Joze Tavcar (2019). Semi-analytical flash temperature model for thermoplastic polymer spur gears with consideration of linear thermo-mechanical material characteristics. *Journal of Computational Design and Engineering*, 6, 617–628.

- Çaydaş, U., Ekici, S. (2012) Support vector machines models for surface roughness prediction in CNC turning of AISI 304 austenitic stainless steel. *J Intell Manuf* 23, pp 639–650.
- Christian Zeller, Binu Surendran & Micheal F. Zaeh (2018). Parameterized Extended Finite Element Method for high thermal gradients. *Journal of Computational Design and Engineering*, 5, 329–336.
- Clarke, A., Sharif, K. J., Evans, H. P. & Snidle, R. W., 2007. Elastohydrodynamic modelling of heat partition in rolling–sliding point contacts. *Proceedings of the Institution of Mechanical Engineers, Part J: Journal of Engineering Tribology*, 221(3), pp. 223-235.
- Cruzado, S.B. Leen, M.A. Urchegui, X. Gómez (2013). “Finite element simulation of fretting wear and fatigue in thin steel wires.” *International Journal of Fatigue*, 55, 7–21.
- Chen, L., Wang, Y., Peng, L., Fu, P. and Jiang, H., 2014. Study on the interfacial heat transfer coefficient between AZ91D magnesium alloy and silica sand. *Experimental thermal and fluid science*, 54, pp.196-203.
- Day, A.J. 2014. *Braking of Road Vehicles*. Elsevier, Amsterdam.
- Douglas Godfrey, *Tribology International*, 28 (1995) 119.
- E.M. Bortoleto, A.C. Rovani, V. Seriacopi, F.J. Profito, D.C. Zachariadis, I.F. Machado, A. Sinatora, R.M. Souza, ,2013. Experimental and numerical analysis of dry contact in the pin on disc test, *Wear*, Volume 301, Issues 1–2, Pages 19-26, ISSN 0043-1648,

- Fei Xue, Zhao-Xi Wang, Wen-Sheng Zhao, Xiao-Liang Zhang, Bao-Ping Qu, Liu Wei (2014). “Fretting fatigue crack analysis of the turbine blade from nuclear power plant.” *Engineering Failure Analysis*, 44, 299–305.
- Gao CH, Lin XZ (2002) Transient temperature field analysis of a brake in a non-axisymmetric three-dimensional model. *J Mat Proc Tech* 129:513–517. doi:10.1016/S0924-0136(02)00622-2.
- Gupta, A. K., Kumar, P., Sahoo, R. K., Sahu, A. K. & Sarangi, S. K. (2017). Performance measurement of plate fin heat exchanger by exploration: ANN, ANFIS, GA, and SA. *Journal of Computational Design and Engineering*, 4, 60–68.
- G.Q. Wu, X.L.Liu, H.H.Li, W.Sha, L.J.Huang (2015). “Effect of contact pressure on fretting fatigue behavior of Ti-1023.” *Wear*, 326-327, 20–27.
- Goto, H. and M. Ashida (1999). The influence of oxygen and water vapour on the friction and wear of an aluminium alloy under fretting conditions. *Wear*, 116, 141–155.
- Gwidon W. Stachowiak (2005). “wear – materials, mechanisms and practice.” Text book.
- H. Murthy, Daniel B. Garcia, John F. Matlik, Thomas N. Farris (2005). “Fretting fatigue of single crystal/polycrystalline nickel subjected to blade/disk contact loading.” *Acta Astronautica*, 57, 1 – 9.
- H. Murthy, K. Vadivuchezhian (2017). “Estimation of friction distribution in partial-slip contacts from reciprocating full-sliding tests.” *Tribology International*, 108, 164–173.

- H. Proudhon, J. Y. Buffiere, S. Fouvry (2006). “Characterisation of fretting fatigue damage using synchrotron X-ray micro-tomography.” *Tribology International*, 39, 1106– 1113.
- Hills, D. and D. Nowell (1994). “Mechanics of fretting fatigue.” Kluwer, Dordrecht, The Netherlands.
- Hinrichs, R., Vasconcellos, M.A.Z., Osterle, W., Prietzel, C.: A TEM snapshot of magnetite formation in brakes: the role of the disc’s cast iron graphite lamellae in third body formation. *Wear* 270, 365–370 (2011).
- Hoepfner, D. W. (2006). “Fretting fatigue case studies of engineering components.” *Tribology International*, 39, 1271 – 1276.
- J.K.M. Kwok, S.C. Lim (1999). “High-speed tribological properties of some Al/SiCp composites: I. Frictional and wear-rate characteristics.” *Composites Science and Technology*, 59, 55-63.
- Jacko, M.G., Tsang, P.H.S., Rhee, S.K.: Wear debris compaction and friction film formation of polymer composites. *Wear* 133, 23–38 (1989).
- Jiang Luqing, Zheng Xilai, Liang Chun, Yue Feng, Zhang Junjie (2011). “The Disposition and Management Strategy of Decommissioning Offshore Oil Platform in Chengdao, China.” *Energy Procedia*, 5, 525–528.
- Johnson, K. L. (1985): *Contact Mechanics*, Cambridge: Cambridge University Press.
- Jones, J., 2000, *Contact Mechanics*, Cambridge University Press, Cambridge, UK, Chap. 6. ISBN: 978-3-16-148410-0
- Johnson, K. L. (1985). “Contact mechanics.” Cambridge University Press

- K.A. Laux, A. Jean-Fulcrand, H.J. Sue, T. Bremner, J.S.S. Wong (2016). "The influence of surface properties on sliding contact temperature and friction for polyetheretherketone (PEEK)." *Polymer*, 103, 397-404.
- K. Arul Raj, M.P. Arunkumar, P.K.C. Kanigalpula, M. Karthikeyan, Tribological and vibrational characteristics of AISI 316L tested at elevated temperature and 600 Torr vacuum, *Defence Technology*, Volume 15, Issue 1, 2019, Pages 58-64, ISSN 2214-9147.
- K. Vadivuchezhian, S. Sundar, H. Murthy (2011). "Effect of variable friction coefficient on contact tractions." *Tribology International*, 44, 1433–1442.
- Kennedy, F. E., Jr. (1981). "Surface Temperatures in Sliding Systems, A Finite Element Analysis." *ASME. J. of Lubrication Tech.* 103(1), pp 90–96.
- Laraqui, N., Alilat, N., Garcia de Maria, J.M., Bairi, A.: Temperature and division of heat in a pin-on-disc frictional device - Exact analytical solution. *Wear* 266, 765–770 (2009).
- Lee H, Mall S, Sathish S (2005). "Investigation into effect of re-shotpeening on fretting fatigue behavior of Ti-6Al-4V." *Materials Science and Engineering, A* 390, 227–232.
- M. Helmi Attia and R. B. Waterhouse (1992). *Standardization of Fretting Fatigue Test Methods and Equipment*.
- M. Martíneza , A. Massettia , H. Svobodaa,b,*2012 "Effect of the pin geometry on the wear behavior of weld deposited hard facing" *Procedia Materials Science* 1, 305 – 312.
- M. Luke, M. Burdack, S. Moroz, I. Varfolomeev (2016). "Experimental and numerical study on crack initiation under fretting fatigue loading." *International Journal of Fatigue*, 86, 24–33.

- M.L. Rahaman, Liangchi Zhang (2014). “On the estimation of interface temperature during contact sliding of bulk metallic glass.” *Wear*, 320, 77–86.
- M. Vilaseca, S. Molas, D. Casellas, High temperature tribological behaviour of tool steels during sliding against aluminium, *Wear*, Volume 272, Issue 1, 2011, Pages 105-109, ISSN 0043-1648, <https://doi.org/10.1016/j.wear.2011.07.007>.
- Majcherczak, D., Dufrenoy, P., Berthier, Y., Nait-Abdelaziz, M(2006) Experimental thermal study of contact with third body. *Wear* 261, pp 467–478.
- Matteo Federici, Giovanni Straffelini, Stefano Gialanella., 2017 Pin-on-Disc Testing of Low-Metallic Friction Material Sliding Against HVOF Coated Cast Iron: Modelling of the Contact Temperature Evolution. *Tribol Lett* 65:121 DOI 10.1007/s11249-017-0904-y.
- Mohammad Asaduzzaman Chowdhury, Dewan Muhammad Nuruzzaman, Biplov Kumar Roy, Asraful Islam, Zakir Hossain and Md. Rakibul Hasan (2013). “Experimental Investigation of Friction Coefficient and Wear Rate of Stainless Steel 202 Sliding against Smooth and Rough Stainless Steel 304 Counter faces” *Friction and Wear Research*, Vol. 1 Iss. 3
- Osterle, W., Urban, I.: Third body formation on brake pads and rotors. *Tribol. Int.* 39, 401–408 (2006).
- P. Palanikumar, N. Gnanasekaran, K. Subrahmanya, Vadivuchezhian Kaliveeran, Effect of sliding speed and rise in temperature at the contact interface on coefficient of friction during full sliding of SS304, *Materials Today: Proceedings*, Volume 27, Part 3, 2020, Pages 1996-1999, ISSN 2214-7853, <https://doi.org/10.1016/j.matpr.2019.09.046>.

- Raghavendra, C.R., Basavarajappa, S. & Sogalad, I. (2019) Analysis of temperature field in dry sliding wear test on pin-on-disc. *Heat Mass Transfer* 55, pp 1545–1552.
- S.C. Sharma, *Wear*, 249 (2001) 1036.
- Saikko, V. (July 10, 2017). "Effect of Contact Area on the Wear and Friction of UHMWPE in Circular Translation Pin-on-Disk Tests." *ASME. J. Tribol.* November 2017; 139(6): 061606.
- Straffelini, G. (2015): *Friction and Wear, Methodologies for Design and Control*. Springer, Berlin
- Sun, Z., Hu, H. and Niu, X., (2011) Determination of heat transfer coefficients by extrapolation and numerical inverse methods in squeeze casting of magnesium alloy AM60. *Journal of Materials Processing Technology*, 211(8), pp 1432-1440.
- Toshio Yoshimura & Kazushige Ikuta (1985). Inverse heat-conduction problem by finite-element formulation. *International Journal of Systems Science*, 16(11), 1365-1375.
- Uthayakumar M, Aravindan S, Rajkumar K, (2013): Wear performance of Al–SiC–B4C hybrid composites under dry sliding conditions, *Materials and Design*, Vol. 47, pp. 456-464.
- Valota, G., De Luca, S., Sodeberg, A.: Use of FEA to clarify pin-on- disc tribometer tests of disc brake materials. In: *EuroBrake 2015 Conference*, Paper EB2015-STQ-004. FISITA, London.
- Verma, P.C., Ciudin, R., Bonfanti, A., Aswath, P., Straffelini, G., Gialanella, S.: Role of the friction layer in the high-temperature pin-on-disc study of a brake material. *Wear* 346–347, 56–65 (2016)

- Vishweshwara, P. S., Gnanasekaran, N. & Arun, M. (2019). Estimation of Interfacial Heat Transfer Coefficient for Horizontal Directional Solidification of Sn-5 wt%Pb Alloy Using Genetic Algorithm as Inverse Method. *Soft Computing for Problem Solving, Advances in Intelligent Systems and Computing*, 816, pp 447-459.
- Vishweshwara, P. S., Gnanasekaran, N. & Arun, M. (2020). Inverse Approach Using Bio-Inspired Algorithm Within Bayesian Framework for the Estimation of Heat Transfer Coefficients During Solidification of Casting. *Journal of Heat Transfer*, 142, pp (012403-1)-(012403-11).
- Zhang, A., Liang, S., Guo, Z. & Xiong, S. (2017). Determination of the interfacial heat transfer coefficient at the metal-sand mold interface in low pressure sand casting. *Experimental Thermal and Fluid Science*, 88, pp 472–482.
- Zhizhong Sun, Henry Hu & Xiaoping Niu (2011). Determination of heat transfer coefficients by extrapolation and numerical inverse methods in squeeze casting of magnesium alloy AM60. *Journal of Materials Processing Technology*, 211, 1432–1440.

PUBLICATIONS BASED ON PRESENT RESEARCH WORK

International Journals

1. **P. Palanikumar**, N. Gnanasekaran, K. Subrahmanya, Vadivuchezhian Kaliveeran (2020) “Effect of sliding speed and rise in temperature at the contact interface on coefficient of friction during full sliding of SS304”, Materials Today: Proceedings, Pages 1996-1999, ISSN 2214-7853, <https://doi.org/10.1016/j.matpr.2019.09.046>. (Scopus Indexed)
2. **P. Palanikumar**, N.Gnanasekaran, K. Subrahmanya, Vadivuchezhian Kaliveeran (2020) “Identification of Effective location of Thermocouples from the Contact Interface” Materials Today: Proceedings, Pages 2811-2814, ISSN 2214-7853, <https://doi.org/10.1016/j.matpr.2019.12.373>. (Scopus Indexed)
3. **P. Palanikumar**, N.Gnanasekaran, K.Subrahmanya, Vadivuchezhian Kaliveeran “Wear, Coefficient of Friction and Contact Temperature Evolution in Full Sliding Experiments on Hertzian Contacts of Aluminium Alloys ” Tribologia - Finnish Journal of Tribology. (Under review).
4. **P.Palanikumar**, N.Gnanasekaran, K.Subrahmanya, Vadivuchezhian Kaliveeran, Raveesh RM, Vishweshwara PS “Effect of Sliding Speed, Normal Load on Evolution of Temperature at Contact Interface during Full Sliding of Stainless Steel (SS304) alloy ” Journal of the Brazilian Society of Mechanical Sciences and Engineering. (Under review).

International Conferences

1. **Palanikumar P.**, Nagaraj M. K., Gnanasekaran N., Vadivuchezhian Kaliveeran “Full sliding Experiments on Hertzian Contacts of Aluminium Alloys Al6061 and Al6082” International Conference Materials and Manufacturing methods-2019, July 5-8, 2019, NIT Tiruchirappalli.
2. **Palanikumar P.**, Nagaraj M. K., Gnanasekaran N. “Effect of frictional heat on coefficient of friction during full slip of Al6061-T6 Hertzian contacts” at 7th International Engineering Symposium -IES 2018, March 7 - 9, 2018, Kumamoto University, Japan.
3. **Palanikumar P.**, Nagaraj M.K., Gnanasekaran N., Gowtham S., Vadivuchezhian Kaliveeran “Dry sliding experiment to understand the effect of sliding speed on coefficient of friction for SS304 and SS304L” International Conference on Recent Advances in Material Chemistry-ICRAMC 2017, February 15 - 17, 2017, SRM University, Tamil Nadu.

CURRICULUM VITAE



Name: PALANI KUMAR. P

Permanent Address:

1/495, Kamarajar Street,
East Lakshmi Nager,
Mudichur,
West Tambaram,
Chennai-600048

Contact No.: +91-9841665070

Email ID: palani161984@gmail.com

Education:

Master of Technology (2012-2014)

Discipline: Internal Combustion Engineering

College : University College of Engineering, Anna University , Villupuram.

Bachelor of Engineering (2008-2011)

Discipline: Madras Institute of Technology,

College : Anna University, Chennai.

Diploma (1985-88)

Discipline: Mechanical Engineering

College : Central Polytechnic college, Chennai.